UNIVERSITY OF OKLAHOMA

GRADUATE COLLEGE

# EXPLORING FUTURE HYDROLOGIC EXTREMES OF THE RED RIVER BASIN

A THESIS

SUBMITTED TO THE GRADUATE FACULTY

in partial fulfillment of the requirements for the

Degree of

MASTER OF SCIENCE IN GEOGRAPHY

By

DARRIAN BERTRAND
Norman, Oklahoma
2017

EXPLORING FUTURE HYDROLOGIC EXTREMES OF THE RED RIVER BASIN

A THESIS APPROVED FOR THE
DEPARTMENT OF GEOGRAPHY AND ENVIRONMENTAL SUSTAINABILITY

BY

_____
Dr. Renee A. McPherson, Chair

_____
Dr. Hernan A. Moreno

_____
Dr. Mark Shafer

## Acknowledgements

I would like to express my deepest gratitude to my committee chair and advisor, Dr. Renee McPherson, for supporting me for two years, being a powerful and positive role model, and providing me with countless opportunities to grow as an early career professional. Without her, my thesis work would not be possible, and I sincerely appreciate her for the opportunity to work with this incredible dataset and for always challenging me. I was able to become a part of the office at the South Central Climate Science Center, which I will be forever grateful for. I thank each and every person there for allowing me to become a team member and for teaching and aiding me through my research hurdles.

Another important mentor and member of my thesis committee that I have had the pleasure to work with and grow from is Dr. Mark Shafer, who has been incredibly positive and encouraging. Without his financial support through the Southern Climate Impacts Planning Program, my thesis studies may not have been possible. Through my graduate research assistantship, I have gained invaluable research experience and had the opportunity to present my results to the scientific community at national conferences.

Furthermore, I would like to thank Dr. Hernan Moreno for being a valuable member of my thesis committee and sharing his ideas to make my project stronger. I am also appreciative to those in the Department of Geography and Environmental Sustainability for teaching me how valuable geography is in solving real-world problems. Finally, I thank my husband, friends, and family for their moral support and always encouraging me to reach for my goals.

# Table of Contents

Acknowledgements ..... iv

List of Tables ..... vii

List of Figures ..... viii

Abstract ..... xvii

Chapter 1: Introduction ..... 1

1. Global Climate Models ..... 2

2. Statistical Downscaling ..... 3

3. Dynamical Downscaling ..... 5

4. Impacts of Hydrologic Extremes ..... 7

5. References ..... 11

Chapter 2: Downscaled Climate Projections for the Red River Basin, South-Central U.S. ..... 17

1. Introduction ..... 17

2. Study Area ..... 19

3. Data ..... 21

3a. Introduction to the Dataset ..... 21

3b. Quantile Mapping Approaches ..... 24

3c. Cumulative Density Function Transform (CDFt) Method ..... 24

3d. Equi-Distant Quantile Mapping (EDQM) Method ..... 25

3e. Bias Correction Quantile Mapping (BCQM) Method ..... 27

4. Results ..... 27

4a. Changes in Precipitation and Temperature ..... 28

4b. Seasonal Changes in Precipitation ..... 33
5. Conclusions ..... 37
6. References ..... 38
Chapter 3: Future Hydrologic Extremes of the Red River Basin ..... 44
1. Introduction ..... 44
2. Study Area ..... 45
3. Methods and Data ..... 47
3a. Research Design ..... 47
3b. Data ..... 48
3c. Heavy Precipitation Definition ..... 49
3d. Severe Drought Definition ..... 51
4. Results ..... 55
4a. Heavy Precipitation ..... 55
4b. Severe Drought ..... 63
5. Conclusion/Discussion ..... 69
6. References ..... 72
Chapter 4: Conclusion ..... 82
1. Precipitation and Temperature ..... 82
2. Hydrologic Extremes ..... 83
3. References ..... 85
Appendix A: Complete List of Figures ..... 86
Appendix B: Survey Questions ..... 106

# List of Tables

Table 1. Ranges in the change between historical and future frequency of extreme precipitation events at the 90th and 99th percentile of the historical period under RCP 2.6 and RCP 8.5 scenarios for each model and statistical downscaling technique (SD); (a) 90th percentile, (b) 99th percentile ..... 58

Table 2. Ranges in the change between historical and future frequency of extreme/severe drought events under RCP 2.6 and RCP 8.5 scenarios for each model and statistical downscaling technique (SD) ..... 65

# List of Figures

Figure 2.1. Red River Basin..... 19

Figure 2.2. Performance assessment of the selected 3 GCMs (CCSM4, MIROC5, MPI-ESM-LR) based on North American (NA) and central North American (CNA) winter (DJF) and summer (JJA) bias in (a) precipitation and (b) temperature, (c) bias in the number of hot days and heavy precipitation days for the south-central U.S. (based on Sheffield et al. (2013)), and (d) Climate sensitivity (based on Forster et al. (2013) and personal communication with Dr. Derek Rosendahl). ..... 23

Figure 2.3. Difference fields for mean daily precipitation (in mm/day) between historical (1981-2005) and end-of-century (2075-2099) timeframes for RCP 8.5. Columns represent the GCMs (CCSM4, MIROC5, and MPI-ESM-LR, from left to right respectively); rows represent downscaling methods, with CDFt on top and EDQM on bottom. Brown and tan colors represent future decreases in precipitation compared to the historical period; blue-green colors represent future increases in precipitation. ..... 29

Figure 2.4. Difference fields for the CCSM4 mean daily precipitation (in mm/day) for the historical (1981-2005) timeframe. Darker shades of blue represent higher rainfall values. ..... 30

Figure 2.5. Difference fields for mean daily minimum temperature (°C) between historical (1981-2005) and end-of-century (2075-2099) timeframes for RCP 8.5. Columns represent the GCMs (CCSM4, MIROC5, and MPI-ESM-LR, from left to right respectively); rows represent downscaling methods, with CDFt on top and EDQM on bottom. Darker shades of red represent higher minimum temperature values. ..... 31

Figure 2.6. Difference fields for mean daily minimum temperature (°C) for the historical (1981-2005) timeframe for CCSM4. Dark shades of red represent higher minimum temperature values..... 32
Figure 2.7. Difference fields for mean daily maximum temperature (°C) between historical (1981-2005) and end-of-century (2075-2099) timeframes for RCP 8.5. Columns represent the GCMs (CCSM4, MIROC5, and MPI-ESM-LR, from left to right respectively); rows represent downscaling methods, with CDFt on top and EDQM on bottom. Darker shades of red represent higher maximum temperature values..... 32
Figure 2.8. Difference field in seasonal changes in mean daily precipitation (mm/day) between the historical (1981-2005) and mid-century (2046-2070) timeframes for RCP 2.6 using the (a) CDFt downscaling technique and (b) EDQM technique. Columns represent seasons (DJF, MAM, JJA, SON). Brown colors represent a decrease in daily precipitation and blues represent an increase..... 35
Figure 2.9. Difference fields in seasonal changes in mean daily precipitation (mm/day) between the historical (1981-2005) and end-of-century (2075-2099) timeframes for RCP 8.5 using the (a) CDFt downscaling technique and (b) EDQM technique. Columns represent seasons (DJF, MAM, JJA, SON). Brown colors represent a decrease in daily precipitation and blues represent an increase..... 36
Figure 3.1. Long-term annual precipitation history for the South Central climate division in Oklahoma (Oklahoma Climatological Survey 2017). ..... 55
Figure 3.2. Annual occurrence of 90th and 99th percentile events in the historical period for three locations in the Red River Basin. The red line represents results for Amarillo,

TX, the black line represents Ardmore, OK, and the blue line represents Shreveport, LA. ..... 56

Figure 3.3. Change in 25-year total frequency of all heavy rainfall days over 25 years at the 90th percentile between the historical period (1981-2005) and mid-century period (2046-2070) under a RCP 2.6 scenario. ..... 61

Figure 3.4. Change in 25-year total frequency of all heavy rainfall days over 25 years at the 90th percentile between the historical period (1981-2005) and end-of-century period (2075-2099) under a RCP 8.5 scenario. ..... 61

Figure 3.5. Change in 25-year total frequency of all heavy rainfall days over 25 years at the 99th percentile between the historical period (1981-2005) and mid-century period (2046-2070) under a RCP 2.6 scenario. ..... 62

Figure 3.6. Change in 25-year total frequency of all heavy rainfall days over 25 years at the 99th percentile between the historical period (1981-2005) and end-of-century period (2075-2099) under a RCP 8.5 scenario. ..... 62

Figure 3.7. Spatial representation of the historical drought frequency for the CCSM4 model ..... 64

Figure 3.8. Palmer Drought Severity Index of the southeast climate division of Arkansas for the historical period (NOAA 2017). ..... 64

Figure 3.9. Change in 25-year total frequency of severe drought at a 1-month timescale between the historical period (1981-2005) and mid-century period (2046-2070) under a RCP 2.6 scenario. Purple colors represent a decrease in events and oranges represent an increase. ..... 68

Figure 3.10. Change in 25-year total frequency of severe drought at a 1-month timescale between the historical period (1981-2005) and end-of-century period (2075-2099) under a RCP 8.5 scenario. Purple colors represent a decrease in events and oranges represent an increase. ..... 68
Figure A1. Difference fields for mean daily precipitation (in mm/day) between historical (1981-2005) and mid-century (2046-2070) timeframes for RCP 2.6. Columns represent the GCMs (CCSM4, MIROC5, and MPI-ESM-LR, from left to right respectively); rows represent downscaling methods, with CDFt on top and EDQM on bottom. Brown and tan colors represent future decreases in precipitation compared to the historical period; blue-green colors represent future increases in precipitation. …87
Figure A2. Difference fields for mean daily precipitation (in mm/day) between historical (1981-2005) and end-of-century (2075-2099) timeframes for RCP 2.6. Columns represent the GCMs (CCSM4, MIROC5, and MPI-ESM-LR, from left to right respectively); rows represent downscaling methods, with CDFt on top and EDQM on bottom. Brown and tan colors represent future decreases in precipitation compared to the historical period; blue-green colors represent future increases in precipitation. …..88
Figure A3. Difference fields for mean daily precipitation (in mm/day) between historical (1981-2005) and mid-century (2046-2070) timeframes for RCP 8.5. Columns represent the GCMs (CCSM4, MIROC5, and MPI-ESM-LR, from left to right respectively); rows represent downscaling methods, with CDFt on top and EDQM on bottom. Brown and tan colors represent future decreases in precipitation compared to the historical period; blue-green colors represent future increases in precipitation. …..89

Figure A4. Difference fields for mean daily precipitation (in mm/day) between historical (1981-2005) and end-of-century (2075-2099) timeframes for RCP 8.5. Columns represent the GCMs (CCSM4, MIROC5, and MPI-ESM-LR, from left to right respectively); rows represent downscaling methods, with CDFt on top and EDQM on bottom. Brown and tan colors represent future decreases in precipitation compared to the historical period; blue-green colors represent future increases in precipitation. …..90
Figure A5. Difference fields for mean daily minimum temperature (°C) between historical (1981-2005) and mid-century (2046-2070) timeframes for RCP 2.6. Columns represent the GCMs (CCSM4, MIROC5, and MPI-ESM-LR, from left to right respectively); rows represent downscaling methods, with CDFt on top and EDQM on bottom. Darker shades of red represent higher minimum temperature values. ……..91
Figure A6. Difference fields for mean daily minimum temperature (°C) between historical (1981-2005) and end-of-century (2075-2099) timeframes for RCP 2.6. Columns represent the GCMs (CCSM4, MIROC5, and MPI-ESM-LR, from left to right respectively); rows represent downscaling methods, with CDFt on top and EDQM on bottom. Darker shades of red represent higher minimum temperature values. ……..92
Figure A7. Difference fields for mean daily minimum temperature (°C) between historical (1981-2005) and mid-century (2046-2070) timeframes for RCP 8.5. Columns represent the GCMs (CCSM4, MIROC5, and MPI-ESM-LR, from left to right respectively); rows represent downscaling methods, with CDFt on top and EDQM on bottom. Darker shades of red represent higher minimum temperature values. …….93
Figure A8. Difference fields for mean daily minimum temperature (°C) between historical (1981-2005) and end-of-century (2075-2099) timeframes for RCP 8.5.

Columns represent the GCMs (CCSM4, MIROC5, and MPI-ESM-LR, from left to right respectively); rows represent downscaling methods, with CDFt on top and EDQM on bottom. Darker shades of red represent higher minimum temperature values. ……..94
Figure A9. Difference fields for mean daily maximum temperature (°C) between historical (1981-2005) and mid-century (2046-2070) timeframes for RCP 2.6. Columns represent the GCMs (CCSM4, MIROC5, and MPI-ESM-LR, from left to right respectively); rows represent downscaling methods, with CDFt on top and EDQM on bottom. Darker shades of red represent higher minimum temperature values. ……..95
Figure A10. Difference fields for mean daily maximum temperature (°C) between historical (1981-2005) and end-of-century (2075-2099) timeframes for RCP 2.6. Columns represent the GCMs (CCSM4, MIROC5, and MPI-ESM-LR, from left to right respectively); rows represent downscaling methods, with CDFt on top and EDQM on bottom. Darker shades of red represent higher minimum temperature values. ……..96
Figure A11. Difference fields for mean daily maximum temperature (°C) between historical (1981-2005) and mid-century (2046-2070) timeframes for RCP 8.5. Columns represent the GCMs (CCSM4, MIROC5, and MPI-ESM-LR, from left to right respectively); rows represent downscaling methods, with CDFt on top and EDQM on bottom. Darker shades of red represent higher minimum temperature values. ……..97
Figure A12. Difference fields for mean daily maximum temperature (°C) between historical (1981-2005) and end-of-century (2075-2099) timeframes for RCP 8.5. Columns represent the GCMs (CCSM4, MIROC5, and MPI-ESM-LR, from left to right respectively); rows represent downscaling methods, with CDFt on top and EDQM on bottom. Darker shades of red represent higher minimum temperature values. ……..98

Figure A13. Difference field in seasonal changes in mean daily precipitation (mm/day) between the historical (1981-2005) and mid-century (2046-2070) timeframes for RCP 2.6 using the (a) CDFt downscaling technique and (b) EDQM technique. Columns represent seasons (DJF, MAM, JJA, SON). Brown colors represent a decrease in daily precipitation and blues represent an increase. ……99
Figure A14. Difference field in seasonal changes in mean daily precipitation (mm/day) between the historical (1981-2005) and end-of-century (2075-2099) timeframes for RCP 2.6 using the (a) CDFt downscaling technique and (b) EDQM technique. Columns represent seasons (DJF, MAM, JJA, SON). Brown colors represent a decrease in daily precipitation and blues represent an increase. ……..100
Figure A15. Change in 25-year total frequency of all heavy rainfall days over 25 years at the 90$^{th}$ percentile between the historical period (1981-2005) and mid-century period (2046-2070) under a RCP 2.6 scenario. Orange colors represent a decrease in events and blue/greens represent an increase. …….101
Figure A16. Change in 25-year total frequency of all heavy rainfall days over 25 years at the 90$^{th}$ percentile between the historical period (1981-2005) and end-of-century period (2075-2099) under a RCP 2.6 scenario. Orange colors represent a decrease in events and blue/greens represent an increase. ……..101
Figure A17. Change in 25-year total frequency of all heavy rainfall days over 25 years at the 90$^{th}$ percentile between the historical period (1981-2005) and mid-century period (2046-2070) under a RCP 8.5 scenario. Orange colors represent a decrease in events and blue/greens represent an increase. …….102

Figure A18. Change in 25-year total frequency of all heavy rainfall days over 25 years at the 90th percentile between the historical period (1981-2005) and end-of-century period (2075-2099) under a RCP 8.5 scenario. Orange colors represent a decrease in events and blue/greens represent an increase. ……..102
Figure A19. Change in 25-year total frequency of all heavy rainfall days over 25 years at the 99th percentile between the historical period (1981-2005) and mid-century period (2046-2070) under a RCP 2.6 scenario. Orange colors represent a decrease in events and blue/greens represent an increase. …….103
Figure A20. Change in 25-year total frequency of all heavy rainfall days over 25 years at the 99th percentile between the historical period (1981-2005) and end-of-century period (2075-2099) under a RCP 2.6 scenario. Orange colors represent a decrease in events and blue/greens represent an increase. ……..103
Figure A21. Change in 25-year total frequency of all heavy rainfall days over 25 years at the 99th percentile between the historical period (1981-2005) and mid-century period (2046-2070) under a RCP 8.5 scenario. Orange colors represent a decrease in events and blue/greens represent an increase. …….104
Figure A22. Change in 25-year total frequency of all heavy rainfall days over 25 years at the 99th percentile between the historical period (1981-2005) and end-of-century period (2075-2099) under a RCP 8.5 scenario. Orange colors represent a decrease in events and blue/greens represent an increase. ……..104
Figure A23. Change in 25-year total frequency of severe drought at a 1-month timescale between the historical period (1981-2005) and mid-century period (2046-2070) under a

RCP 2.6 scenario. Purple colors represent a decrease in events and oranges represent an increase. ……105
Figure A24. Change in 25-year total frequency of severe drought at a 1-month timescale between the historical period (1981-2005) and end-of-century period (2075-2099) under a RCP 2.6 scenario. Purple colors represent a decrease in events and oranges represent an increase. ……...105
Figure A25. Change in 25-year total frequency of severe drought at a 1-month timescale between the historical period (1981-2005) and mid-century period (2046-2070) under a RCP 8.5 scenario. Purple colors represent a decrease in events and oranges represent an increase. ……106
Figure A26. Change in 25-year total frequency of severe drought at a 1-month timescale between the historical period (1981-2005) and end-of-century period (2075-2099) under a RCP 8.5 scenario. Purple colors represent a decrease in events and oranges represent an increase. ……...106

# Abstract

Hydrologic extremes of drought and flooding stress water resources and damage communities in the Red River Basin, located in the south-central U.S. For example, the summer of 2011 was the third driest summer in Oklahoma state history and the driest in Texas state history. These states suffered great loss from prolonged drought conditions, with D4 (exceptional drought) conditions affecting almost the entire state of Texas and nearly seventy percent of Oklahoma. When the long-term drought conditions finally ended in the spring of 2015 as El Niño brought record amounts of precipitation to the region, there were also catastrophic floods that caused loss of life and property. Hydrologic extremes, such as these, have occurred throughout the historical record; however, decision makers need to know how the frequency of these events is expected to vary in a changing climate so that they can mitigate for these impacts and losses. Therefore, the goals of this study focus on how these hydrologic extremes impact water resources in the Red River Basin, how the frequency of such events is expected to change in the future, and how this study can aid local water resource managers and decision makers. To accomplish these goals, this study uses statistically downscaled climate projections of daily minimum and maximum temperature and daily precipitation. These projections were used to first detect the mean daily changes in temperature and precipitation through the end of the century, and then to identify the future trends in heavy precipitation events at the historical $90^{th}$ and $99^{th}$ percentiles and severe drought events at a threshold of the Standardized Precipitation Evapotranspiration Index's value of less than or equal to -1.5.

# Chapter 1: Introduction

Hydrologic extremes are phenomena that negatively impact communities and water resources in the Red River Basin, located in the south-central United States. In the basin's history, heavy precipitation and severe events have created multiple billion-dollar disasters. For example, the most extreme U.S. Drought Monitor category of D4 (exceptional drought) occurred in 2011 across most of Texas and nearly 70% of Oklahoma. Oklahoma experienced its third driest summer and Texas faced its driest summer since records began in 1895 (Crouch 2015). Both states tied for the highest mean temperature recorded in the U.S. in July, adding further stress to the already-dry conditions. Oklahoma and Texas suffered significant losses, and $2 billion in agricultural damages accumulated between 2011 and 2012 (Wertz 2012).

This drought prolonged for nearly 5 years and abruptly ended in May of 2015 as El Niño conditions brought heavy downpours, breaking many precipitation records. Conditions changed from widespread drought to extreme flooding very quickly, causing more harm and loss of life. This extreme rainfall event created an additional $2.6 billion in damages (NOAA 2016). While this was a long-lasting event, Durant, OK received a daily rainfall value of 2 inches and Newport, OK received as much as 10.5 inches on June 18, 2015 (OCS 2015).

Hydrologic extremes of drought and rainfall have impacted the Red River Basin throughout the historical record; however, decision makers need to know how the frequency of these events may alter in a changing climate so they can mitigate future losses. Therefore, this research has assessed how hydrologic extremes impact water resources in the Red River Basin, how the frequency of these events is expected to

change in the future, and how the results of this study can aid local water resource managers and decision makers.

## 1. Global Climate Models

In order to answer the research question and the goals of this work, this study uses a dataset of statistically downscaled climate projections that apply empirical relationships between a predictor, or large-scale climate variable, and a predictand, or local-scale surface variable (Wilby et al. 2004). These high-resolution projections capture local and detailed information that is more useful to decision makers, researchers, and resource managers than coarse-resolution global climate models (GCMs; Maurer et al. 2014, Thrasher et al. 2013).

GCMs are models that numerically represent Earth's atmospheric and oceanic processes by projecting climate variables, such as temperature and precipitation, for various representative concentration pathways (RCPs; IPCC 2013). RCPs are trajectories that provide information about the future anthropogenic causes of increased radiative forcings, including changing concentrations of greenhouse gas emissions (Moss et al. 2010). For example, RCP 2.6 represents a future scenario with a peak in radiative forcing at 3.1 $W/m^2$ and a greenhouse gas concentration of 490 parts per million (ppm) that is reached in 2100, followed by a decrease; RCP 8.5 exhibits a radiative forcing of 8.5 $W/m^2$ and increasing greenhouse gas emissions of 1,370 ppm by 2100.

While GCMs present a large picture of the climate system, community planning and decision making requires a higher resolution output with local information. GCMs typically have a spatial resolution of several hundred kilometers (IPCC 2013, UCAR

2011, Semenov and Barrow 1997, Prudhomme et al. 2002, Feser et al. 2011), which lacks details in topography, mountain meteorology processes, local convection, and land-sea interactions (Feser et al. 2011, Schmidli et al. 2006, Eden et al. 2012). In addition, each GCM has its own inherent bias. Downscaled climate projections correct some of these biases and limitations while providing decision makers and resource managers with information at a resolution that allows them to make more informed decisions about their area (Wilby et al. 2004).

## 2. Statistical Downscaling

There are two approaches to performing a downscaled climate projection: statistical and dynamical. Statistical downscaling computes the relationships between large-scale climate variables, or predictors, and small-scale surface variables, or predictands (Wilby et al. 2004). Because this approach includes empirical data, it is applied only in regions with sufficient data, thus it tends to be limited in its geographic scope. For example, there is a lack of data over oceans, less inhabited areas, and poor nations that cannot afford the necessary monitoring equipment (Lupo and Kininmonth 2013). However, statistical downscaling is computationally inexpensive, causing it to be a popular downscaling approach (Salameh et al. 2008). Statistical downscaling has been used in a variety of studies, such as research in synoptic climatology, numerical weather prediction, and climate change studies (Giorgi et al. 2001), and understanding the relationships between predictors and predictands can provide information about the performance and biases of the model (Goodess et al. 2007).

Methods for statistical downscaling include weather typing, regression models, and weather generators, described in detail in Wilby et al. (2004). Weather typing

classifies data into weather "types" based on synoptic, or large-scale, weather patterns. In this method, the predictand is assigned to the predominant weather type and then simulated with new climate conditions through a regression analysis (Wilby et al. 2004). For example, Cheng et al. (2010) used weather typing to simulate daily rainfall events in Ontario, Canada by identifying the synoptic patterns that were associated with these rainfall events and using regression methods.

Another technique for statistical downscaling is the use of regression models, which determine the presence of a linear or nonlinear relationship between a predictor and predictand. The relationship between a predictor and predictand is also called a transfer function (Giorgi et al. 2001). An example of a regression model can be found in Huth (1999), where three multiple regression models and a canonical correlation analysis were used to determine how well their statistical downscaling model simulated daily mean temperatures in central Europe. They were able to make generalizations of the conditions; however, there were uncertainties in whether or not their results applied to other seasons outside of their study and other geographic regions.

The last mentioned technique of statistical downscaling is the use of a weather generator, which is a model that simulates daily weather conditions through simple statistics, such as means, variances, and covariances (Wilks and Wilby 1999). Fowler et al. (2007) explained that weather generators can determine daily precipitation by training the model variables with specific climate statistics, such as precipitation frequency, rather than weather patterns.

Statistical downscaling has many advantages and disadvantages. This approach is versatile, can aid a wide community of users because it is computationally

inexpensive, and can provide point values for extremes (Goodess et al. 2007). A drawback is related to the importance of choosing the correct predictor and predictand, in addition to the statistical technique (Wilby et al. 2004), as there are many decisions that must be carefully made to reach the best outcome. Whether or not statistical downscaling is appropriate is dependent on the study area, since it is not applicable for areas without a sufficient data record (Giorgi et al. 2001). Additionally, statistical downscaling includes the assumption that the relationship between the predictor and predictand will not change under future conditions; however, there is no guarantee that the same atmospheric processes as present day will remain stationary in the future (Goodess et al. 2007, Hewitson and Crane 2006).

## 3. Dynamical Downscaling

The second approach to downscaling is dynamical downscaling, which is much more complex and computationally expensive, often requiring the use of supercomputers. This method uses output from a GCM as an input to a regional climate model (RCM; Schmidli et al. 2006), or, in other words, the fine-resolution RCM is nested into the coarse-resolution GCM (Kitoh et al. 2016). Like statistical downscaling, climate scientists have various techniques for implementing dynamical downscaling as well. For example, spectral nudging is a technique that recognizes that small-scale features, like topography and land-sea distribution, and large-scale processes both affect regional-scale climate model data (von Storch et al. 2000). Rather than having constant boundary conditions as a synoptic feature propagates, spectral nudging forces external conditions to influence local processes in the smaller-scale model (Waldron et al. 1996). Others have built off of the concept of spectral nudging for climate change studies, such

as von Storch et al. (2000), who concludes that spectral nudging can be advantageous when there is a need for regional climate statistics, such as for climate change and historical climate reconstruction applications.

Castro et al. (2005) proposed four types of dynamical downscaling methods: (1) uses numerical weather prediction (NWP), (2) neglects initial conditions but results take into account the lateral boundary conditions, with a horizontal grid spacing of 20-50 km (Wilby et al. 2002) from a NWP GCM, (3) has lateral boundary conditions from a GCM with forced surface conditions, and (4) uses lateral boundary conditions from a coupled earth system GCM with interacting elements. Rockel et al. (2008) applied the second type of simulation with spectral nudging in order to assess the value of the second technique from Castro et al. (2005), concluding that the dynamical downscaling technique adds value to small-scale characteristics and the values remain close to observations. However, they stated that if there is a large bias in the GCM, then dynamical downscaling is not beneficial.

An advantage of dynamical downscaling is the ability to represent physical and mesoscale processes better than course-resolution GCMs due to the high spatial resolution and reduction of GCM biases (Murphy 1999). This attribute is also an advantage over statistical downscaling since the latter uses statistical relationships rather than representing the physics behind the processes. High-resolution details, including topography and coastlines, add value to the model and take local processes and convective precipitation into account (Kitoh et al. 2016). Furthermore, this method can be used in areas where there are not long data records (Kitoh et al. 2016). The key disadvantage of this approach is the amount of computational power required, which

only allows the user to simulate a small time period of a few ensembles (Goodess et al. 2007).

Taking these points into consideration, statistical downscaling was the best technique for this study. It allowed us to project multiple climate variables for different timeframes and RCP scenarios in order to estimate changes in the future frequency of heavy rainfall and severe drought for the Red River Basin. Chapter 2 presents the details of the statistically downscaled dataset used for our analysis.

## 4. Impacts of Hydrologic Extremes

According to the Intergovernmental Panel on Climate Change (IPCC) and the National Climate Assessment, many regions of the world, including the United States, are likely to experience a higher frequency of drought conditions and heavy rainfall events in the future. As temperatures rise in the future, there is more evapotranspiration at the surface which affects drought further by creating a moisture deficit (Venkataraman et al. 2016). The IPCC's Fifth Assessment Report declared that drought is likely to increase by the end of the 21$^{st}$ century in some regions (IPCC 2014). Downscaled climate projections created for the National Climate Assessment indicated that drought conditions in 2071-2099 are expected to become more severe by at least 30%, compared to 1970-1999, in the northwest U.S. during the summer while the southwest U.S. will likely experience more drought in spring months under a high emission scenario (Walsh et al. 2014).

Furthermore, in the Great Plains, especially southern portions, an increase in the number of consecutive dry days is estimated to occur (Shafer et al. 2014). Drought affects many sectors, such as energy, agriculture, and water resources, and an increase

in these events only stresses these sectors further. In addition, heavy precipitation events are also expected to increase by the end of the 21st century in the Southern Plains (Shafer et al. 2014). Heavy rainfall events have increased during the last several decades in this region and are expected to continue (Walsh et al. 2014). Christian et al. (2015) also discovered that wet years are increasingly following drought years in the Southern Plains. Therefore, it is important to understand how these events impact our study area.

On the large scale, the Red River Basin region is expected to have a drier and warmer climate with intermittent heavy rainfall events, which are dangerous under these conditions because soils are too dry to absorb enough rainfall to prevent flooding (UCAR 2010). These periods of flash flooding are a hazard to human health, as raw sewage and other toxic chemicals often contaminate the water supply (Lee 2015, Taylor et al. 2011). Heavy rainfall also causes a large economic impact from inundated streets and structures and may require structures to be updated sooner than previously planned (National Research Council 2011). On the other hand, drought stresses the water system by reducing the amount of surface water supply and increasing the water demand, which affects the agricultural and energy industries, as well as public water supply (Shafer et al. 2014). For example, a precipitation deficiency leads to reduced ground water recharge, soil water content, and inflow to water bodies (Wilhite 2000).

Some of these impacts have affected stakeholders in the Red River Basin as well. A short (10-minute), online survey was sent to various stakeholders who work and make decisions in the Red River Basin, such as natural resource managers, engineers, and energy producers. The goal of this survey was to seek information about the

impacts of heavy rainfall and drought events across the Red River Basin and the actions that jurisdictions take during these events. For heavy rainfall, impacts listed were inundated buildings and streets, decreased water quality, damage to infrastructure, and substantial negative economic impacts. During these events, the participants' jurisdictions have provided safety resources to their population and participated in outreach. Drought impacts included a reduction in groundwater levels, decreased water quality and quantity, reduced lake levels for energy production, and lower survival rates of species in the basin. The actions described were outreach to stakeholders, water conservation, drought committee meetings, and water storage. This valuable information aided the understanding of the impacts of these extreme events and how an increase in the future frequency of these events may affect communities. The full list of survey questions is located in Appendix B.

In conclusion, our study sought to identify impacts of hydrologic extremes, determine the change in future frequency of these events, and aid water resource managers and decision makers in mitigating for future impacts by providing a high-resolution analysis that offers localized results. Chapter 2 of this manuscript provides detailed information about the dataset of statistically downscaled climate projections and the study region, along with an analysis of mean daily changes in future temperature and precipitation across the basin. Chapter 2 will be submitted for publication to the *Journal of Applied Meteorology and Climatology*, which is a journal of the American Meteorological Society. An analysis of future heavy rainfall and severe drought events in the Red River Basin is then presented in Chapter 3. This chapter will

be submitted to the *Weather and Climate Extremes* journal, which is an Elsevier journal. Chapter 4 then summarizes the study and provides overall conclusions.

## 5. References


Castro, C. L., R. A. Pielke, and G. Leoncini, 2005: Dynamical downscaling: assessment of value retained and added using the Regional Atmospheric Modeling System (RAMS). *Journal of Geophysical Research: Atmospheres*, **110,** 2156-2202.

Cheng, C. S., G. Li, Q. Li, and H. Auld, 2010: A synoptic weather typing approach to simulate daily rainfall and extremes in Ontario, Canada: potential for climate change projections. *Journal of Applied Meteorology and Climatology*, **49,** 845-866.

Christian, J., K. Christian and J.B. Basara, 2016: Drought and pluvial dipole events within the Great Plains of the United States. *Journal of Applied Metr. And Clim*, **54,** 1886-1898.

Crouch, J., 2015: Reflections on a really big drought. NOAA, Accessed 15 March 2016. [Available online at https://www.climate.gov/news-features/blogs/beyond-data/reflections-really-big-drought.]

Eden, J. M., M. Widmann, D. Grawe, and S. Rast, 2012: Skill, correction, and downscaling of GCM-simulated precipitation. *Journal of Climate*, **25,** 3970-3984.

Feser, F., B. Rockel, H. von Storch, J. Winterfeldt, and M. Zahn, 2011: Regional climate models add value to global model data: a review and selected examples. *Bulletin of the American Meteorological Society*, **92,** 1181.

Fowler, H., S. Blenkinsop, and C. Tebaldi, 2007: Linking climate change modelling to impacts studies: recent advances in downscaling techniques for hydrological modelling. *International Journal of Climatology*, **27,** 1547-1578.

Giorgi, F., B. Hewitson, J. Christensen, M. Hulme, and H. von Storch, 2001: Regional climate information - evaluation and projections. *Climate Change 2001: The Scientific Bases*, Cambridge University Press, 583-638.

Goodess, C. M., and Coauthors, 2007: An intercomparison of statistical downscaling methods for Europe and European regions–assessing their performance with respect to extreme temperature and precipitation events. *Climatic Change*.

Hewitson, B. C., and R. G. Crane, 2006: Consensus between GCM climate change projections with empirical downscaling: precipitation downscaling over South Africa. *International Journal of Climatology*, **26,** 1315-1337.

Huth, R., 1999: Statistical downscaling in central Europe: evaluation of methods and potential predictors. *Climate Research*, **13,** 91-101.

IPCC, 2013: What is a GCM? Accessed 12 July 2016. [Available online at http://www.ipcc-data.org/guidelines/pages/gcm_guide.html.]

IPCC, 2014: Climate Change 2014: Synthesis Report. Contribution of Working Groups I, II and III to the Fifth Assessment Report of the Intergovernmental Panel on Climate Change [Core Writing Team, R.K. Pachauri and L.A. Meyer (eds.)]. IPCC, Geneva, Switzerland, 151 pp.

Kitoh, A., T. Ose, and I. Takayabu, 2016: Dynamical downscaling for climate projection with high-resolution MRI AGCM-RCM. *Journal of the Meteorological Society of Japan. Ser. II*, **94A,** 1-16.

Lee, J., 2015: Texas, Oklahoma floodwaters contain sewage, other pollutants. National

Geographic, Accessed 15 Nov. 2016. [Available online at http://news.nationalgeographic.com/2015/05/150528-floodwater-chemicals-texas-oklahoma-environment-science-runoff/.]

Lupo, A., and W. Kininmonth, 2013: Global climate models and their limitations. *Climate Change Reconsidered II: Physical Science*, C.D. Idso, R.M. Carter and S.F. Singer, Eds., The Heartland Institute, 7-148.

Maurer, E. P., and Coauthors, 2014: An enhanced archive facilitating climate impacts and adaptation analysis. *Bulletin of the American Meteorological Society*, **95,** 1011-1019.

Moss, R. H., and Coauthors, 2010: The next generation of scenarios for climate change research and assessment. *Nature*, **463,** 747-756.

Murphy, J., 1999: An evaluation of statistical and dynamical techniques for downscaling local climate. *Journal of Climate*, **12,** 2256-2284.

National Research Council, 2011: *Global change and extreme hydrology: testing conventional wisdom*. Washington, DC: The National Academies Press. doi:https://doi.org/10.17226/13211.

NOAA National Centers for Environmental Information, 2016: U.S. billion-dollar weather and climate disasters. Accessed 13 Oct. 2016. [Available online at https://www.ncdc.noaa.gov/billions/.]

Oklahoma Climatological Survey, 2015: Oklahoma Monthly Climate Summary June 2015. Accessed 10 Aug. 2017. [Available online at climate.ok.gov/summaries/monthly/2015/MCS_June_2015.pdf.]

Prudhomme, C., N. Reynard, and S. Crooks, 2002: Downscaling of global climate

models for flood frequency analysis: where are we now? *Hydrological Processes*, **16**, 1137-1150.

Rockel, B., C.L. Castro, R.A. Pielke, H. von Storch, and G. Leoncini, 2008: Dynamical downscaling: assessment of model system dependent retained and added variability for two different regional climate models. *Journal of Geophysical Research: Atmospheres*, **113,** 2156-2202.

Salameh, T., P. Drobinski, M. Vrac, and P. Naveau, 2008: Statistical downscaling of near-surface wind over complex terrain in southern France. *Meteorology and Atmospheric Physics*, **103,** 253-265.

Schmidli, J., C. Frei, and P.L. Vidale, 2006: Downscaling from GCM precipitation: a benchmark for dynamical and statistical downscaling methods. *International Journal of Climatology*, **26,** 679-689.

Semenov, M. A., and E. M. Barrow, 1997: Use of a stochastic weather generator in the development of climate change scenarios. *Climatic Change*, **35**, 397-414.

Shafer, M., D. Ojima, J. M. Antle, D. Kluck, R. A. McPherson, S. Petersen, B. Scanlon, and K. Sherman, 2014: Ch. 19: Great Plains. *Climate Change Impacts in the United States: The Third National Climate Assessment*, J. M. Melillo, Terese (T.C.) Richmond, and G. W. Yohe, Eds., U.S. Global Change Research Program, 441-461. doi:10.7930/J0D798BC.

Taylor, J., K. man Lai, M. Davies, D. Clifton, I. Ridley, and P. Biddulph, 2011: Flood management: prediction of microbial contamination in large-scale floods in urban environments. *Environment International*, **37,** 1019-1029.

Thrasher, B., J. Xiong, W. Wang, F. Melton, A. Michaelis, and R. Nemani, 2013:

Downscaled climate projections suitable for resource managers. *EOS, Trans. AGU*, **94,** 321-323.

UCAR, 2010: Flash flood early warning system reference guide. UCAR, ISBN 978-0-615-37421-5.

UCAR, 2011: Climate Modeling. Accessed 10 July 2016. [Available online at http://scied.ucar.edu/longcontent/climate-modeling.]

Venkataraman, K., S. Tummuri, A. Medina, and J. Perry, 2016: 21st century drought outlook for major climate divisions of Texas based on CMIP5 multimodel ensemble: Implications for water resource management. *Journal of Hydrology*, **534,** 300-316.

von Storch, H., H. Langenberg, and F. Feser, 2000: A spectral nudging technique for dynamical downscaling purposes. *Monthly Weather Review*, **128,** 3664-3673.

Waldron, K. M., J. Paegle, and J. D. Horel, 1996: Sensitivity of a spectrally filtered and nudged limited-area model to outer model options. *Monthly Weather Review*, **124,** 529.

Walsh, J., and Coauthors, 2014: Our Changing Climate. *Climate Change Impacts in the United States: The Third National Climate Assessment*, T. C. R. J.M. Melillo, and G.W. Yohe, Ed., U.S. Global Change Research Program, 19-67.

Wertz, J., 2012: The cost of Oklahoma's drought: $2 Billion in two years. NPR State Impact, Accessed 24 Jul. 2017. [Available online at https://stateimpact.npr.org/oklahoma/2012/12/04/the-cost-of-oklahomas-drought-2-billion-in-two-years/.]

Wilby, R. L., C. W. Dawson, and E. M. Barrow, 2002: SDSM — a decision support

tool for the assessment of regional climate change impacts. *Environmental Modelling & Software*, **17,** 145-157.

Wilby, R. L., S. P. Charles, E. Zorita, B. Timbal, P. Whetton, and L. O. Mearns, 2004: Guidelines for use of climate scenarios developed from statistical downscaling methods. Data Distribution Centre of the Intergovernmental Panel on Climate Change.

Wilhite, D. A., 2000: Drought as a natural hazard: concepts and definitions. *Drought: A Global Assessment*, Routledge.

Wilks, D. S., and R. L. Wilby, 1999: The weather generation game: a review of stochastic weather models. *Progress in Physical Geography*, **23,** 329-357.

# Chapter 2: Downscaled Climate Projections for the Red River Basin, South-Central U.S.

## 1. Introduction

As the global climate changes, numerical projections from climate models provide information that aids resource managers, policy makers, and researchers in planning for the future (Maurer et al. 2014, Thrasher et al. 2013). While water resource managers and decision makers can view global climate models (GCMs) for basic information, the associated low spatial-resolution output lacks the local information that they need to plan for their community (Thrasher et al. 2013). Therefore, high-resolution climate projections that are either model-generated in high resolution (less common) or are downscaled to high resolution (more common) are more useful to these local managers. In the Red River Basin, located in the south-central U.S., this detailed climate information helps those who make long-term (e.g., 50 years) water plans. This study discusses the creation of a downscaled dataset that includes historical and future projections of daily minimum and maximum temperature and daily precipitation that stakeholders in the Red River Basin can use to make more informed decisions.

GCMs are numerical models that represent atmospheric and oceanic processes (IPCC 2013) and can offer a large-scale view of future climate conditions, such as projected temperature and precipitation, under different representative concentration pathways (RCPs). The RCPs serve as scenarios of various radiative forcing trajectories from anthropogenic greenhouse gas emissions and changes in land cover (Moss et al. 2010). Moss et al. (2010) discussed the four RCPs — RCP 2.6, RCP 4.5, RCP 6.0, and RCP 8.5 — where RCP 2.6 represents a scenario where radiative forcing peaks at 3.1

$W/m^2$ and the concentration of greenhouse gases reaches 490 parts per million in 2100 then decreases and RCP 8.5 represents a scenario with more than 8.5 $W/m^2$ of radiative forcing and a concentration of greenhouse gases that exceeds 1,370 parts per million by 2100.

Although GCMs provide an overall depiction of possible future conditions, they do not take local processes into account, having a coarse-resolution range of 50 kilometers to several hundred kilometers depending on the model, but 250- to 600-kilometer resolution is the most common (IPCC 2013, UCAR 2011, Semenov and Barrow 1997, Prudhomme et al. 2002, Feser et al. 2011). These local processes can include mountain meteorology and land-sea interactions (Feser et al. 2011). Other GCM limitations include biases in rainfall intensity, response to climate forcing, natural variability, and simulated precipitation with a shortfall in convection and across mountainous areas (Schmidli et al. 2006, Eden et al. 2012). Downscaling can correct some of these GCM biases (Schmidli et al. 2006) and provide greater detail, with higher-resolution data that allow local decision makers and resource managers to make more informed decisions about their area and to understand local phenomena to a higher degree (Wilby et al. 2004).

Thrasher et al. (2013) provided an example of the significance of downscaled climate projections to resource managers and decision makers. The spatial resolution of the projections offered enough detail to determine the changes in the freezing line in mountainous regions, relating to the amount of melting snowpack that affects the water supply. Resource managers also can learn about how their area may be affected by drought, causing them to change their community's water plans and usage of the water

supply (Venkataraman et al. 2016). In addition, knowing how their region's climate is expected to change may alter food production areas, causing alteration in land use (Zhang and Zhang 2016), especially where crops are rainfed. Downscaled climate projections provide more localized information than GCMs through high-resolution data for applications by decision makers and can help them to create better drought and water resource management strategies (Nam et al. 2015).

## 2. Study Area

This study focuses on the Red River Basin of the South (hereafter Red River Basin), with headwaters in far eastern New Mexico (Figure 2.1), flowing west to east through Texas, Oklahoma, and Arkansas, and exiting into the Mississippi River in Louisiana. The basin covers 239,361 $km^2$ and crosses a west-to-east gradient of precipitation with average yearly rainfall totals of approximately 500 to 1300 millimeters (20 to 50 inches). Because of this moisture gradient, the Red River Basin is home to many different ecoregions, from the High Plains in the west to the South Central Plains in the east (U.S. EPA 2013).

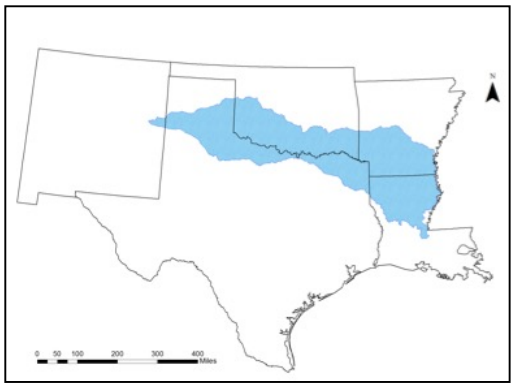

**Figure 2.1. Red River Basin**

This basin is vital for the area's drinking water supply and recreational and cultural activities (Xue et al. 2015). However, because the basin benefits multiple states and metropolitan cities, such as Fort Worth, TX, and Oklahoma City, OK, there have been disagreements regarding water rights in this basin. Oklahoma, Texas, Arkansas, and Louisiana signed a water compact in 1978 to share the water resource fairly

(OWRB 2016); however, because Texas had been routinely exceeding its allotment of water, the Oklahoma Legislature restricted the state's apportioned water to remain within state boundaries in 2002, excluding Texas from any option to buy water from Oklahoma (Malewitz 2013). This new statute, Title 82-1B, upset decision makers in Texas because Tarrant County, including Fort Worth, previously bought water from Oklahoma. The issue eventually rose to a legal case that was brought before the U.S. Supreme Court — *Tarrant Regional Water District vs. Hermann* (2013) — that wished to declare Oklahoma's new law as unconstitutional under interstate commerce laws. The case was dismissed, however, allowing Oklahoma to determine how to use its apportioned water.

Similarly, in 2016, a water rights issue between the City of Oklahoma City and both the Choctaw Nation of Oklahoma and Chickasaw Nation was resolved. This dispute arose in 2011, during a period of extreme drought in Oklahoma and Texas, when officials in Oklahoma City purchased rights to water in Sardis Lake, a reservoir in southeast Oklahoma that is within tribal boundaries of the Choctaw Nation. Both tribes had views of water rights that conflicted with those of Oklahoma City, but all governments came to an agreement that allowed the State of Oklahoma to manage the water supply while ensuring that the Tribes continued to have a voice in water resource and conservation issues for the region. These disagreements are important examples of the extremes that communities under pressure from water stress will undertake to gain or maintain their rights to water. With drought ravaging the U.S. Southern Plains in the current decade, states have been forced to look for new water resources or reduce water

use. Therefore, precipitation, temperature, and streamflow projections have become of important interest to water planners in the basin.

## 3. Data

### *3a. Introduction to the Dataset*

This study employs an ensemble of statistically downscaled, high-resolution climate projections that were created by the Geophysical Fluid Dynamics Laboratory of the National Oceanic and Atmospheric Administration and disseminated by the South Central Climate Science Center of the U.S. Geological Survey. One purpose of the ensemble was to examine the representativeness of the dataset to aid water resource managers in the Red River Basin with their long-term water plans. The dataset was generated by statistically downscaling output from three representative GCMs using empirical relationships between a predictor, or large-scale climate variable, and a predictand, or local-scale surface variable, by diverse techniques (Giorgi et al. 2001). Appropriate transfer functions, described below, were used to link the predictor and the predictand. Statistical downscaling was a better option for this study, compared to dynamical downscaling, because it allowed us to create projections for multiple models and scenarios without being as computationally demanding and expensive.

Downscaled daily surface maximum and minimum temperatures and daily precipitation were projected for historical and future periods using over 3600 grid points throughout the region. The historical projections were trained from an observational dataset from Livneh et al. (2013) that originally included daily minimum and maximum temperature and daily precipitation data from 1915-2011 with a 0.16-degree resolution. From these data, a timeframe of January 1$^{st}$, 1961 to December 31$^{st}$, 2005 was selected

and the data were interpolated to 0.1°. The downscaled projections included a timeframe of 1961-2005 for the historical period and 2006-2099 for the future period, seeking results for the end of the 21st century.

To force the projections on the large scale, three GCMs were chosen from the Coupled Model Intercomparison Project Phase 5 (CMIP5; Taylor et al. 2012): the low-resolution version of the Max Planck Institute's Earth System Model (MPI-ESM-LR; Giorgetta et al. 2013), the Community Climate System Model (CCSM4; Gent et al. 2011), and the fifth version of the Model for Interdisciplinary Research on Climate (MIROC5; Watanabe et al. 2010). The CCSM4 model has a resolution of 0.9° by 1.3° and couples the atmosphere, ocean, land surface, and sea ice, and the sixth realization was used for this study, which spans from 1850 to 2005. For the MPI-ESM-LR model with a 1.9-degree resolution, the r1 realization was used, which has a timeframe from 1880 through 2005; future simulations included natural forcings but excluded volcanic aerosols after 2005. The r1 realization was used for the MIROC5 model with a resolution of 1.4°. In addition, the first version of the perturbed physics model was used for all models.

These models were selected based on their historical performance from the evaluation of Sheffield et al. (2013) which included consideration of model biases in seasonal temperature and precipitation in central North America and the frequency of hot days and heavy rainfall days in the south-central U.S. Additionally, the climate sensitivity of the models was included in the overall selection process (Forster et al. 2013). These final three GCMs selected have relatively smaller biases compared to the full suite of CMIP5 models and represent a portion of the models' uncertainties,

generally spanning the range of one standard deviation above and below the ensemble mean. For example, CCSM4 falls on the mean and MIROC5 and MPI-ESM-LR are on each end of the inner 50% of model sensitivities (Figure 2.2).

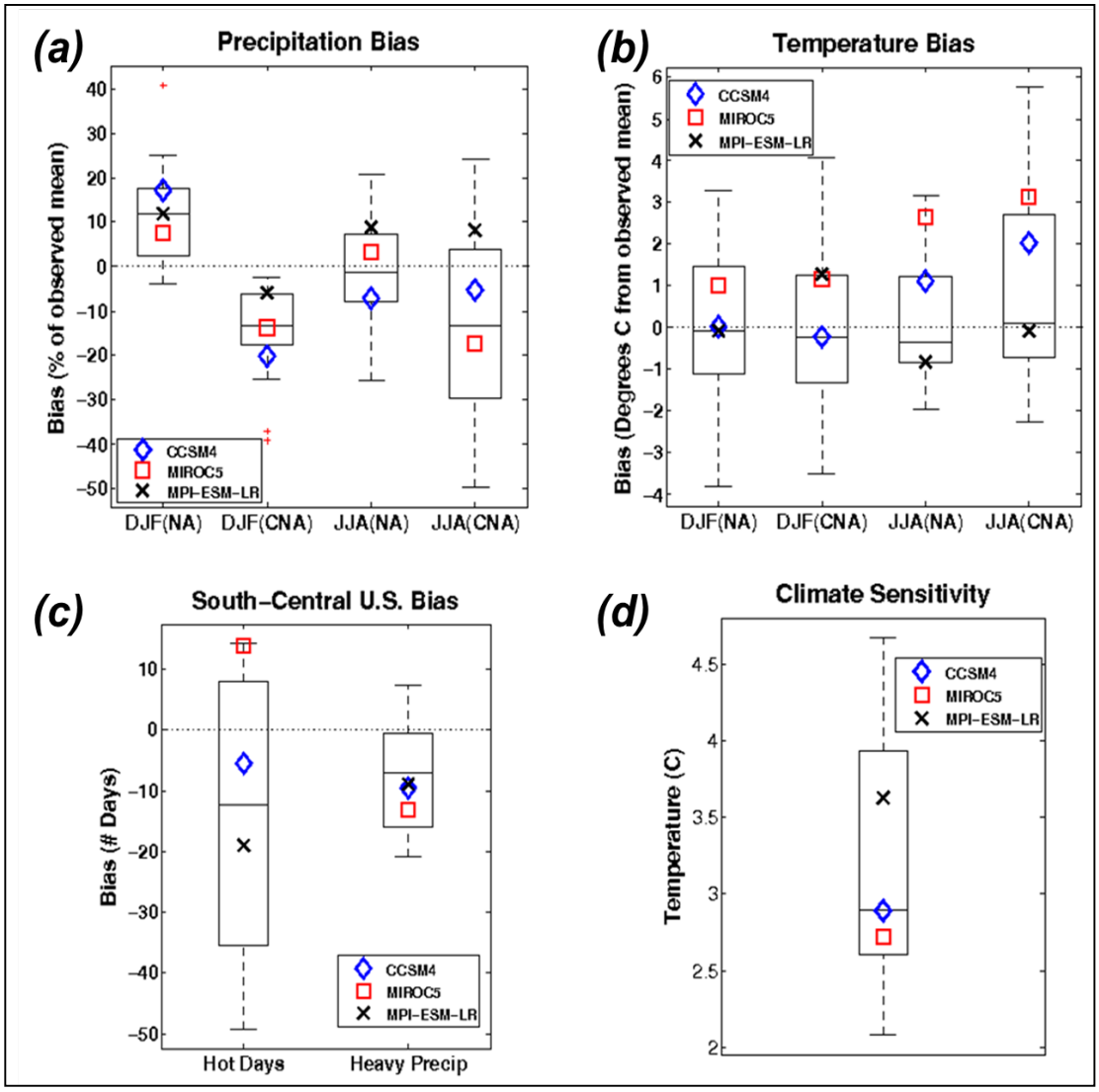


**Figure 2.2. Performance assessment of the selected 3 GCMs (CCSM4, MIROC5, MPI-ESM-LR) based on North American (NA) and central North American (CNA) winter (DJF) and summer (JJA) bias in (a) precipitation and (b) temperature, (c) bias in the number of hot days and heavy precipitation days for the south-central U.S. (based on Sheffield et al. (2013)), and (d) Climate sensitivity (based on Forster et al. (2013) and personal communication with Dr. Derek Rosendahl).**

### *3b. Quantile Mapping Approaches*

After model selection, we selected three of the four available RCP scenarios (RCP 2.6, RCP 4.5, and RCP 8.5) because they represent the full range of existing scenarios. Using these for each of the three GCMs, we implemented quantile mapping techniques to downscale the output, also reducing biases in the large-scale climate models during post-processing (Themeßl et al. 2011). For example, all three chosen models have been shown to underestimate precipitation in the winter, and two of the models overestimate temperature in the summer for the central North America region (Fig. 2.2, Sheffield et al. 2013). In this case, quantile mapping helped to correct these biases in the probability distributions of the GCMs and were tested to find the sensitivity of the projections. Quantile mapping incudes a stationarity assumption, meaning that biases and patterns that occur in the historical period are assumed to also occur in the future period (Cannon et al. 2015, Mauran 2012, Milly et al. 2008). In addition, for precipitation downscaling, we used a threshold of 0.127 mm to classify rainfall days, while dry days were defined as those days with precipitation amounts falling below the threshold.

### *3c. Cumulative Density Function Transform (CDFt) Method*

We selected the downscaling techniques of Cumulative Density Function Transform (CDFt; Michelangeli et al. 2009), Equi-Distant Quantile Mapping (EDQM; Li et al. 2010, Cannon et al. 2015), and Bias Correction Quantile Mapping (BCQM; Ho et al. 2012). The CDFt downscaling technique uses a transfer function, shown in Equation 2.1 (Li et al. 2010), to identify the quantitative relationship between the

modeled historical and the observed cumulative distribution functions and uses the same relationship to generate the future cumulative distribution function (Pierce et al.

$$\hat{x}_{m,p}(t) = F^{-1}{}_{o,h}\left(F_{m,h}\left(x_{m,p}\right)\right) \quad \text{Eq. 2.1}$$

2015). Subscripts represent observed (o), historical (h), modeled (m), and predicted (p) data, $x_{m,p}$ is the modeled climate variable that is being predicted, and $\hat{x}_{m,p}$ is the bias corrected climate variable. This equation improves the tail behavior of the projections by keeping the distribution within the bounds of the observed data, and the technique preserves the initial GCM means in the downscaled output by transforming the mean of the GCMs to match the historical observed means.

The two parameters used by CDFt are *dev*, the coefficient of development, which is the difference between the historical and future GCM mean and is used to extend the range for quantiles to be calculated, and *npas*, the number of quantiles that are being estimated. For this study, *dev*=1 and *npas*=100, the default. Pierce et al. (2015) analyzed the CDFt method and their results revealed that this method generally produces lower precipitation estimates across the U.S. However, in the Red River Basin region, their findings indicated a wet bias across a large part of the region, especially during the summer. Daily maximum temperature was underestimated in their end-of-century projections for much of the basin in the summer as well.

### *3d. Equi-Distant Quantile Mapping (EDQM) Method*

The second method we used was EDQM and the downscaling was performed through the transfer functions in Equation 2.2 (Cannon et al. 2015) and 2.3 (Li et al. 2010). The modeled mean for the historical and predicted period is represented by $\bar{x}_{m,h}$ and $\bar{x}_{m,p}(t)$ (Cannon et al. 2015). A ratio approach (Eq. 2.2) for EDQM versus an

additive approach (Eq. 2.3) for precipitation eliminates the possibility of negative precipitation values occurring after bias correction, which generally arises when a

$$\hat{x}_{m,p}(t) = F^{-1}_{o,h}\left\{F_{m,h}\left[\frac{\bar{x}_{m,h}x_{m,p}(t)}{\bar{x}_{m,p}(t)}\right]\right\}\frac{\bar{x}_{m,p}(t)}{\bar{x}_{m,h}} \quad \text{Eq. 2.2}$$

$$\hat{x}_{m,p}(t) = x_{m,p} + F^{-1}_{o,h}\left(F_{m,p}\left(x_{m,p}\right)\right) - F^{-1}_{m,h}\left(F_{m,p}\left(x_{m,p}\right)\right) \quad \text{Eq. 2.3}$$

model has a wet bias and projects a decrease in precipitation (Wang and Chen 2014). Therefore, both methods were applied in the calculation of EDQM, with a ratio approach being implemented for precipitation and an additive approach for temperature.

EDQM assumes that the historical model error will persist in the future, and the technique bias corrects future temperature values by adding the historical bias value to the modeled change in that estimate at a given quantile across the gridpoints (Pierce et al. 2015). This method also upholds the modeled median change in the future. Pierce et al. (2015) projected very wet and dry regions to have a higher error; however, in the Red River Basin region, their estimates showed an underestimation of precipitation in the winter with a smaller mean error of 0 to -1 degrees Celsius and an overestimation in the summer with mean error of 0 to 0.5 degrees Celsius.

Quantile mapping methods do not require a temporal structure, or sequence, that represents the historical record; however, the resulting downscaled projections are used for hydrologic impacts studies, applying the Variable Infiltration Capacity model (Liang et al. 1994) for rainfall runoff and input to the RiverWare (Zagona et al. 2001; Xue et al. 2016) water management tool. Thus, it was essential to link the daily variability of the GCM and downscaled output from both techniques to create temporal consistency by creating an algorithm to reorganize the downscaled output to improve the correlation of

the projections with the coarse-resolution GCM time-sequenced values. Once this process was complete, the downscaled data were quality controlled.

### *3e. Bias Correction Quantile Mapping (BCQM) Method*

It is worth noting that we intended to use the BCQM method (Ho et al. 2012) as a third downscaling technique; however, there were substantive issues found with this method. BCQM uses the transfer equation in Eq. 2.1, but it only includes historical observations for data training and disregards information from future projections (Cannon et al. 2015). This technique can alter the trends of the GCMs after bias correction substantially, which affects precipitation analyses and skews the data distribution (Maurer and Pierce 2014). The tail distribution becomes skewed when the model projects values that fall outside of the historical range used for training. When the variance is overestimated in the historical period, the mean and quantiles also are overestimated after bias correction, and vice versa for underestimation (Cannon et al. 2015). Therefore, the BCQM technique was not used for this study and cannot be recommended to decision makers in the Red River Basin at this time.

## 4. Results

The resulting dataset of statistically downscaled climate projections for the Red River Basin is publically available in NetCDF format. The data include daily minimum and maximum temperatures (in degrees Kelvin) and daily precipitation (in $kg/m^2s$) from the described three GCMs and two downscaling techniques for the historical time period (1961-2005) and future period (2006-2099). There are 72 statistically downscaled projections created at a resolution of 0.1°, or approximately 11 kilometers latitude by 9 kilometers longitude, including 18 projections for the historical period and

54 projections for the future period. The gridded observational dataset (Livneh et al. 2013) used as the downscaling training dataset is also available for validation purposes.

Many analyses can be executed from these data. For example, in Section 4a, we provide an analysis for the difference in mean daily values between the most recent 25 years in the historical period (1981-2005) and two 25-year segments of the future period (2046-2070 and 2075-2099) under RCP 2.6 and RCP 8.5 scenarios. We then computed the mean daily changes of precipitation for each season, which we discuss in Section 4b.

### *4a. Changes in Precipitation and Temperature*

Our first example of an analysis that can be conducted from these data include a simple calculation of the projected changes in mean daily precipitation and daily minimum and maximum temperature between the historical and future timeframes. We converted temperature to degrees Celsius and precipitation to millimeters per day. Overall, we determined that the models generally project an increasing precipitation trend in eastern portions of the Red River Basin and a decreasing trend in the west for both downscaling techniques, especially during the end-of-century period under RCP 8.5 (Fig. 2.3). Under the CDFt technique, the CCSM4 and MPI-ESM-LR models estimate mean daily precipitation to decrease in the west up to 0.5 mm/day and increase in the east by up to 0.7 mm/day (Figure 2.3). In the historical period, 4-5 mm/day of mean daily precipitation occurred in the east, which indicates a 15% increase by the end of the 21$^{st}$ century (Fig. 2.4). In the west, historical mean daily precipitation ranged from 1-3 mm/day, which is a 15% decrease in the future.

The EDQM technique yielded a smaller range in precipitation differences, spanning from a 0.5-mm/day decrease to a 0.4-mm/day increase but exhibited the same spatial patterns as CDFt. On the other hand, the MIROC5 simulations demonstrated a basin-wide increase in precipitation for all RCPs and timeframes with the exception of the end-of-century scenario with RCP 8.5, where a basin-wide decrease was projected from both downscaling techniques. Sillmann et al. (2013) found that the MIROC5 model projects the highest precipitation totals among the CMIP5 models, which may explain the model's generally higher estimates. The differing results between models represent uncertainties in the models, downscaling methods, emission scenarios, and natural variability (Knutti and Sedláček 2013).

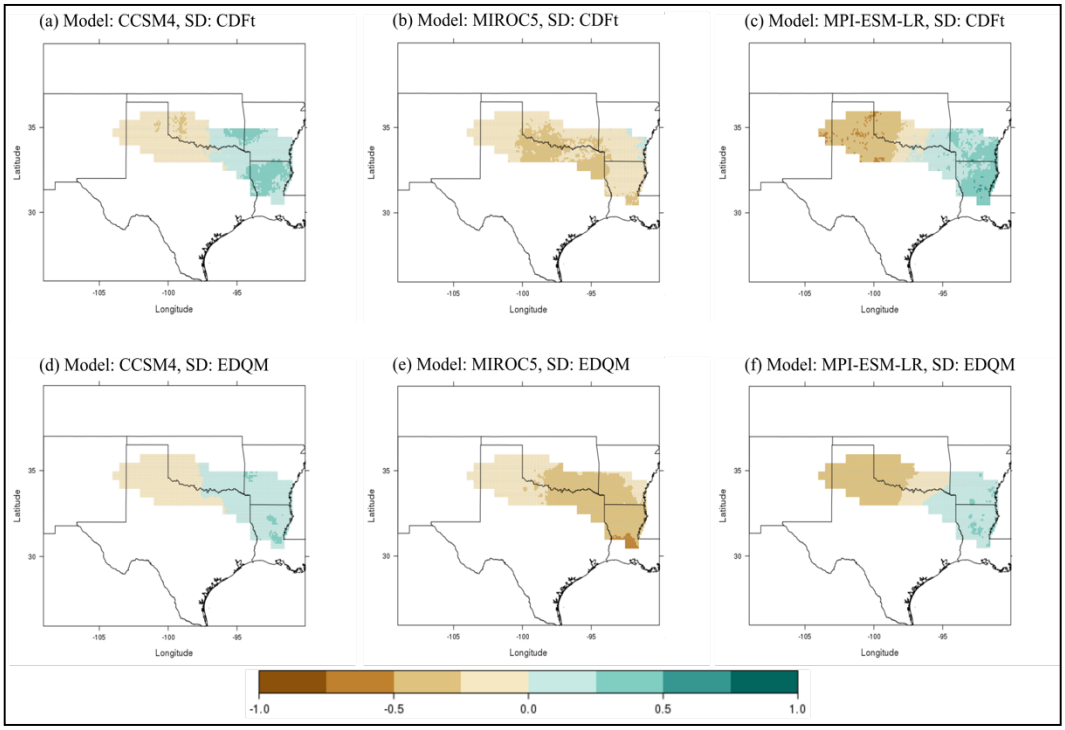


**Figure 2.3. Difference fields for mean daily precipitation (in mm/day) between historical (1981-2005) and end-of-century (2075-2099) timeframes for RCP 8.5. Columns represent the GCMs (CCSM4, MIROC5, and MPI-ESM-LR, from left to right respectively); rows represent downscaling methods, with CDFt on top and EDQM on bottom. Brown and tan colors represent future decreases in precipitation compared to the historical period; blue-green colors represent future increases in precipitation.**

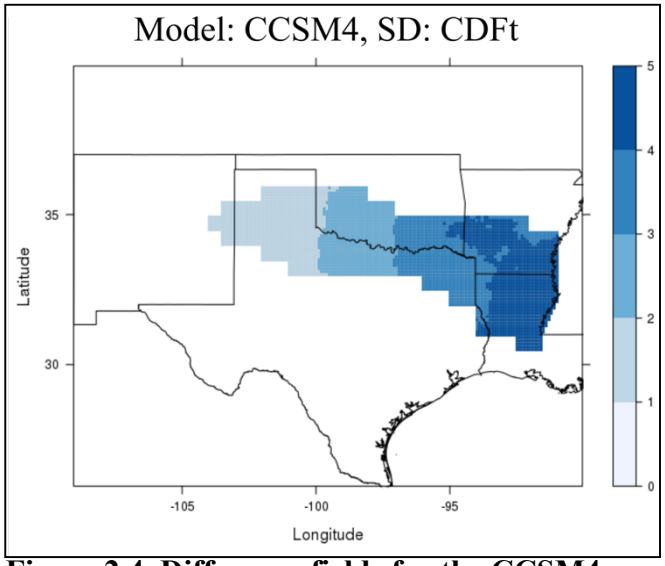


**Figure 2.4. Difference fields for the CCSM4 mean daily precipitation (in mm/day) for the historical (1981-2005) timeframe. Darker shades of blue represent higher rainfall values.**

Projections for mean daily minimum temperature differed greatly between RCP 2.6 and RCP 8.5 scenarios. In a lower emission scenario, mean minimum daily temperatures increased up to 2°C for both timeframes, while estimates in the higher emission scenario increased by as much as 6.6°C by the end of the century (Fig. 2.5) compared to the historical value of approximately 10°C (Fig. 2.6). Mean daily maximum temperature is similar, and each projection revealed a basin-wide increase with no decreases in either minimum or maximum temperature (Fig. 2.7).

The largest warming was projected to occur in the end-of-century time period of 2075-2099 under the RCP 8.5 scenario for all models and downscaling methods. Although, MIROC5 exhibited warmer mean temperatures in the future time periods, with values being 1°C higher than the other two models. This difference can be explained by the warm bias in MIROC5 temperatures, shown in Figure 2b and described in Sheffield et al. (2013). Sheffield also estimated a warm bias in MPI-ESM-

LR for the central North America region. The CDFt and EDQM results were nearly equivalent in regard to temperature variables.

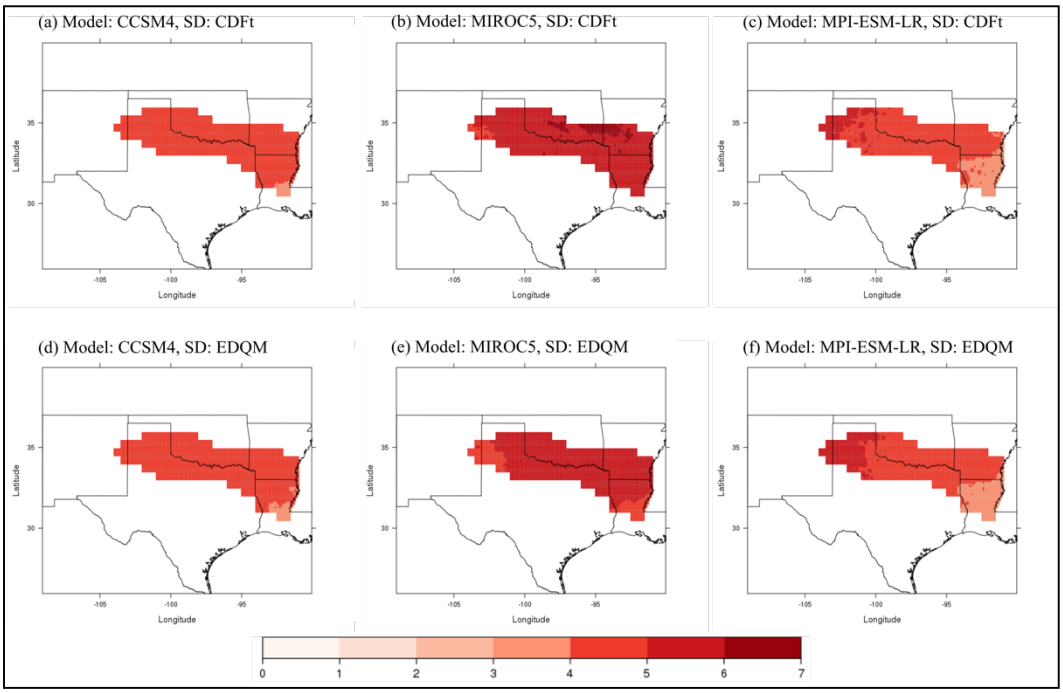


**Figure 2.5. Difference fields for mean daily minimum temperature (°C) between historical (1981-2005) and end-of-century (2075-2099) timeframes for RCP 8.5. Columns represent the GCMs (CCSM4, MIROC5, and MPI-ESM-LR, from left to right respectively); rows represent downscaling methods, with CDFt on top and EDQM on bottom. Darker shades of red represent higher minimum temperature values.**

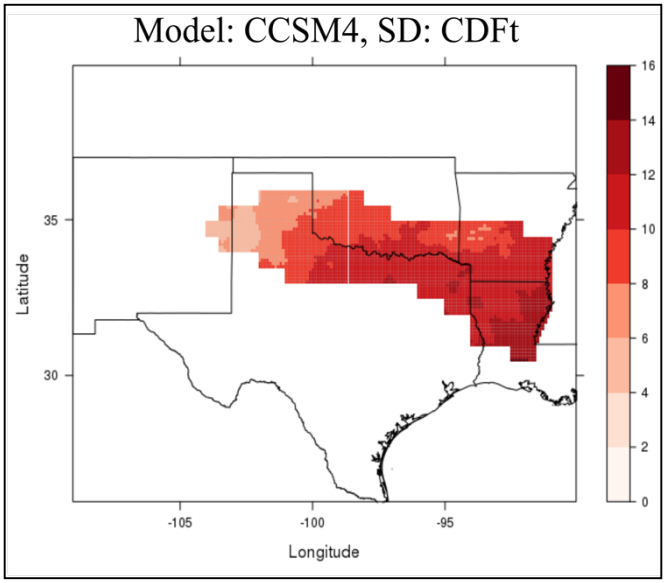


**Figure 2.6. Difference fields for mean daily minimum temperature (°C) for the historical (1981-2005) timeframe for CCSM4. Dark shades of red represent higher minimum temperature values.**

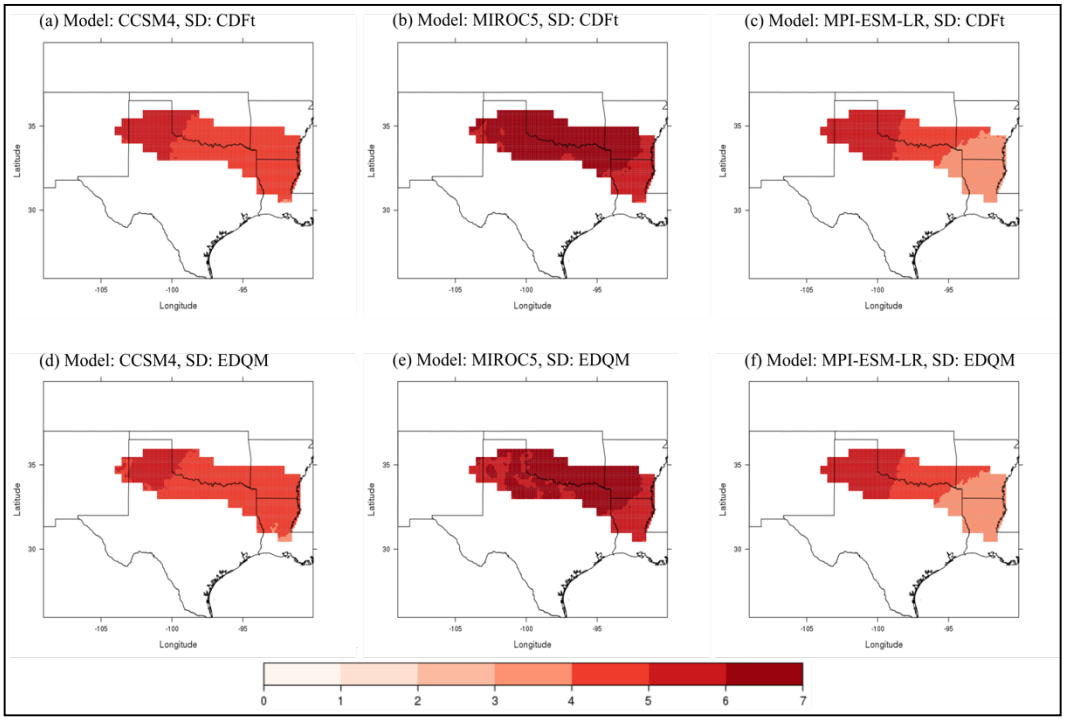


**Figure 2.7. Difference fields for mean daily maximum temperature (°C) between historical (1981-2005) and end-of-century (2075-2099) timeframes for RCP 8.5. Columns represent the GCMs (CCSM4, MIROC5, and MPI-ESM-LR, from left to right respectively); rows represent downscaling methods, with CDFt on top and EDQM on bottom. Darker shades of red represent higher maximum temperature values.**

### *4b. Seasonal Changes in Precipitation*

To better understand the changes seen in Section 4a, we computed the mean daily precipitation differences between the historical and future periods for each climatological season, categorized as December through February (DJF), March through May (MAM), June through August (JJA), and September through November (SON). Because modeled precipitation is more variable than temperature, we chose to only analyze the seasonal precipitation changes. Model projections indicated that the two downscaling techniques yielded similar results and spatial patterns.

In the mid-century period, the models generally projected a change of 0.5 mm/day from the historical value; however, there were distinct patterns in some models. For example, the CCSM4 model exhibited the largest changes in mean daily precipitation. This model estimated the mean daily precipitation to increase by 2 mm/day in the MAM timeframe, compared to less than 0.5 mm/day in the other models (Fig. 2.8). This substantial amount revealed a 40% increase compared to historical values. Furthermore, the model projected a basin-wide decrease in the JJA timeframe with some locations having a reduction of 0.85 mm/day, while the other two models included a large-scale increase in mean daily precipitation. This result shows that the CCSM4 model projects more extreme values during the spring and balances its annual average by a widespread reduction during the summer in the mid-century period. Qiao et al. (2017) analyzed seasonal precipitation in the Red River Basin and used the same dataset as our study for the mid-century timeframe. Their results showed that the highest increases in precipitation occur in the spring and largest decreases were in the fall for the mid-century period. In addition, they discovered that precipitation amounts

in the upper quantiles are driving the precipitation totals in spring, which may validate that CCSM4 projects more extreme events in spring. Their results are consistent with ours.

On the other hand, larger changes were seen in the end-of-century period under RCP 8.5. We noticed the same previous patterns for the CCSM4 model, but the largest changes emerged in the MPI-ESM-LR model (Fig. 2.9). For example, mean daily precipitation in the DJF period increased by 1.68 mm in the eastern basin, which is more than 30% greater than the historical value. Precipitation increased in the JJA period as well, along with a decrease of 1.3 mm/day in the Texas Panhandle. Furthermore, this model projected the largest MAM decreases. Meanwhile, the MIROC5 model included small changes throughout most of the year. Precipitation uncertainties are evident by the end of the 21$^{st}$ century and two of the three models show that extreme values are likely driving the seasonal trends.

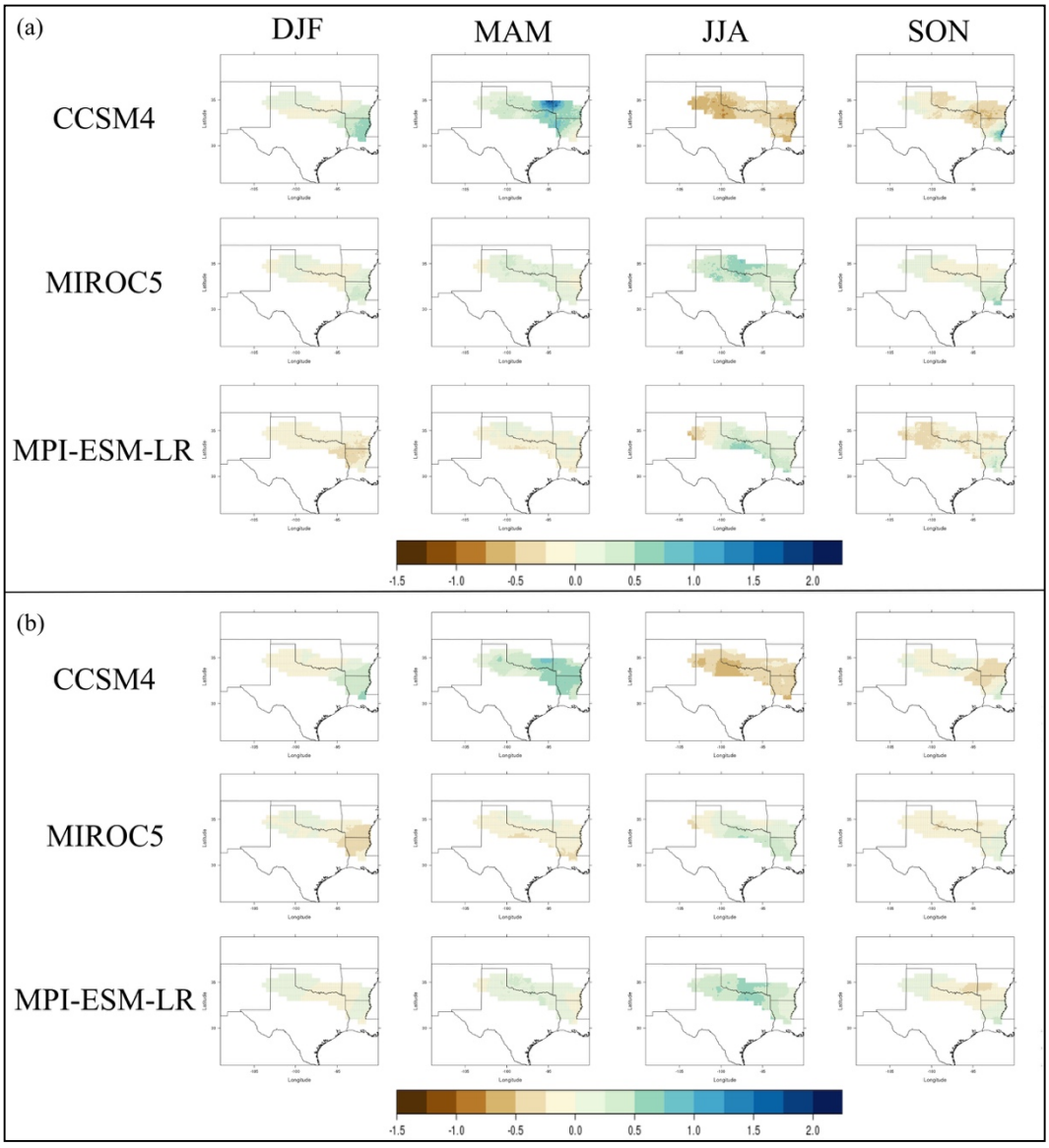


**Figure 2.8. Difference field in seasonal changes in mean daily precipitation (mm/day) between the historical (1981-2005) and mid-century (2046-2070) timeframes for RCP 2.6 using the (a) CDFt downscaling technique and (b) EDQM technique. Columns represent seasons (DJF, MAM, JJA, SON). Brown colors represent a decrease in daily precipitation and blues represent an increase.**

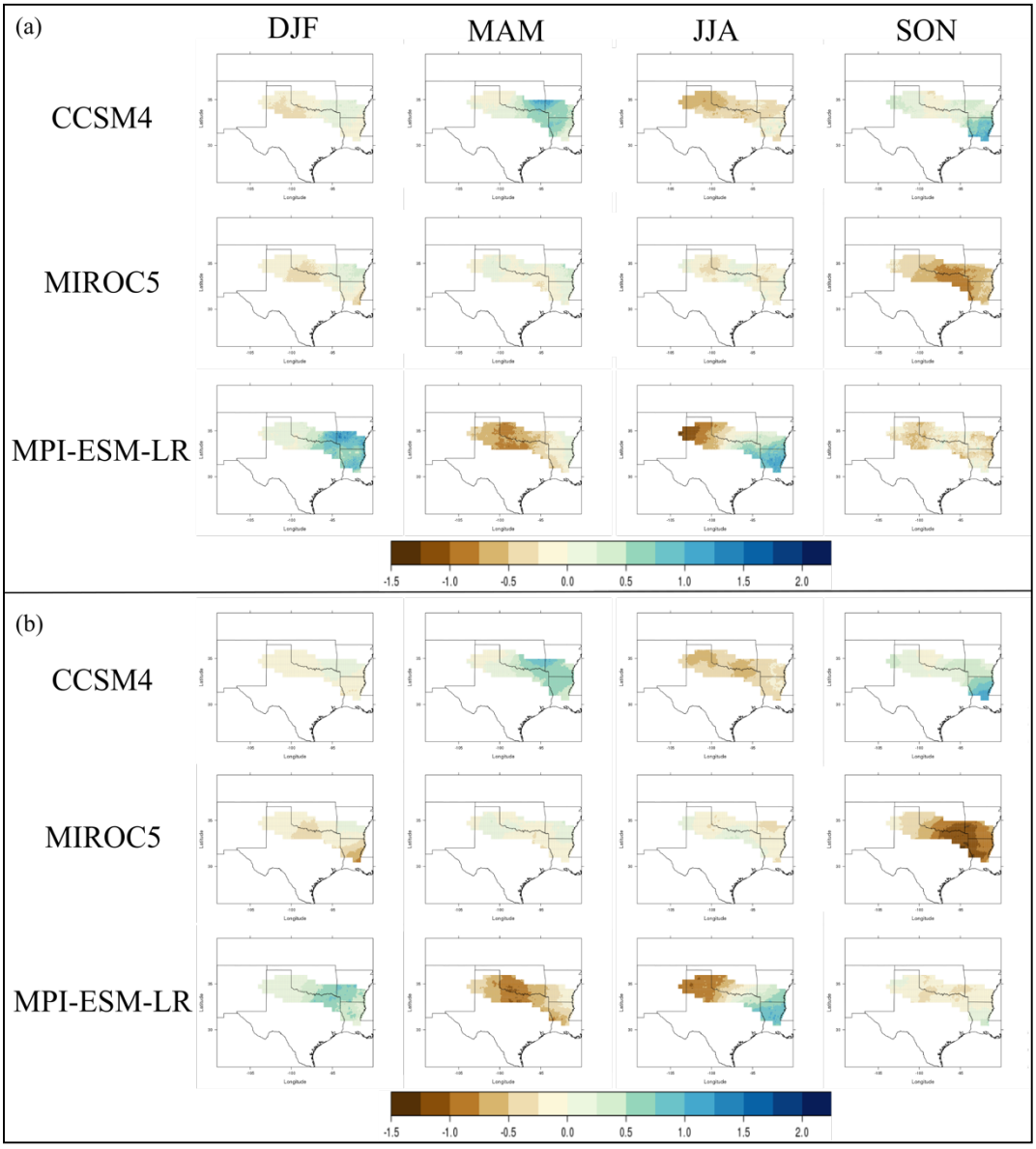


**Figure 2.9. Difference fields in seasonal changes in mean daily precipitation (mm/day) between the historical (1981-2005) and end-of-century (2075-2099) timeframes for RCP 8.5 using the (a) CDFt downscaling technique and (b) EDQM technique. Columns represent seasons (DJF, MAM, JJA, SON). Brown colors represent a decrease in daily precipitation and blues represent an increase.**

## 5. Conclusions

Statistically downscaled climate projections provide high-resolution output that is more useful to water managers, decision makers, and researchers than coarse-resolution global climate models. This study introduced a dataset that includes downscaling from three GCMs (CCSM4, MPI-ESM-LR, and MIROC5) using two statistical downscaling techniques (CDFt and EDQM) at a resolution of 0.1° for the Red River Basin. The dataset contains a historical time period (1961-2005) and a future period (2006-2099) and projects daily minimum and maximum temperature and daily precipitation through the end of the 21$^{st}$ century.

While there are uncertainties in the models, downscaling techniques, and future emissions, results of the mean daily differences between historical and future climate variables indicate a decrease in mean daily precipitation in western portions of the basin and an increase in the east by the end of the century. Our seasonal analysis indicates that extreme values in some seasons may be driving the trends in mean daily precipitation, especially in the end-of-century period under RCP 8.5. In addition, daily minimum and maximum temperatures were projected to increase across the basin by up to 7°C, especially toward the end of the century and under a higher emission scenario. Results suggest that water resource managers and decision makers may need to plan for drier and hotter conditions in the western Red River Basin and wetter and hotter conditions in the east. This analysis explores one possibility of the use of this dataset; however, it can be beneficial for many other studies regarding climatological and hydrological aspects in the region.

## 6. References


Cannon, A. J., S. R. Sobie, and T. Q. Murdock, 2015: Bias correction of GCM precipitation by quantile mapping: how well do methods preserve changes in quantiles and extremes? *Journal of Climate*, **28,** 6938-6959.

Eden, J. M., M. Widmann, D. Grawe, and S. Rast, 2012: Skill, correction, and downscaling of GCM-simulated precipitation. *Journal of Climate*, **25,** 3970-3984.

Feser, F., B. Rockel, H. von Storch, J. Winterfeldt, and M. Zahn, 2011: Regional climate models add value to global model data: a review and selected examples. *Bulletin of the American Meteorological Society*, **92,** 1181.

Forster, P. M., T. Andrews, P. Good, J. M. Gregory, L. S. Jackson, and M. Zelinka, 2013: Evaluating adjusted forcing and model spread for historical and future scenarios in the CMIP5 generation of climate models. *Journal of Geophysical Research: Atmospheres*, **118,** 1139-1150.

Gent, P. R., and Coauthors, 2011: The community climate system model version 4. *Journal of Climate*, **24,** 4973-4991.

Giorgetta, M. A., and Coauthors, 2013: Climate and carbon cycle changes from 1850 to 2100 in MPI-ESM simulations for the Coupled Model Intercomparison Project phase 5. *Journal of Advances in Modeling Earth Systems*, **5,** 572-597.

Giorgi, F., B. Hewitson, J. Christensen, M. Hulme, and H. von Storch, 2001: Regional climate information - evaluation and projections. *Climate Change 2001: The Scientific Bases*, Cambridge University Press, 583-638.

Ho, C. K., D. B. Stephenson, M. Collins, C. A. Ferro, and S. J. Brown, 2012:

Calibration strategies: a source of additional uncertainty in climate change projections. *Bulletin of the American Meteorological Society*, **93,** 21-26.

IPCC, 2013: What is a GCM? Accessed 12 July 2016. [Available online at http://www.ipcc-data.org/guidelines/pages/gcm_guide.html.]

Knutti, R., and J. Sedláček, 2013: Robustness and uncertainties in the new CMIP5 climate model projections. *Nature Climate Change*, **3,** 369-373.

Li, H., J. Sheffield, and E. F. Wood, 2010: Bias correction of monthly precipitation and temperature fields from Intergovernmental Panel on Climate Change AR4 models using equidistant quantile matching. *Journal of Geophysical Research: Atmospheres*, **115**.

Liang, X., D. P. Lettenmaier, E. F. Wood, and S. J. Burges, 1994: A simple hydrologically based model of land surface water and energy fluxes for general circulation models. *Journal of Geophysical Research: Atmospheres*, **99,** 14415-14428.

Livneh, B., E. A. Rosenberg, C. Lin, B. Nijssen, V. Mishra, K. M. Andreadis, E. P. Maurer, and D. P. Lettenmaler, 2013: A long-term hydrologically based dataset of land surface fluxes and states for the conterminous United States: Update and extensions. *Journal of Climate*, **26,** 9384-9392.

Malewitz, J., 2013: Red river showdown: Texas-Oklahoma water war could reverberate across US. *McClatchy - Tribune Business News*, Tribune Content Agency LLC.

Maraun, D., 2012: Nonstationarities of regional climate model biases in European seasonal mean temperature and precipitation sums. *Geophysical Research*

*Letters*, **39**.

Maurer, E.P., and Coauthors, 2014: An enhanced archive facilitating climate impacts and adaptation analysis. *Bulletin of the American Meteorological Society*, **95**, 1011-1019.

Maurer, E. P., and D. W. Pierce, 2014: Bias correction can modify climate model simulated precipitation changes without adverse effect on the ensemble mean. *Hydrol. Earth Syst. Sci.*, **18,** 915-925.

Michelangeli, P. A., M. Vrac, and H. Loukos, 2009: Probabilistic downscaling approaches: application to wind cumulative distribution functions. *Geophysical Research Letters*, **36**.

Milly, P. C. D., J. Betancourt, M. Falkenmark, R. M. Hirsch, Z. W. Kundzewicz, D. P. Lettenmaier, and R. J. Stouffer, 2008: Stationarity is dead: whither water management? *Science*, **319,** 573.

Moss, R. H., and Coauthors, 2010: The next generation of scenarios for climate change research and assessment. *Nature*, **463,** 747-756.

Nam, W.-H., M. J. Hayes, M. D. Svoboda, T. Tadesse, and D. A. Wilhite, 2015: Drought hazard assessment in the context of climate change for South Korea. *Agricultural Water Management*, **160,** 106-117.

Oklahoma Water Resources Board, 2016: Red river compact commission. [Available online at https://www.owrb.ok.gov/rrccommission/rrccommission.html.]

Pierce, D. W., D. R. Cayan, E. P. Maurer, J. T. Abatzoglou, and K. C. Hegewisch, 2015: Improved bias correction techniques for hydrological simulations of climate change. *Journal of Hydrometeorology*, **16,** 2421-2442.

Prudhomme, C., N. Reynard, and S. Crooks, 2002: Downscaling of global climate models for flood frequency analysis: where are we now? *Hydrological Processes*, **16**, 1137-1150.

Qiao, L., C. B. Zou, C. F. Gaitán, Y. Hong, and R. A. McPherson, 2017: Analysis of precipitation projections over the climate gradient of the Arkansas Red River Basin. *Journal of Applied Meteorology and Climatology*, **56,** 1325-1336.

Schmidli, J., C. Frei, and P.L. Vidale, 2006: Downscaling from GCM Precipitation: A benchmark for dynamical and statistical downscaling methods. *International Journal of Climatology*, **26,** 679-689.

Semenov, M. A., and E. M. Barrow, 1997: Use of a stochastic weather generator in the development of climate change scenarios. *Climatic Change*, **35**, 397-414.

Sheffield, J., and Coauthors, 2013: North American climate in CMIP5 experiments. Part I: evaluation of historical simulations of continental and regional climatology. *Journal of Climate*, **26,** 9209-9245.

Sillmann, J., V. Kharin, X. Zhang, F. Zwiers, and D. Bronaugh, 2013: Climate extremes indices in the CMIP5 multimodel ensemble: Part 1. Model evaluation in the present climate. *Journal of Geophysical Research: Atmospheres*, **118,** 1716-1733.

*Tarrant Regional Water Dist.* v. *Herrmann,* 569 U. S. ___ (2013).

Taylor, K. E., R. J. Stouffer, and G. A. Meehl, 2012: An overview of CMIP5 and the experiment design. *Bulletin of the American Meteorological Society*, **93,** 485-498.

Themeßl, M. J., A. Gobiet, and A. Leuprecht, 2011: Empirical-statistical downscaling

and error correction of daily precipitation from regional climate models. *International Journal of Climatology*, **31,** 1530-1544.

Thrasher, B., J. Xiong, W. Wang, F. Melton, A. Michaelis, and R. Nemani, 2013: Downscaled climate projections suitable for resource managers. *EOS, Trans. AGU*, **94,** 321-323.

UCAR, 2011: Climate Modeling. Accessed 10 July 2016. [Available online at http://scied.ucar.edu/longcontent/climate-modeling.]

U.S. Environmental Protection Agency, 2013: Level III ecoregions of the continental United States. Accessed 5 July 2015. [Available online at ftp://newftp.epa.gov/EPADataCommons/ORD/Ecoregions/us/Eco_Level_III_US.pdf.]

Venkataraman, K., S. Tummuri, A. Medina, and J. Perry, 2016: 21st Century drought outlook for major climate divisions of Texas based on CMIP5 multimodel ensemble: implications for water resource management. *Journal of Hydrology*, **534,** 300-316.

Wang, L., and W. Chen, 2014: Equiratio cumulative distribution function matching as an improvement to the equidistant approach in bias correction of precipitation. *Atmospheric Science Letters*, **15,** 1-6.

Watanabe, M., and Coauthors, 2010: Improved climate simulation by MIROC5: mean states, variability, and climate sensitivity. *Journal of Climate*, **23,** 6312-6335.

Wilby, R. L., S. P. Charles, E. Zorita, B. Timbal, P. Whetton, and L. O. Mearns, 2004: Guidelines for use of climate scenarios developed from statistical downscaling methods.

Xue, X., K. Zhang, Y. Hong, J. Gourley, W. Kellogg, R. A. McPherson, Z. Wan, and B. Austin, 2015: New multisite cascading calibration approach for hydrological models: case study in the Red River Basin using the VIC Model. *Journal of Hydrologic Engineering*, **21,** 05015019.

Zagona, E. A., T. J. Fulp, R. Shane, T. Magee, and H. M. Goranflo, 2001: RiverWare: A generalized tool for complex reservoir system modeling. *JAWRA Journal of the American Water Resources Association*, **37,** 913-929.

Zhang, Q., and J. Zhang, 2016: Drought hazard assessment in typical corn cultivated areas of China at present and potential climate change. *Natural Hazards*, **81,** 1323-1331.

# Chapter 3: Future Hydrologic Extremes of the Red River Basin

## 1. Introduction

Hydrologic extremes of heavy precipitation and severe drought stress water resources and damage communities in the Red River Basin, located in the south-central United States. For example, the summer of 2011 was the third driest summer in Oklahoma state history and the driest in Texas history since records began in 1895. These states suffered great losses from prolonged drought conditions, with U.S. Drought Monitor category D4 (exceptional drought) conditions affecting almost all of Texas and nearly seventy percent of Oklahoma by area. As the long-term drought conditions finally ended in the spring of 2015, El Niño brought record amounts of precipitation to the region, resulting in catastrophic floods that caused loss of life and property. For example, daily rainfall values on June 18, 2015 included 2 inches in Durant, OK and as much as 10.5 inches in Newport, OK (OCS 2015).

Hydrological extremes, hereby defined as heavy rainfall and severe drought events, have occurred throughout the historical record and are expected to continue in the future; however, decision makers need to know if and how the frequency of these events may vary in a changing climate so that they can mitigate these losses. Therefore, this research has examined how these hydrologic extremes impact water resources in the Red River Basin, how the frequency of such events is expected to change in the future, and how this study can aid local water resource managers and decision makers.

To analyze the future frequency of hydrological extremes, this study used statistically downscaled climate projections, which use quantifiable relationships between large-scale climate variables, or predictors, and small-scale surface variables,

or predictands (Wilby et al. 2004). Downscaling generates high-resolution, detailed output that is more useful to decision makers and local resource managers than coarse-resolution global climate models (GCMs; Maurer et al. 2014, Thrasher et al. 2013). GCMs are numerical models that simulate Earth's large-scale atmospheric and oceanic processes and take greenhouse gas concentrations into account (IPCC 2013). GCMs calculate the evolution of climate variables, such as temperature and precipitation, that quantitatively describe future climatic changes; however, they currently only provide output in a coarse resolution of generally several hundreds of kilometers (Wilby et al. 2004, IPCC 2013, UCAR 2011, Prudhomme et al. 2002). In addition, GCMs have limitations, including biases in climate forcings of greenhouse gases, natural variability, and rainfall (Lupo and Kininmonth 2013, Eden et al. 2012, Schmidli et al. 2006). To correct for these biases and gain local-scale information that is more beneficial for impact assessments and for decision makers and water resource managers, downscaling is typically the solution.

## 2. Study Area

The Red River Basin has a diverse climate, with average yearly rainfall totals ranging from approximately 500 to 1300 millimeters (20 to 50 inches) from the west to the east, respectively. The basin, covering 239,361 $km^2$, spans from New Mexico to the Mississippi River (Fig. 2.1) and is important for many ecoregions, the water supply, and cultural and recreational activities (Xue et al. 2015, Bertrand and McPherson 2017, in prep.). Conflicts over water resources in the basin have occurred in the past, such as the Supreme Court case, *Tarrant Regional Water District vs. Hermann* (2013), that arose after Oklahoma legislatures prohibited out-of-state water distribution in 2002,

preventing Tarrant County, and therefore, Fort Worth, Texas, from continuing to buy water from the state (Malewitz 2013). Another major water rights conflict occurred between the City of Oklahoma City and the Choctaw Nation of Oklahoma and Chickasaw Nation from 2011-2016, during a time of extreme drought in Oklahoma. These examples shine a light on the issues of water resources in the Red River Basin and the local stresses that arise during drought.

On the other end of the spectrum, the Red River Basin has experienced heavy and extensive rainfall in the past, resulting in river and flash flooding. For example, record-breaking precipitation amounts in Texas and Oklahoma in May and June of 2015 brought flooding that caused a loss of lives and property (Crouch 2015). Southern Oklahoma's May monthly rainfall was 400% above average, with over 20 inches of rain (Di Liberto 2015). One Oklahoma City station recorded a 1-in-1000-year rainfall event for an accumulated period of 30 days. In northern Texas, levees broke, leading to flooded homes and voluntary evacuations (Breslin 2015). While this was a long-lasting event, daily rainfall values reached 2 inches in Durant, OK and 10.5 inches in Newport, OK on June 18, 2015 (OCS 2015). Periods of flash flooding are a hazard to human health not only from high flood waters, but from raw sewage and other toxic chemicals often contaminating the water supply from the stormwater runoff (Lee 2015, Taylor et al. 2011). Oklahoma and Texas experienced this, with various levels of sewage, oil, and insecticides released into the stormwater. This rainfall event caused at least 31 fatalities (Breslin 2015).

Climate change studies of the Southern Plains have discussed a drier and warmer pattern in the future (Gutzler and Robbins 2010, Shafer et al. 2014,

Venkataraman et al. 2016). When intermittent heavy rainfall events occur in this pattern, soils can be too dry to absorb rainfall quickly enough to prevent flooding (UCAR 2010). Thus, even during drought conditions, it is important for water resource managers and decision makers to understand how flooding is expected to impact their community. In some cases, increased frequency of these events in the future may make it necessary for water infrastructure to be updated (National Research Council 2011). Taking these points into consideration, this study identifies if heavy rainfall and severe drought events may be expected to continue in the future for the region.

## 3. Methods and Data

### *3a. Research Design*

The goal of this study was to identify the future changes in frequency of hydrologic extremes in the Red River Basin in order to aid water resource managers and decision makers in the region. For our study, hydrologic extremes include heavy rainfall and severe drought events. Our study applies a dataset of statistically downscaled climate projections for the Red River Basin (Bertrand and McPherson 2017, in prep.) in order to determine any future changes in the frequency of these events in our future periods (2046-2070 and 2075-2099) compared to the historical period (1981-2005). To answer this research question, we first defined a heavy rainfall and severe drought threshold for our study area. We then selected a peak-over-threshold (POT) approach for both event types in order to identify the frequency of events that exceeded the thresholds in our selected timeframes. Because our goal was to find changes and trends in the future periods, we then computed the 25-year difference in event frequency between the historical and each future period across the basin. Our study provides

information on a grid cell basis, allowing us to discover spatial patterns that are also useful to decision makers and communities. The remainder of this section discusses the specific methodology we used for our study, as well as information about the dataset.

*3b. Data*

Bertrand and McPherson (2017, in prep.) provided details of the dataset, which uses statistical downscaling methods to project a 0.1-degree resolution of climate variables, such as minimum and maximum temperature and precipitation on a daily scale. The dataset was created by the Geophysical Fluid Dynamics Laboratory (of the National Oceanic and Atmospheric Administration) and was shared by the South Central Climate Science Center (of the U.S. Department of the Interior) in order to aid decision makers and water resource managers in the basin with local-scale information for long-term water plans (Bertrand and McPherson 2017, in prep.). The climate variables were projected for a recent historical period of 1961-2005 and through the end of the 21$^{st}$ century, or 2006-2099, for various representative concentration pathway (RCP) scenarios.

After an evaluation of GCMs from the Coupled Model Intercomparison Project Phase 5 (CMIP5; Taylor et al. 2012), three models were selected to be downscaled: the Community Climate System Model (CCSM4; Gent et al. 2011), the fifth version of the Model for Interdisciplinary Research on Climate (MIROC5; Watanabe et al. 2010), and the low-resolution version of the Max Planck Institute's Earth System Model (MPI-ESM-LR; Giorgetta et al. 2013). The dataset includes two quantile mapping methods that statistically downscaled the data and reduced GCM biases, which are the Cumulative Density Function Transform (CDFt; Michelangeli et al. 2009) and Equi-

Distant Quantile Mapping (EDQM; Li et al. 2010) with RCPs of 2.6, 4.5, and 8.5. For more information about the quantile mapping techniques, model selection, and model evaluation, refer to Bertrand and McPherson (2017, in prep.).

For our comparative analysis, 25-year time periods were chosen from the dataset, which include a historical period of 1981-2005 and two future periods of 2046-2070 and 2075-2099 to offer a mid-century and end-of-century analysis. In addition, RCP scenarios 2.6 and 8.5 were selected to provide a range of possible future radiative forcings.

### *3c. Heavy Precipitation Definition*

Literature has shown that there is no standard definition of an extreme or heavy precipitation event, for the term is dependent on the climatology of the region (Liu et al. 2013, Schoof and Robeson 2016). For example, in a dry location where it is typical to have little precipitation, the threshold of heavy rainfall is different than in an area prone to convective storms with heavy downpours. While there is a lack of clarity in heavy rainfall definitions, there are various criteria of these events in the literature for different study areas. Some researchers use a specific daily rainfall value that is set as the threshold. For example, a study in India defined a "heavy [rainfall] event" as 100 mm/day of precipitation and a "very heavy event" as 150 mm/day (Goswami et al. 2006). In addition, Vavrus et al. (2015) classified a heavy precipitation event in the northeast U.S. as having at least 2 inches of rainfall in one day.

Return periods and Generalized Extreme Value (GEV) distributions have also been used to study extreme rainfall. For example, results from Kharin et al. (2013) revealed that the historical 20-year return period is reduced to as much as 6 years in the

future for CMIP5 models. Cheng and AghaKouchak (2014) assess intensity-duration curves with GEV distributions to compute several return periods under a stationary and nonstationary climate, revealing more extremes in a nonstationary environment. Furthermore, Tryhorn and DeGaetano (2011) developed GEV distributions to validate their statistical downscaling techniques by analyzing extreme precipitation events in the northeast U.S. They found that the simulated return periods were within the 95% confidence interval of the observations and the GEV distributions.

On the other hand, many studies utilize a percentile approach. Zhang et al. (2011) states that using percentile thresholds and the number of days exceeding those thresholds allows us to compare frequencies spatially. This method is also termed a peak-over-threshold (POT) approach, which Villarini et al. (2013) similarly uses to assess precipitation values at the 95$^{th}$ percentile. Schoof and Robeson (2016) list indicators created by the Expert Team on Climate Change Detection and Indices (ETCCDI) from the World Meteorological Organization Commission for Climatology (CCI)/World Climate Research Programme's Climate Variability and Predictibility (CLIVAR) project (Vavrus et al. 2015) in which "extremely wet days" are calculated by the 99$^{th}$ percentile of annual total precipitation.

Another instance of a 99$^{th}$ percentile method is shown in Emori and Brown (2005), where they use this threshold with daily precipitation from six climate models. Other percentile values have been found in the literature as well, such as Zhai et al. (2005) that determines the frequency of extreme rainfall events over time in China, which are classified as days with rainfall greater than the 95$^{th}$ percentile for a selected time period. Therefore, implementing a POT approach from a set percentile is

commonly found in the literature and is implemented in this study to analyze the frequency of heavy precipitation events occurring from a spatial perspective.

In our study, we selected the POT approach with thresholds of the 90$^{th}$ and 99$^{th}$ percentiles of rain days in the 25-year historical period of 1981-2005, based on the statistically downscaled dataset used in this study. The percentiles of the historical period and the number of daily events exceeding each of these thresholds in the historical and future periods (2046-2070 and 2075-2099) were calculated across the Red River Basin through R version 3.3.2 (R Core Team 2016). From here on, the number of events that exceed the 90$^{th}$ and 99$^{th}$ percentiles of the historical period are referred to as the "frequency of heavy precipitation events," and the future events at these thresholds are denoted as "90$^{th}$ and 99$^{th}$ percentile events". The differences, or changes, between the historical frequency and each future frequency across the basin were then computed to determine whether there were any increasing or decreasing trends in heavy precipitation events. Our computed values thus represent the change in the number of days *during a 25-year period*, not yearly differences.

### *3d. Severe Drought Definition*

The second type of hydrologic extreme analyzed in this study is drought. Drought also has many definitions, depending on the application, and there are various types of drought, such as meteorological, agricultural, and hydrological (Palmer 1965). For the purpose of finding short-term hydrologic extremes, this study focused on meteorological drought. Even focusing on this one type of drought, much of the literature highlights that there is not a standard way to define or measure the hazard (Dracup et al. 1980, Wilhite and Glantz 1985, Wilhite 2000). A concise definition by

the National Weather Service is, “a deficiency of moisture that results in adverse impacts on people, animals, or vegetation over a sizeable area” (NOAA 2016).

One method to empirically measure drought is through drought indices, such as the Standardized Precipitation Index (SPI; McKee et al. 1993). The SPI is user friendly, allowing the user to calculate the drought conditions for specific timeframes and determine how many droughts, and at what magnitude, have occurred in that time frame (McKee et al. 1993, Guttman 1998, Keyantash and Dracup 2002). This index can be computed by creating probability distribution functions for the long-term precipitation of a location for a selected time scale and then calculating the cumulative probability of a certain precipitation amount (McKee et al. 1993, Guttman 1999). The SPI value is then estimated by applying an inverse normal function to the probabilities with a mean of zero and standard deviation of one. Therefore, the SPI provides the probability of a wet or dry event occurring by showing the number of standard deviations the values are from the mean. Negative SPI values represent a deficiency in moisture relative to local climatology and positive values are above the median precipitation (Guttman 1999).

Unfortunately, SPI does not take evapotranspiration into consideration and thus is insufficient to use in a warming world. Instead, the Standardized Precipitation Evapotranspiration Index (SPEI) accounts for the SPI’s limitations and provides the ability to perform a multiscalar analysis (Vicente-Serrano et al. 2010). SPEI can be calculated by Equation 3.1, where P is monthly total precipitation and PET is the potential evapotranspiration (Vicente-Serrano et al. 2010). There is an R package, *SPEI*, for simple calculation of the drought index at various timescales (Beguería and

$$SPEI = P - PET \quad \text{Eq. 3.1}$$

Vicente-Serrano 2013). Through this software package, users can choose different methods for the calculation of potential evapotranspiration (PET). Examples include the Thornthwaite equation (Thornthwaite 1948) that uses mean daily temperature and latitude and the Hargreaves equation (Hargreaves and Samani 1985) that uses monthly average minimum and maximum temperature. Equation 3.2 displays the Hargreaves

$$ET_0 = 0.0023R_a(TC + 17.8)TR^{0.5} \quad \text{Eq. 3.2}$$

equation, where $ET_0$ is reference evapotranspiration, $R_a$ is the radiation component, TC is the mean temperature in degrees Celsius for the time period, and TR is the daily temperature range (Hargreaves and Samani 1985). The Thornthwaite and Hargreaves equations require different data variables for calculation of PET but do not have specific requirements for the number of observations.

Venkataraman et al. (2016) utilized this package to calculate SPEI in Texas under three emission scenarios through the end of the 21$^{st}$ century. They chose to calculate PET, and thus SPEI, with the Hargreaves method because other research has shown that the Thornthwaite equation is not ideal for climate change studies due to the method overestimating drought conditions with increased temperatures (Lockwood 1999). Amatya et al. (1995) analyzed several methods of calculating PET, including Thornthwaite and Hargreaves, and found that the Thornthwaite method performed the worst for their humid study area of North Carolina. Furthermore, Lu et al. (2005) discovered that PET values calculated from the Thornthwaite equation were the lowest among six methods used to calculate PET in the southeast U.S., including a watershed in Arkansas.

For our study, the SPEI was the most suitable drought index because it could easily be calculated from limited climatological variables, such as monthly minimum and maximum temperature and monthly precipitation (UCAR 2014), as recommended by Beguería et al. (2014). The *SPEI* R package also allows the user to input the time scale desired for the calculation, which is important for multiscalar analyses whereby drought is examined at different time scales, such as for long-term assessments and impacts.

The variables of daily minimum and maximum temperature and daily precipitation in our downscaled dataset enabled a simple calculation of PET using the Hargreaves method and then further computation of SPEI. To run the package in R, monthly average minimum and maximum temperatures and monthly total precipitation were required for both the historical and future time periods. We then calculated PET and SPEI values for each grid cell in the Red River Basin at a one-month timescale from these monthly averages and totals, then computed the frequency of severe drought events for each grid cell in the basin.

The SPEI classifies extreme drought as a value of less than or equal to –2 (McKee et al. 1993); however, our study discovered that these events are rare, especially during 25-year periods; hence, we selected a threshold of SPEI less than or equal to –1.5 to encompass severe drought. Our study's historical period of 1981-2005 was a wetter period than other 25-year periods on record (Fig. 3.1), and it did not contain the high-magnitude drought of the 1950s or 1960s, thus clarifying the small number of extreme drought events and length of drought found (Fig. 3.1). Similar to the heavy precipitation analysis, the differences between the historical frequency and each

future frequency across the grid were calculated in order to determine any changes in severe drought through the 21st century.

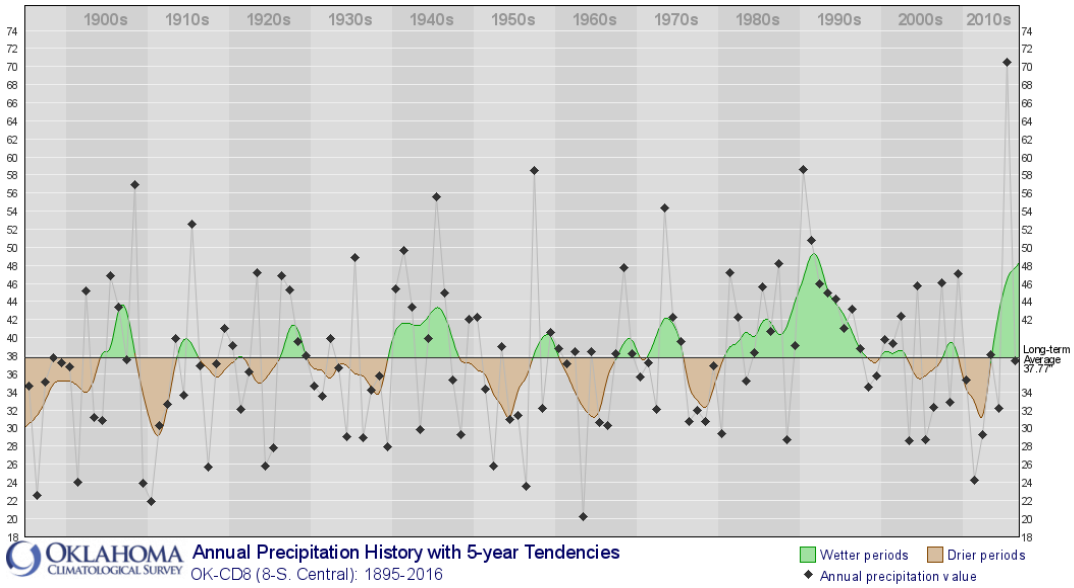


**Figure 3.1. Long-term annual precipitation history for the South Central climate division in Oklahoma (Oklahoma Climatological Survey 2017).**

## 4. Results

### *4a. Heavy Precipitation*

The difference between the number of heavy precipitation events in the historical period (1981-2005) and each future period (2046-2070 and 2075-2099) was calculated for the ensemble that used CCSM4, MIROC5, and MPI-ESM-LR models with CDFt and EDQM downscaling techniques for RCP 2.6 and RCP 8.5 across the Red River Basin. The 90th percentile of precipitation during the historical period ranged from approximately 7 to 35 millimeters (0.3 to 1.4 inches) per day across the basin, while the 99th percentile spanned from 22 to 88 millimeters (0.9 to 3.5 inches) per day. Heavy precipitation thresholds increased to the east, coinciding with the average annual

precipitation gradient of approximately 500 to 1300 millimeters (20 to 50 inches) per year (USGS 2017, Bertrand and McPherson 2017, in prep).

For example, the threshold for the grid cell that encompassed Amarillo, TX, which is located in the Texas Panhandle, in the CCSM4 model was 12.3 millimeters (0.5 inches) for the historical 90$^{th}$ percentile and 32 millimeters (1.3 inches) for the 99$^{th}$ percentile. In the center of the basin, the heavy precipitation threshold near Ardmore, OK, was 17.6 millimeters (0.7 inches) for the 90$^{th}$ percentile and 42.6 millimeters (1.7 inches) for the 99$^{th}$ percentile. Eastern locations exhibited higher thresholds, such as a 90$^{th}$ percentile of 17.6 millimeters (0.7 inches) and a 99$^{th}$ percentile of 52.2 millimeters (2.1 inches) in the grid cell that Shreveport, LA was within. Because the thresholds were calculated from rain days, the annual number of 90$^{th}$ and 99$^{th}$ percentile events in

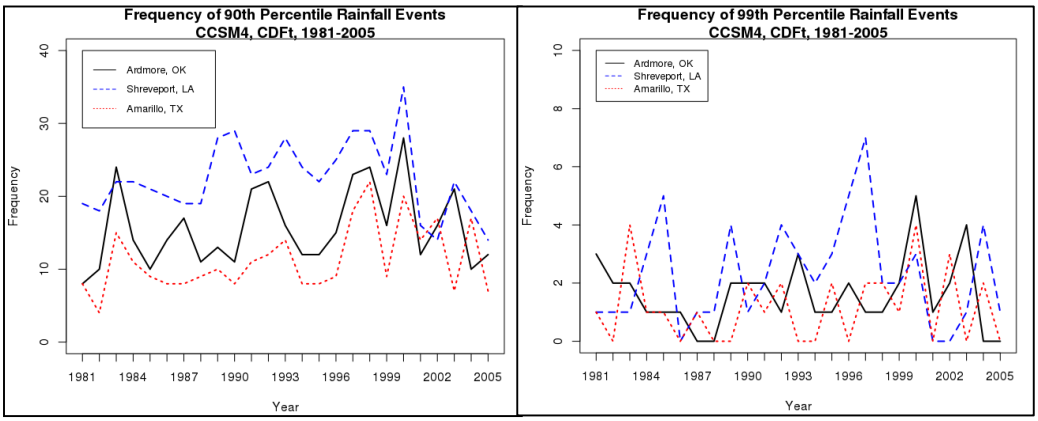


**Figure 3.2. Annual occurrence of 90th and 99th percentile events in the modeled historical period for three locations in the Red River Basin. The red line represents results for Amarillo, TX, the black line represents Ardmore, OK, and the blue line represents Shreveport, LA.**

the historical period were dependent on location and followed the west to east gradient as well, as seen in Figure 3.2. It is worth noting that gridded data produce a lower frequency of heavy rainfall events, because the grid cell is averaging what would be several point observations (Ensor and Robeson 2008, Contractor et al. 2015).

The future projected change in the amount of precipitation associated with the historical 90$^{th}$ percentile threshold varies between models, statistical downscaling techniques, and RCP scenarios and is shown in Table 1, where negative values are associated with decreasing events and positive values show increasing events. Overall, we discovered a decreasing trend of events exceeding the historical 90$^{th}$ percentile thresholds in the west and an increase in these events in the east for the future scenarios. However, these trends were not consistent across all models and all RCP scenarios. For example, the mid-century (2046-2070) results for RCP 2.6 included an increase in heavy precipitation events across much of the basin for the MIROC5 model, but a basin-wide decrease in events for the CCSM4 model (Fig. 3.3). In addition, the CCSM4 mid-century results for RCP 8.5 included a basin-wide decrease in 90$^{th}$ percentile days and results for MIROC5 were variable on each run.

The largest decreases in extreme precipitation events at the 90$^{th}$ percentile occurred in the RCP 8.5 scenario, especially for the end-of-century period. For example, projections from the MPI-ESM-LR model and CDFt downscaling technique estimated locations in the far western portion of the basin to have a decrease in the number of 90$^{th}$ percentile daily events by as many as 249 days compared to approximately 900 events that occurred in the historical 25-year period (Table 1a, Figure 3.4). The EDQM technique demonstrated the same pattern; however, the change in number of events was not as large as the CDFt results, with the greatest decrease being 98 days in this scenario and timeframe. There were projected increases in heavy rainfall events as well, most noticeably in the MPI-ESM-LR model. This model estimated some locations in the east to have approximately 113 more 90$^{th}$ percentile rainfall days by the end of the

**Table 1. Change of the number of days in the 25-year period of heavy precipitation events at the (a) 90th percentile and (b) 99th percentile of the historical period. Change in the number of days is calculated under RCP 2.6 and RCP 8.5 scenarios (columns) for each model and statistical downscaling technique (SD), and the range across the basin is displayed as the basin minimum (left side of each column) and maximum (right side).**

| Minimum and Maximum Number of Days for the Change in Historical versus Future Heavy Precipitation Events | | | | | | | | | | |
|---|---|---|---|---|---|---|---|---|---|---|
| **Model, SD** | **Mid-century (2046-2070)** | | | | **End-of-century (2075-2099)** | | | | **Historical (1981-2005)** | |
| | **RCP 2.6** | | **RCP 8.5** | | **RCP 2.6** | | **RCP 8.5** | | | |
| | **Min** | **Max** | **Min** | **Max** | **Min** | **Max** | **Min** | **Max** | **Min** | **Max** |
| ***(a) 90th Percentile*** | | | | | | | | | | |
| CCSM4, CDFt | –76 | 47 | –123 | 4 | –108 | 47 | –84 | 74 | 0 | 691 |
| MIROC5, CDFt | –23 | 105 | –71 | 92 | –37 | 111 | –133 | 27 | 0 | 627 |
| MPI-ESM-LR, CDFt | –112 | 57 | –185 | 71 | –112 | 112 | –247 | 76 | 0 | 913 |
| CCSM4, EDQM | –70 | 59 | –104 | 13 | –90 | 59 | –75 | 59 | 0 | 499 |
| MIROC5, EDQM | –27 | 92 | –82 | 66 | –48 | 116 | –119 | 12 | 0 | 499 |
| MPI-ESM-LR, EDQM | –61 | 68 | –85 | 97 | –49 | 101 | –98 | 113 | 0 | 419 |
| | | | | | | | | | | |
| ***(b) 99th Percentile*** | | | | | | | | | | |
| CCSM4, CDFt | –24 | 68 | –24 | 65 | –29 | 40 | –23 | 72 | 0 | 70 |
| MIROC5, CDFt | –18 | 45 | –21 | 51 | –21 | 45 | –12 | 51 | 0 | 63 |
| MPI-ESM-LR, CDFt | –24 | 44 | –23 | 53 | –23 | 53 | –14 | 71 | 0 | 92 |
| CCSM4, EDQM | –22 | 34 | –19 | 34 | –24 | 15 | –20 | 32 | 0 | 50 |
| MIROC5, EDQM | –12 | 43 | –9 | 45 | –15 | 46 | –9 | 68 | 0 | 50 |
| MPI-ESM-LR, EDQM | –10 | 30 | –16 | 35 | –16 | 35 | –11 | 49 | 0 | 42 |

century under a RCP 8.5 scenario for both downscaling techniques compared to 900 events that occurred in the historical period.

Results for rainfall events associated with the 99$^{th}$ percentile of the historical period showed similar patterns to those of the 90$^{th}$ percentile, with the most common pattern being an increase in heavy rainfall days in the east and many fewer occurring in the west. However, there were model differences in trends compared to the 90$^{th}$ percentile events. For example, while the MPI-ESM-LR model exhibited the highest decrease in extreme events in the basin for the 90$^{th}$ percentile, the MIROC5 (during the end-of-century period for RCP 8.5) and the CCSM4 portrayed this characteristic in the 99$^{th}$ percentile for both CDFt and EDQM techniques (Figs. 3.5 and 3.6). All three models projected a decrease in mean daily precipitation in the western Red River Basin (Bertrand and McPherson 2017, in prep.); however, the models were handling extremes differently.

When we compared results for the mid-century period under RCP 2.6 (Fig. 3.5) versus the end-of-century period under RCP 8.5 (Fig. 3.6), we noticed that heavy rainfall events are affected by different emission scenarios and timeframes as well. The largest decreases in events occurred in the 2075-2099 timeframe for the CCSM4 model where the western and central portions of the basin were estimated to experience up to nearly 30 fewer heavy rainfall days, compared to 70 events that the CCSM4 modeled for the historical period (Table 1b).

Increases in 99$^{th}$ percentile events were variable and dependent on the model and RCP scenario. Most model runs projected an increase in heavy precipitation events in the eastern Red River Basin. These results agree with Wuebbles et al. (2014) who used

CMIP5 models to indicate that rainfall in the U.S. is projected to increasingly fall in the 99$^{th}$ percentile of their long-term historical period, especially in the RCP 8.5 scenario. The most widespread increases in the end-of-century period occurred using the MPI-ESM-LR model, especially in the RCP 8.5 scenario, which includes approximately 70 more heavy rainfall days than the historical period. The difference is a sizeable change and indicates that the number of heavy precipitation events may increase by more than 75% in this area as compared to the historical period.

Sillmann et al. (2013) analyzed the performance of the CMIP5 models for extreme indices and stated that the MPI-ESM-LR model produces the greatest simple daily intensity, an extremes index from ETCCDI, in millimeters per day versus other models, which could explain a higher number of events occurring with this model. Dosio (2016) found that the MPI-ESM-LR model overestimates precipitation. This overestimation also occurred in the mean daily precipitation analysis of the Red River Basin compared to observational data (Bertrand and McPherson 2017, in prep.). While there were differences between models for different timeframes and RCP scenarios, the most common trend included an increase in the number of heavy rainfall events in the eastern Red River Basin, where average annual rainfall is higher, and a decrease in events in the drier, western portions of the basin.

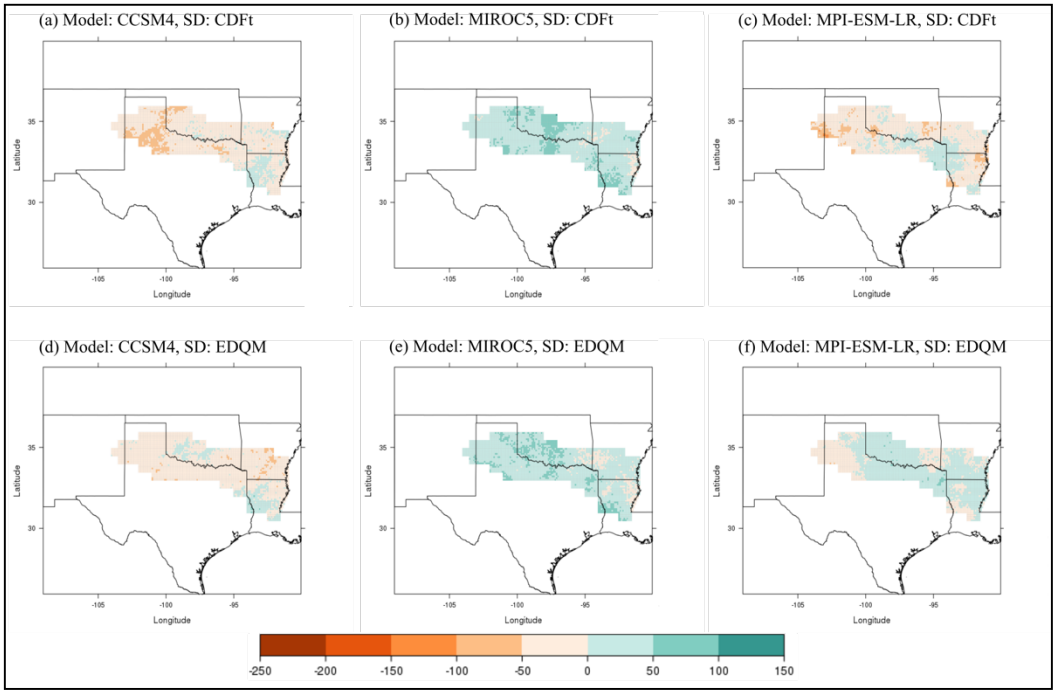


**Figure 3.3. Change in 25-year total frequency of all heavy rainfall days over 25 years at the 90$^{th}$ percentile between the historical period (1981-2005) and mid-century period (2046-2070) under a RCP 2.6 scenario.**

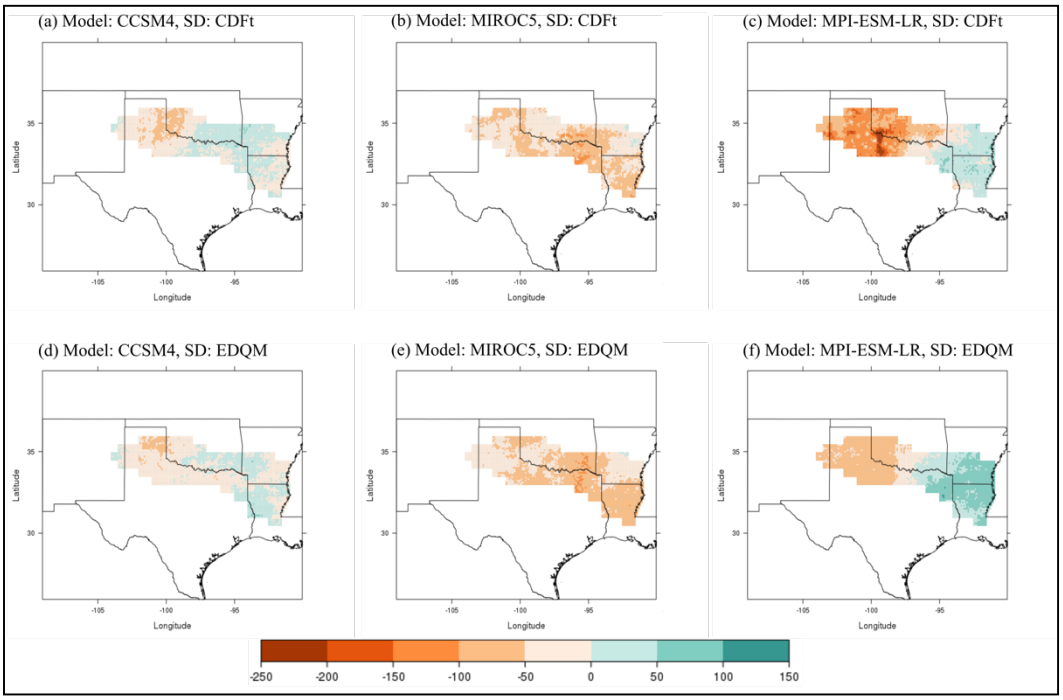


**Figure 3.4. Change in 25-year total frequency of all heavy rainfall days over 25 years at the 90$^{th}$ percentile between the historical period (1981-2005) and end-of-century period (2075-2099) under a RCP 8.5 scenario.**

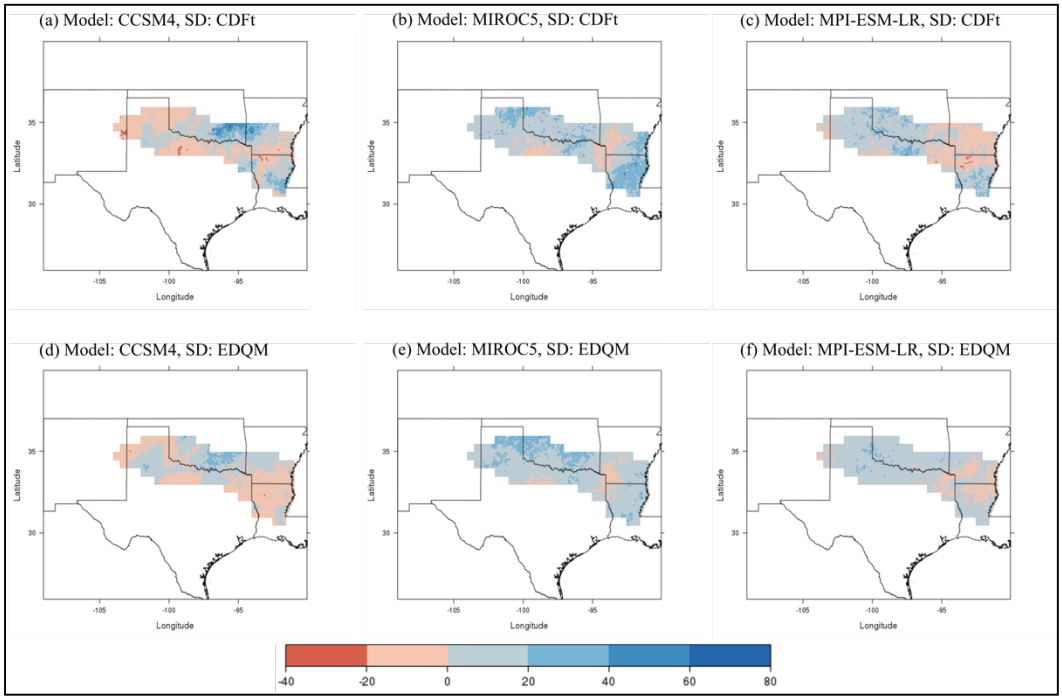


**Figure 3.5. Change in 25-year total frequency of all heavy rainfall days over 25 years at the 99th percentile between the historical period (1981-2005) and mid-century period (2046-2070) under a RCP 2.6 scenario.**

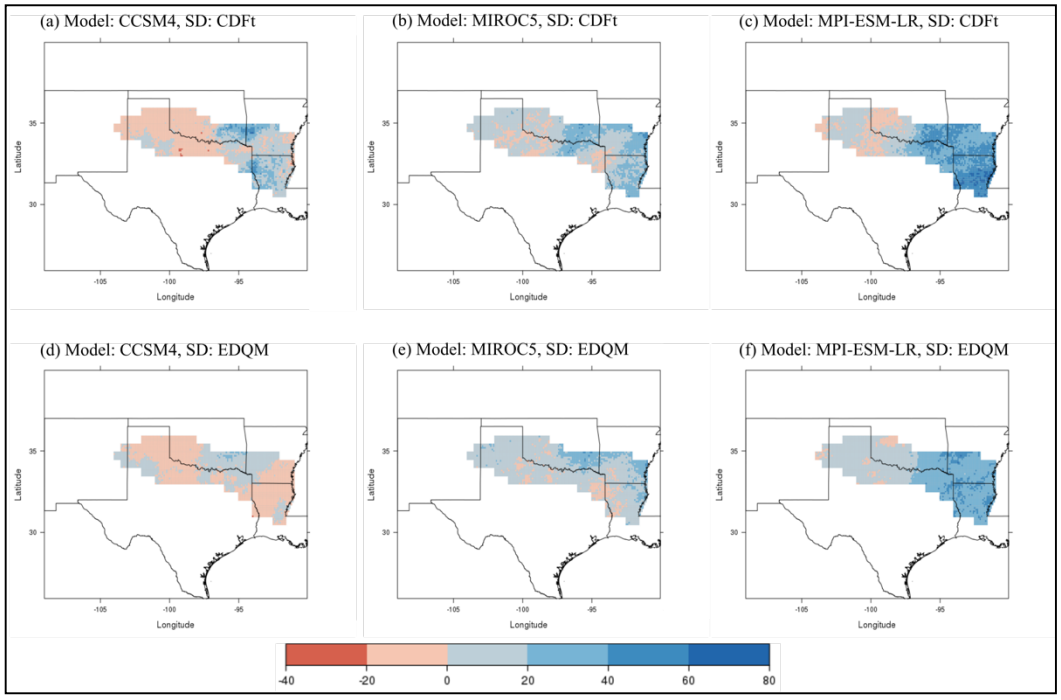


**Figure 3.6. Change in 25-year total frequency of all heavy rainfall days over 25 years at the 99$^{th}$ percentile between the historical period (1981-2005) and end-of-century period (2075-2099) under a RCP 8.5 scenario.**

### *4b. Severe Drought*

Similar to the heavy rainfall analysis, a frequency analysis of severe drought was also computed for each grid cell in the Red River Basin for each model, statistical downscaling technique, and RCP scenario for the historical and future timeframes. To gauge how meteorological drought may change in the future, we calculated monthly averages of SPEI and counted the number of events when SPEI was less than or equal to –1.5. Because the analysis included monthly events, consecutive months of severe drought were considered to be separate events. Drought often occurs for several consecutive months, so we acknowledge that this could have affected our results. During the 25-year historical period, the downscaled models indicated that the highest frequency of severe drought in the basin was 24 events, which occurred in southeast Arkansas and north-central Louisiana (Fig. 3.7). This result is consistent with NOAA's time series of drought in the southeast climate division of Arkansas (2017; Fig. 3.8). A similar number of historical severe drought events were also located in the Texas Panhandle.

Table 2 displays the ranges for the projected change in number of severe drought events for each future setting, with negative and positive values indicating decreasing or increasing events in the basin, respectively. Overall, the change in severe drought included a range of increasing and decreasing events across the basin. As Table 2 shows, the difference between the number of severe drought events was relatively consistent from historical to future periods for each model.

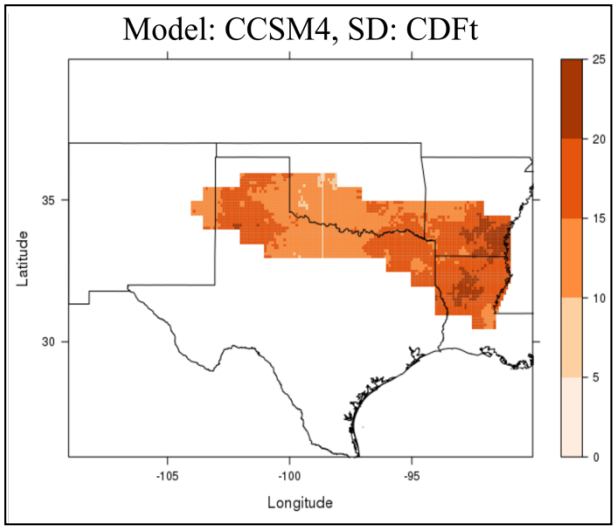


**Figure 3.7. Spatial representation of the historical drought frequency for the CCSM4 model**

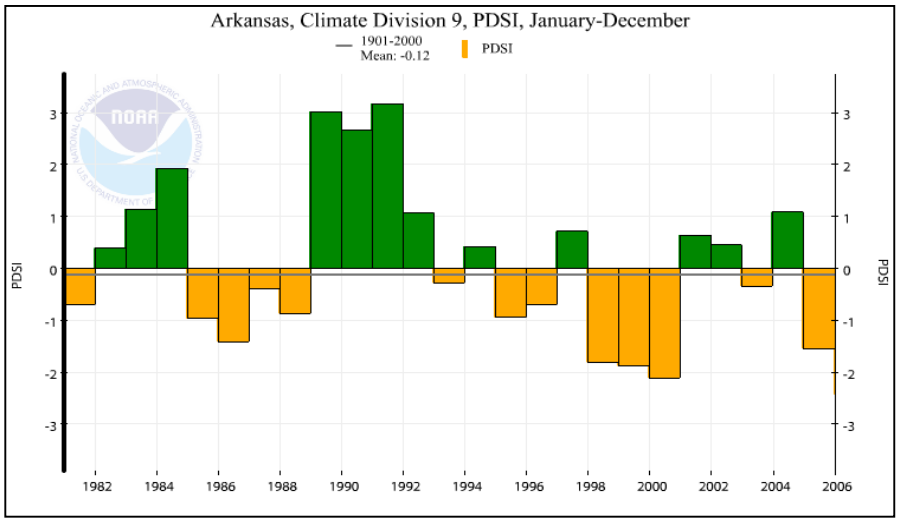


**Figure 3.8. Palmer Drought Severity Index of the southeast climate division of Arkansas for the historical period (NOAA 2017).**

**Table 2. Ranges in the change between historical and future frequency of 1-month severe drought events under RCP 2.6 and RCP 8.5 scenarios for each model and statistical downscaling technique (SD)**

| Minimum and Maximum Number for the Change in Historical versus Future 1-Month Severe Drought Events | | | | | | | | | | |
|---|---|---|---|---|---|---|---|---|---|---|
| **Model, SD** | **Mid-century (2046-2070)** | | | | **End-of-century (2075-2099)** | | | | **Historical (1981-2005)** | |
| | **RCP 2.6** | | **RCP 8.5** | | **RCP 2.6** | | **RCP 8.5** | | | |
| | **Min** | **Max** | **Min** | **Max** | **Min** | **Max** | **Min** | **Max** | **Min** | **Max** |
| CCSM4, CDFt | -9 | 8 | -12 | 10 | -8 | 8 | -10 | 12 | 0 | 24 |
| MIROC5, CDFt | -9 | 14 | -8 | 13 | -8 | 11 | -8 | 11 | 0 | 21 |
| MPI-ESM-LR, CDFt | -10 | 10 | -6 | 9 | -8 | 10 | -12 | 8 | 9 | 21 |
| CCSM4, EDQM | -10 | 9 | -12 | 8 | -11 | 8 | -12 | 11 | 0 | 26 |
| MIROC5, EDQM | -13 | 12 | -12 | 10 | -9 | 7 | -12 | 9 | 0 | 22 |
| MPI-ESM-LR, EDQM | -13 | 12 | -12 | 10 | -9 | 7 | -12 | 9 | 0 | 23 |

Although the minimum and maximum values were similar throughout, there were some spatial trends for each model. For example, the CCSM4 model projected an increase in the number of severe drought events across northwestern and central portions of the basin and a decline across the southwest and east (Figs. 3.9 and 3.10). This pattern was demonstrated in both the mid-century period under RCP 2.6 and the end-of-century period under RCP 8.5; however, the magnitude of this change was greater for the latter. For example, southwest Oklahoma and north-central Texas may receive up to 12 more severe drought events between 2075-2099, as compared to the historical frequency of 10-15 events over 25 years. Doubling the frequency of these events is likely to cause great damage to communities. Bertrand and McPherson (2017,

in prep.) identified a decrease in mean daily precipitation in the western part of the Red River Basin and a rise in both minimum and maximum temperatures, consistent with the projections of more drought events across the west in the future.

The MIROC5 model projected the trend of more severe drought events in the west and fewer in the east as well. The largest change in these events occurred in the mid-century period under RCP 2.6 for both downscaling techniques, when higher frequencies of severe drought were projected to occur and expand through the central Red River Basin. For example, we estimated an increase of at most 14 more events during a 25-year period throughout the basin, but especially across southeast Oklahoma and northeast Texas, and up to nine fewer events in the east, particularly in southern Arkansas (Table 2, Fig. 3.9). These results indicate that the frequency of severe drought may double in the western and central areas of the basin; however, southern Arkansas may experience a decline of these events by one third in the mid-century period compared to historical events.

Our analysis for the end-of-century timeframe under RCP 8.5 exhibited the same spatial pattern but had a much weaker signal, indicating a smaller range of severe drought occurrence compared to the historical period (Fig. 3.10). However, under this same RCP scenario for the end-of-century period, there were more widespread areas of decreasing severe drought events throughout the basin. These results support those of Venkataraman et al. (2016), who computed SPEI values across Texas to assess drought through the 21$^{st}$ century. They discovered that locations like Lubbock, located in far-west Texas, just south of the Texas Panhandle, are expected to experience more droughts by the end of the century under RCP 8.5 conditions.

Lastly, the MPI-ESM-LR results included the similar pattern of more severe drought events in the west and fewer events in the east; however, the signal was small compared to the other two models, and the location of the highest frequency of future events both shifted farther westward and expanded across the southeast (Figs. 3.9 and 3.10). This pattern was similar to that of the historical period, as seen in Figure 3.7. For example, we estimated an increase of as many as 12 events near the New Mexico/Texas border and northeast Texas during the 25-year, mid-century period, especially for the EDQM downscaling technique, compared to 15-20 events that occurred in the historical period. By the end of the century, however, our projections indicate less prominence in the increasing trend of events for the EDQM downscaling technique and a widespread decrease in the number of severe drought events throughout the basin, with scattered pockets of more events using the CDFt technique (Figs. 3.10c and 3.10f).

While there is variability between GCMs, we document an overall increase in drought events in portions of the western Red River Basin and a decline in the east. Wuebbles et al. (2014) found that CMIP5 models project an increase in the risk of drought in the RCP 8.5 scenario in the U.S. due to projected increases in evaporation and decreases in precipitation, which further validates our end-of-century results. Furthermore, with both temperature and precipitation taken into account for the calculation of SPEI, the models were more consistent for our estimation of these events than for our extreme precipitation analysis.

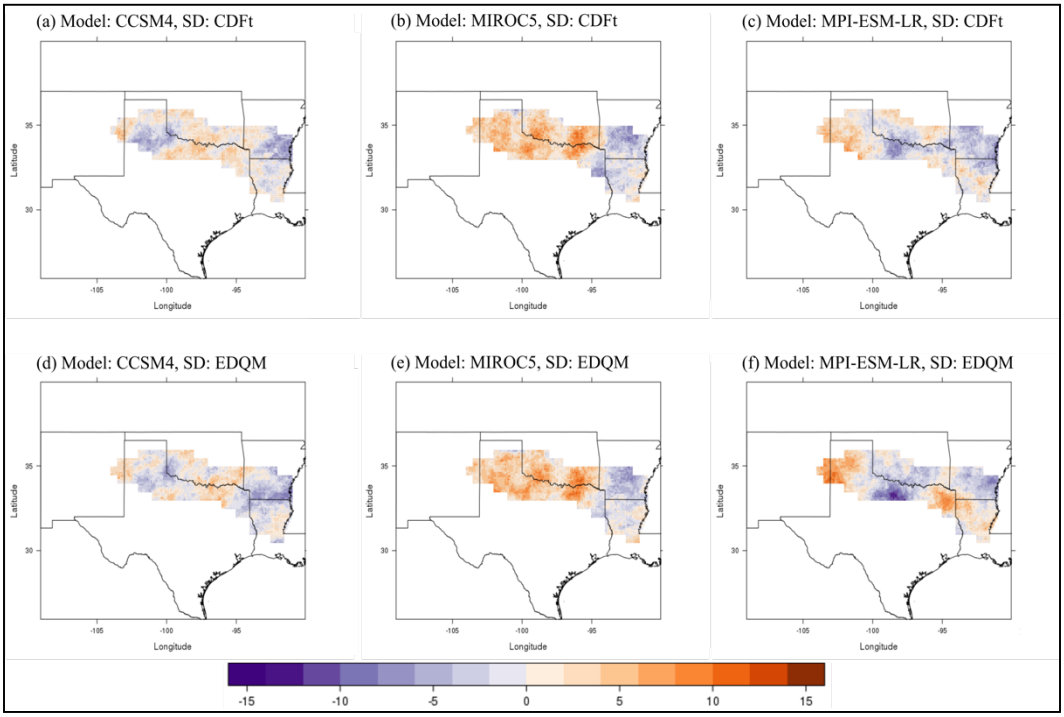


**Figure 3.9. Change in 25-year total frequency of severe drought at a 1-month timescale between the historical period (1981-2005) and mid-century period (2046-2070) under a RCP 2.6 scenario. Purple colors represent a decrease in events and oranges represent an increase.**

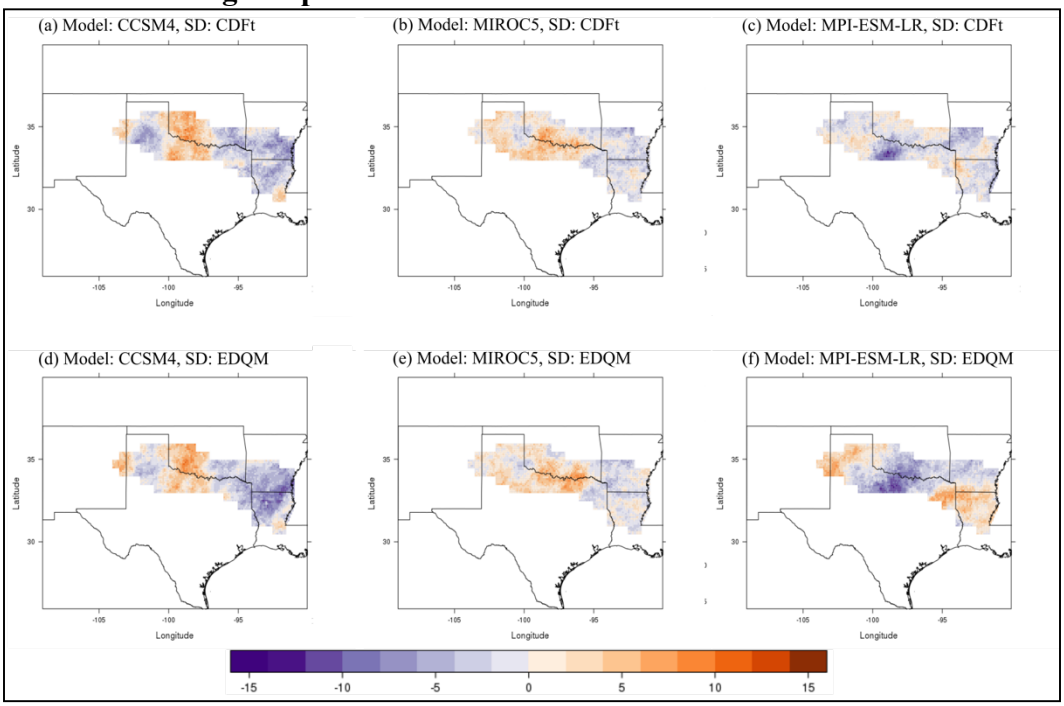


**Figure 3.10. Change in 25-year total frequency of severe drought at a 1-month timescale between the historical period (1981-2005) and end-of-century period (2075-2099) under a RCP 8.5 scenario. Purple colors represent a decrease in events and oranges represent an increase.**

## 5. Conclusion/Discussion

Hydrologic extremes of rainfall and drought have affected the Red River Basin in the past, creating negative economic impacts and causing damage to infrastructure and water quality and quantity. In order to alleviate for future losses, this study intended to identify the trends in the frequency of future heavy rainfall and severe drought events in the basin by using statistically downscaled climate projections through the end of the 21$^{st}$ century. By using a peak-over-threshold approach for heavy rainfall events at the 90$^{th}$ and 99$^{th}$ percentiles of the historical period, we discovered that the selected models generally show an increase in heavy rainfall events in the eastern portion of the basin and a decrease in the west, especially during the 2075-2099 period under a RCP 8.5 scenario. However, results for the RCP 2.6 scenario, when emissions are reduced, still indicate this trend. Heavy rainfall events cause large economic impacts from inundated homes and streets, erosion around infrastructure, and reduced water quality. Those in the eastern Red River Basin, such as across northeast Louisiana, may need to prepare for more of these events and their consequences in order to prevent future damages as well as possible.

We detected severe drought events by using the Standardized Precipitation Evapotranspiration Index (SPEI) at a one-month timescale, and values of less than or equal to -1.5 were classified as severe drought. This analysis also included a POT approach to identify the frequency of historical and future severe drought events. The results from this analysis differed between models, as each model projects precipitation differently. The most common result, although not unanimous among all three models,

was an increasing trend in number of severe drought events in the western Red River Basin and a declining trend in the east.

For the eastern basin, a decrease in severe drought would be good news, as drought impacts energy production, water quality and quantity, the ecology of the area, and agriculture. For example, the drought in 2011 led to $13 billion in damages in the Southern Plains (NOAA 2016) and caused a 6% increase in energy demand and 30% reduction in reservoir storage for cooling power plants in Texas (Scanlon et al. 2013). During this event, groundwater levels of aquifers in the region were below normal (Andrews 2013). For the western portion of the basin, an increase in extreme drought events, coupled with mean precipitation expected to decline, would create a more dire situation for water resources in this already arid or semi-arid region.

As one of the goals of this study was to aid stakeholders in the region, these results will be communicated to stakeholders through a webinar that will present the details of the study and what communities may expect in the future in regard to heavy rainfall and severe drought events. The results of this research will also be displayed on the South Central Climate Science Center's website to reach other stakeholders.

There are many factors of uncertainty with our study. First, the time period of the historical observations in which the projections were trained from plays a role in the statistics of the downscaled projections. The observation dataset is constrained to the 1961-2005 time period and our 25-year selection of 1981-2005 was wetter than other 25-year periods; therefore, having a longer time-series would potentially impact the threshold of the $90^{th}$ and $99^{th}$ percentiles. There is also uncertainty with the GCMs, downscaling techniques, and RCP scenarios. For example, Chen et al. (2011) discussed

uncertainty in GCMs and various downscaling techniques and found that GCMs have the largest uncertainty but the choice of downscaling technique has an impact on results for climate change studies. Taking this into account, we still found common patterns throughout our results. This study aimed to provide information and awareness of the possible scenarios of future hydrologic extremes of the Red River Basin and to help stakeholders to understand their future risks so they can mitigate for potential losses.

## 6. References


Amatya, D., R. Skaggs, and J. Gregory, 1995: Comparison of methods for estimating REF-ET. *Journal of irrigation and drainage engineering*, **121,** 427-435.

Andrews, W. J., 2013: Oklahoma's climate, droughts, and projected future climate. USGS, Accessed 3 Aug. 2017. [Available online at https://ok.water.usgs.gov/projects/tesnar/2013/Drought.Climate.ppt.WJA_5_2013.pdf.]

Beguería, S. and S. M. Vicente-Serrano, 2013. SPEI: Calculation of the Standardised Precipitation-Evapotranspiration Index.R package version 1.6. https://CRAN.R-project.org/package=SPEI.

Beguería, S., S. M. Vicente-Serrano, F. Reig, and B. Latorre, 2014: Standardized precipitation evapotranspiration index (SPEI) revisited: parameter fitting, evapotranspiration models, tools, datasets and drought monitoring. *International Journal of Climatology*, **34,** 3001-3023.

Bertrand, D. and R. A. McPherson, 2017: Downscaled climate projections for the Red River Basin, south-central U.S. In preparation.

Breslin, S., 2015: Southern Plains flooding: 31 killed in Texas and Oklahoma; Dry weather finally arrives. The Weather Channel, Accessed 17 Feb. 2017. [Available online at https://weather.com/safety/floods/news/flash-flooding-heavy-rain-texas-oklahoma-catastrophic-impacts.]

Chen, J., F. P. Brissette, and R. Leconte, 2011: Uncertainty of downscaling method in quantifying the impact of climate change on hydrology. *Journal of Hydrology*, **401,** 190-202.

Cheng, L., and A. AghaKouchak, 2014: Nonstationary precipitation intensity-duration-frequency curves for infrastructure design in a changing climate. *Scientific reports*, **4**.

Contractor, S., L. V. Alexander, M. G. Donat, and N. Herold, 2015: How well do gridded datasets of observed daily precipitation compare over Australia? *Advances in Meteorology*, **2015**.

Crouch, J., 2015: Reflections on a really big drought. NOAA, Accessed 15 March 2016. [Available online at https://www.climate.gov/news-features/blogs/beyond-data/reflections-really-big-drought.]

Di Liberto, T., 2015: Flood disaster in Texas and Oklahoma. NOAA, Accessed 17 Feb. 2017. [Available online at https://www.climate.gov/news-features/event-tracker/flood-disaster-texas-and-oklahoma.]

Donohue, R. J., T. R. McVicar, and M. L. Roderick, 2010: Assessing the ability of potential evaporation formulations to capture the dynamics in evaporative demand within a changing climate. *Journal of Hydrology*, **386,** 186-197.

Dosio, A., 2016: Projections of climate change indices of temperature and precipitation from an ensemble of bias-adjusted high-resolution EURO-CORDEX regional climate models. *Journal of Geophysical Research: Atmospheres*, **121,** 5488-5511.

Dracup, J. A., K. S. Lee, and E. G. Paulson, 1980: On the definition of droughts. *Water Resources Research*, **16,** 297-302.

Eden, J. M., M. Widmann, D. Grawe, and S. Rast, 2012: Skill, correction, and downscaling of GCM-simulated precipitation. *Journal of Climate*, **25,** 3970-

3984.

Emori, S., and S. J. Brown, 2005: Dynamic and thermodynamic changes in mean and extreme precipitation under changed climate. *Geophysical Research Letters*, **32**, L10776.

Ensor, L. A., and S. M. Robeson, 2008: Statistical characteristics of daily precipitation: comparisons of gridded and point datasets. *Journal of Applied Meteorology and Climatology*, **47,** 2468-2476.

Gent, P. R., and Coauthors, 2011: The community climate system model version 4. *Journal of Climate*, **24,** 4973-4991.

Giorgetta, M. A., and Coauthors, 2013: Climate and carbon cycle changes from 1850 to 2100 in MPI- ESM simulations for the Coupled Model Intercomparison Project phase 5. *Journal of Advances in Modeling Earth Systems*, **5,** 572-597.

Goswami, B. N., V. Venugopal, D. Sengupta, M. S. Madhusoodanan, and P. K. Xavier, 2006: Increasing trend of extreme rain events over India in a warming environment. *Science*, **314,** 1442-1445.

Guttman, N. B., 1998: Comparing the Palmer Drought Index and the Standardized Precipitation Index. *Journal of the American Water Resources Association*, **34,** 113-121.

Guttman, N. B., 1999: Accepting the standardized precipitation index: a calculation algorithm. *Journal of the American Water Resources Association*, **35,** 311-322.

Gutzler, D. S., and T. O. Robbins, 2010: Climate variability and projected change in the western United States: regional downscaling and drought statistics. *Climate Dynamics*, **37,** 835-849.

Hargreaves, G. H., and Z. A. Samani, 1985: Reference crop evapotranspiration from temperature. *Applied engineering in agriculture*, **1,** 96-99.

IPCC, 2013: What is a GCM? Accessed 12 July 2016. [Available online at http://www.ipcc-data.org/guidelines/pages/gcm_guide.html.]

Keyantash, J., and J. A. Dracup, 2002: The quantification of drought: an evaluation of drought indices. *Bulletin of the American Meteorological Society*, **83,** 1167-1180.

Kharin, V. V., F. Zwiers, X. Zhang, and M. Wehner, 2013: Changes in temperature and precipitation extremes in the CMIP5 ensemble. *Climatic change*, **119,** 345-357.

Lee, J., 2015: Texas, Oklahoma floodwaters contain sewage, other pollutants. National Geographic, Accessed 15 Nov. 2016. [Available online at http://news.nationalgeographic.com/2015/05/150528-floodwater-chemicals-texas-oklahoma-environment-science-runoff/.]

Li, H., J. Sheffield, and E. F. Wood, 2010: Bias correction of monthly precipitation and temperature fields from Intergovernmental Panel on Climate Change AR4 models using equidistant quantile matching. *Journal of Geophysical Research: Atmospheres*, **115**.

Liu, B., J. Chen, X. Chen, Y. Lian, and L. Wu, 2013: Uncertainty in determining extreme precipitation thresholds. *Journal of Hydrology*, **503,** 233-245.

Lockwood, J. G., 1999: Is potential evapotranspiration and its relationship with actual evapotranspiration sensitive to elevated atmospheric CO2 levels? *Climatic Change*, **41,** 193-212.

Lu, J., G. Sun, S. G. McNulty, and D. M. Amatya, 2005: A comparison of six potential

evapotranspiration methods for regional use in the southeastern United States. *Journal of the American Water Resources Association*, **41,** 621-633.

Lupo, A., and W. Kininmonth, 2013: Global climate models and their limitations. *Climate Change Reconsidered II: Physical Science*, C.D. Idso, R.M. Carter and S.F. Singer, Eds., The Heartland Institute, 7-148.

Malewitz, J., 2013: Red River showdown: Texas-Oklahoma water war could reverberate across US. *McClatchy - Tribune Business News*, Tribune Content Agency LLC.

Maurer, E. P., and Coauthors, 2014: An enhanced archive facilitating climate impacts and adaptation analysis. *Bulletin of the American Meteorological Society*, **95,** 1011-1019.

McKee, T. B., N. J. Doesken, and J. Kleist, 1993: Drought monitoring with multiple timescales. *Eighth Conf. on Applied Climatology*, Amer. Meteor. Soc., 179-184.

Michelangeli, P. A., M. Vrac, and H. Loukos, 2009: Probabilistic downscaling approaches: application to wind cumulative distribution functions. *Geophysical Research Letters*, **36**.

National Research Council. 2011. *Global change and extreme hydrology: testing conventional wisdom*. Washington, DC: The National Academies Press. doi:https://doi.org/10.17226/13211.

NOAA, 2016: National Weather Service glossary. Accessed 15 March 2016. [Available online at http://w1.weather.gov/glossary.]

NOAA National Centers for Environmental information, 2017: Climate at a glance:

U.S. time series, Palmer Drought Severity Index (PDSI). Accessed 7, July 2017. [Available online at http://www.ncdc.noaa.gov/cag/.]

Oklahoma Climatological Survey, 2015: Oklahoma Monthly Climate Summary June 2015. Accessed 10 Aug. 2017. [Available online at climate.ok.gov/summaries/monthly/2015/MCS_June_2015.pdf.]

Oklahoma Climatological Survey, 2017: Precipitation history: Annual, South Central. Accessed 6 July 2017. [Available online at http://climate.ok.gov/index.php/climate/climate_trends/precipitation_history_annual_statewide/CD08/prcp/Annual.]

Palmer, W. C., 1965: *Meteorological drought.* Vol. 30, US Department of Commerce, Weather Bureau Washington, DC, USA.

Prudhomme, C., N. Reynard, and S. Crooks, 2002: Downscaling of global climate models for flood frequency analysis: where are we now? *Hydrological Processes*, **16,** 1137-1150.

R Core Team (2016). R: A language and environment for statistical computing. R Foundation for Statistical Computing, Vienna, Austria. URL https://www.R-project.org/.

Scanlon, B. R., I. Duncan, and R. C. Reedy, 2013: Drought and the water–energy nexus in Texas. *Environmental Research Letters*, **8,** 045033.

Schmidli, J., C. Frei, and P.L. Vidale, 2006: Downscaling from GCM precipitation: A benchmark for dynamical and statistical downscaling methods. *International Journal of Climatology*, **26,** 679-689.

Schoof, J. T., and S. M. Robeson, 2016: Projecting changes in regional temperature and

precipitation extremes in the United States. *Weather and Climate Extremes*, **11,** 28-40.

Shafer, M., D. Ojima, J. M. Antle, D. Kluck, R. A. McPherson, S. Petersen, B. Scanlon, and K. Sherman, 2014: Ch. 19: Great Plains. *Climate change impacts in the United States: the Third National Climate Assessment*, J. M. Melillo, Terese (T.C.) Richmond, and G. W. Yohe, Eds., U.S. Global Change Research Program, 441-461. doi:10.7930/J0D798BC.

Sillmann, J., V. Kharin, X. Zhang, F. Zwiers, and D. Bronaugh, 2013: Climate extremes indices in the CMIP5 multimodel ensemble: Part 1. Model evaluation in the present climate. *Journal of Geophysical Research: Atmospheres*, **118,** 1716-1733.

*Tarrant Regional Water Dist.* v. *Herrmann,* 569 U. S. ___ (2013).

Taylor, J., K. man Lai, M. Davies, D. Clifton, I. Ridley, and P. Biddulph, 2011: Flood management: prediction of microbial contamination in large-scale floods in urban environments. *Environment international*, **37,** 1019-1029.

Taylor, K. E., R. J. Stouffer, and G. A. Meehl, 2012: An overview of CMIP5 and the experiment design. *Bulletin of the American Meteorological Society*, **93,** 485-498.

Thornthwaite, C. W., 1948: An approach toward a rational classification of climate. *Geographical Review*, **38,** 55-94.

Thrasher, B., J. Xiong, W. Wang, F. Melton, A. Michaelis, and R. Nemani, 2013: Downscaled climate projections suitable for resource managers. *EOS, Trans. AGU*, **94,** 321-323.

Tryhorn, L., and A. DeGaetano, 2011: A comparison of techniques for downscaling extreme precipitation over the Northeastern United States. *International Journal of Climatology*, **31,** 1975-1989.

UCAR, 2010: Flash flood early warning system reference guide. UCAR, ISBN 978-0-615-37421-5.

UCAR, 2011: Climate modeling. Accessed 10 July 2016. [Available online at http://scied.ucar.edu/longcontent/climate-modeling.]

UCAR, 2014: Standardized Precipitation Evapotranspiration Index (SPEI) expert guidance. UCAR, Accessed 27 March 2016. [Available online at https://climatedataguide.ucar.edu/climate-data/standardized-precipitation-evapotranspiration-index-spei.]

USGS, 2017: The National Map Small Scale. Accessed 6 July 2017. [Available online at https://nationalmap.gov/small_scale/printable/climatemap.html#list.]

Vavrus, S. J., M. Notaro, and D. J. Lorenz, 2015: Interpreting climate model projections of extreme weather events. *Weather and Climate Extremes*, **10,** 10-28.

Venkataraman, K., S. Tummuri, A. Medina, and J. Perry, 2016: 21st century drought outlook for major climate divisions of Texas based on CMIP5 multimodel ensemble: Implications for water resource management. *Journal of Hydrology*, **534,** 300-316.

Vicente-Serrano, S. M., S. Beguería, J. I. López-Moreno, M. Angulo, and A. El Kenawy, 2010: A new global 0.5 gridded dataset (1901–2006) of a multiscalar drought index: comparison with current drought index datasets based on the Palmer Drought Severity Index. *Journal of Hydrometeorology*, **11,** 1033-1043.

Villarini, G., J. A. Smith, and G. A. Vecchi, 2013: Changing frequency of heavy rainfall over the central United States. *Journal of Climate*, **26,** 351-357.

Watanabe, M., and Coauthors, 2010: Improved climate simulation by MIROC5: mean states, variability, and climate sensitivity. *Journal of Climate*, **23,** 6312-6335.

Wilby, R. L., S. P. Charles, E. Zorita, B. Timbal, P. Whetton, and L. O. Mearns, 2004: Guidelines for use of climate scenarios developed from statistical downscaling methods. Data Distribution Centre of the Intergovernmental Panel on Climate Change.

Wilhite, D. A., 2000: Drought as a natural hazard: concepts and definitions. *Drought: A Global Assessment*, Routledge.

Wilhite, D. A., and M. H. Glantz, 1985: Understanding the drought phenomenon: the role of definitions. *Water International*, **10,** 111.

Wuebbles, D., and Coauthors, 2014: CMIP5 climate model analyses: climate extremes in the United States. *Bulletin of the American Meteorological Society*, **95,** 571-583.

Xue, X., and Coauthors, 2015: New multisite cascading calibration approach for hydrological models: Case study in the Red River Basin using the VIC model. *Journal of Hydrologic Engineering*, **21,** 05015019.

Zhai, P., X. Zhang, H. Wan, and X. Pan, 2005: Trends in total precipitation and frequency of daily precipitation extremes over China. *Journal of climate*, **18,** 1096-1108.

Zhang, X., L. Alexander, G. C. Hegerl, P. Jones, A. K. Tank, T. C. Peterson, B. Trewin,

and F. W. Zwiers, 2011: Indices for monitoring changes in extremes based on daily temperature and precipitation data. *Wiley Interdisciplinary Reviews: Climate Change*, **2,** 851-870.

# Chapter 4: Conclusion

Hydrologic extremes of rainfall and drought have created billions of dollars in damages and stressed water resources in the Red River Basin in the past. These events have occurred throughout the historical record; however, it is important to know how the frequency of these events is expected to vary in a changing climate so that decision makers can mitigate for these losses. Therefore, this study used statistically downscaled climate projections to determine the change in frequency of these events through the end of the 21$^{st}$ century. While global climate models provide a general idea of future conditions for water resource managers and decision makers, the coarse resolution does not compare to high-resolution statistically downscaled data (Thrasher et al. 2013). Therefore, this study introduced a dataset of statistically downscaled climate projections from three GCMs (CCSM4, MIROC5, and MPI-ESM-LR) and two downscaling techniques (CDFt and EDQM) at a 0.1-degree resolution for the Red River Basin under RCP 2.6 and RCP 8.5. The data were projected for a historical period (1961-2005) and future period (2006-2099) and included daily minimum and maximum temperature and daily precipitation.

## 1. Precipitation and Temperature

To explore the data, mean daily changes in all three climate variables were calculated between the most recent historical period of 1981-2005 and two future periods of 2046-2070 and 2075-2099 to deliver a mid-century and end-of-century analysis. The general pattern of precipitation showed mean daily precipitation declining in the western Red River Basin and increasing in the east by the end of the century. Compared to the historical period, this indicates a 15% change across the basin. In

addition, mean daily minimum and maximum temperature were projected to increase up to 7°C across the basin, especially toward the end of the century and under RCP 8.5. The mean daily minimum temperature was estimated to double for this scenario compared to historical projections. A seasonal analysis was then performed for precipitation, and we found that some seasons include more extreme values that are driving the overall trend in mean daily precipitation, especially for the end-of-century timeframe with a higher emission scenario. These results indicated that water resource managers and decision makers need to prepare for a much warmer climate with drier conditions in the west. The conditions seen in this analysis were confirmed in the literature (Shafer et al. 2014, Qiao et al. 2017).

**2. Hydrologic Extremes**

The next step of this study included an examination of future hydrologic extremes of the Red River Basin. After we examined the literature, a peak-over-threshold approach was decided for both the heavy rainfall and severe drought analyses. Heavy rainfall events were defined by the daily $90^{th}$ and $99^{th}$ percentiles of rain days in the historical period for each grid cell in the basin. Severe drought events were classified by the Standardized Precipitation Evapotranspiration Index (SPEI) value of less than or equal to -1.5 for a 1-month timescale. Using the same conditions that were previously described (three GCMs, two statistical downscaling techniques, and two RCP scenarios), the frequency of both types of events was found for the historical period and each future period. The difference between the historical and future frequency of these events was then computed in order to identify any changes in heavy rainfall and severe drought through the end of the century.

Similar to the analysis of mean daily precipitation, we discovered that the models generally projected an increase in both tiers of heavy rainfall events in the eastern Red River Basin, such as northeast Louisiana, and a decrease in the west, especially under a RCP 8.5 scenario for the end of the century. For the 99$^{th}$ percentile events, some areas in the east were projected to receive over twice as many heavy rainfall events than in the modeled historical period, which is a substantial change.

On the other hand, the most common trend for the change in severe drought events included an increase of future events in the west and a reduction in the east. For this analysis, we discovered variability between RCP scenarios and downscaling techniques, but each model tended to sustain similar spatial patterns throughout. For example, the CCSM4 model projected events in southwestern Oklahoma and north-central Texas to double by the end of the century. Meanwhile, the MPI-ESM-LR model had a smaller signal of increasing events and a widespread pattern of decreasing events had more prominence. However, the overall trend remained with an east versus west pattern of decreasing and increasing events, respectively.

The main results of this study include drier and warmer conditions with increasing severe drought events in the western Red River Basin and wetter and warmer conditions with increasing extreme rainfall events in the east. For both cases, water resources are likely to be affected. While there is uncertainty in the models, our downscaling techniques, and future emission amounts, this study aimed to provide localized information for decision makers and water resource managers in this region to be able to make more informed decisions for resilience against these life-threatening and damaging events in the future.

## 3. References

Qiao, L., C. B. Zou, C. F. Gaitán, Y. Hong, and R. A. McPherson, 2017: Analysis of precipitation projections over the climate gradient of the Arkansas Red River Basin. *Journal of Applied Meteorology and Climatology*, **56,** 1325-1336.

Shafer, M., D. Ojima, J. M. Antle, D. Kluck, R. A. McPherson, S. Petersen, B. Scanlon, and K. Sherman, 2014: Ch. 19: Great Plains. *Climate change impacts in the United States: the Third National Climate Assessment*, J. M. Melillo, Terese (T.C.) Richmond, and G. W. Yohe, Eds., U.S. Global Change Research Program, 441-461. doi:10.7930/J0D798BC.

Thrasher, B., J. Xiong, W. Wang, F. Melton, A. Michaelis, and R. Nemani, 2013: Downscaled climate projections suitable for resource managers. *EOS, Trans. AGU*, **94,** 321-323.

# Appendix A: Complete List of Figures

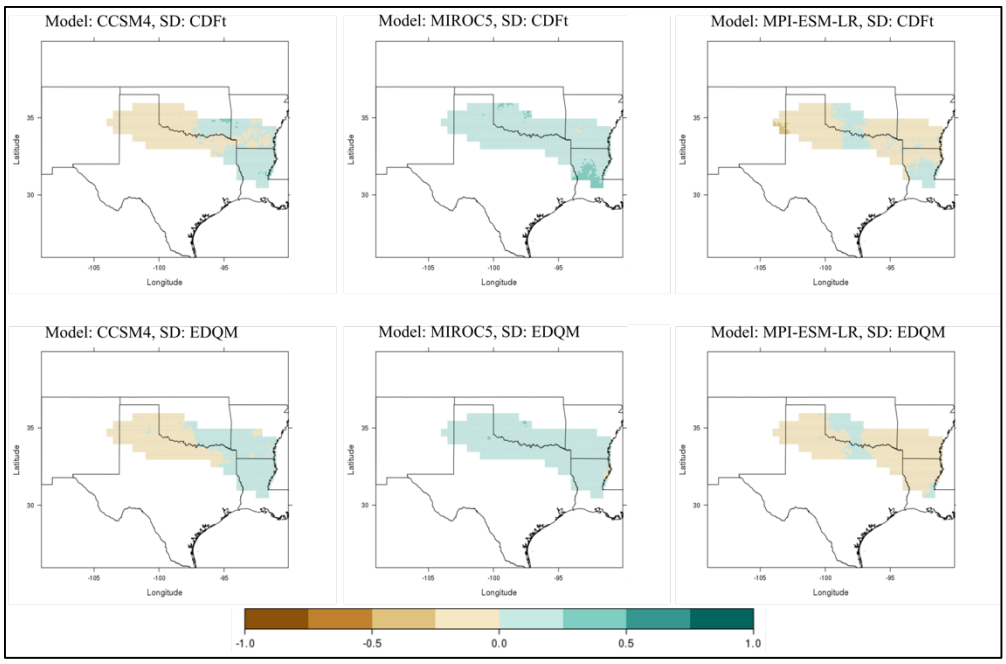


**Figure A1. Difference fields for mean daily precipitation (in mm/day) between historical (1981-2005) and mid-century (2046-2070) timeframes for RCP 2.6. Columns represent the GCMs (CCSM4, MIROC5, and MPI-ESM-LR, from left to right respectively); rows represent downscaling methods, with CDFt on top and EDQM on bottom. Brown and tan colors represent future decreases in precipitation compared to the historical period; blue-green colors represent future increases in precipitation.**

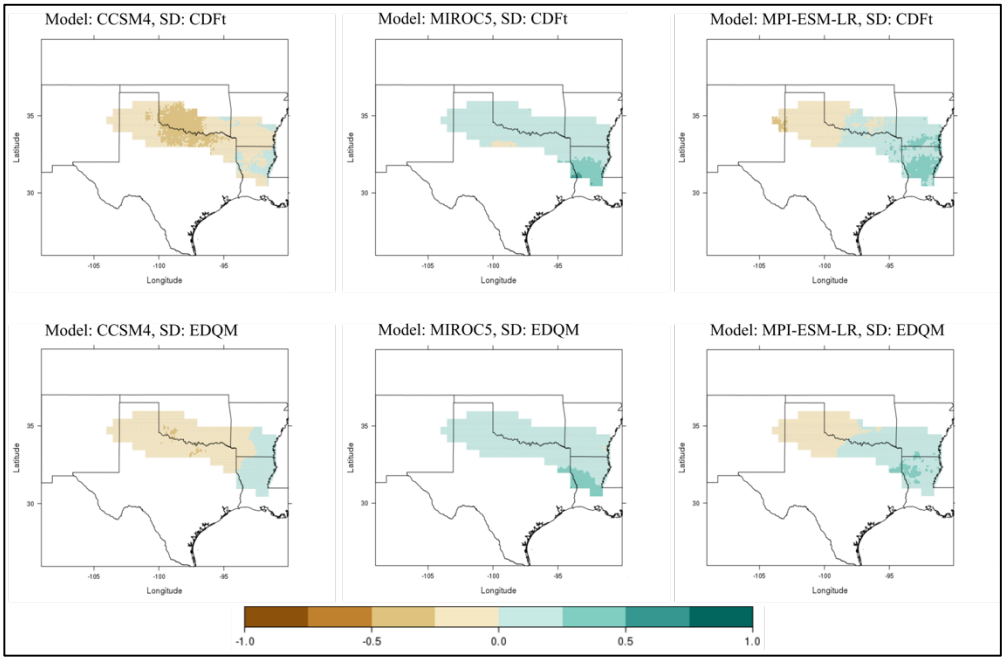


**Figure A2. Difference fields for mean daily precipitation (in mm/day) between historical (1981-2005) and end-of-century (2075-2099) timeframes for RCP 2.6. Columns represent the GCMs (CCSM4, MIROC5, and MPI-ESM-LR, from left to right respectively); rows represent downscaling methods, with CDFt on top and EDQM on bottom. Brown and tan colors represent future decreases in precipitation compared to the historical period; blue-green colors represent future increases in precipitation.**

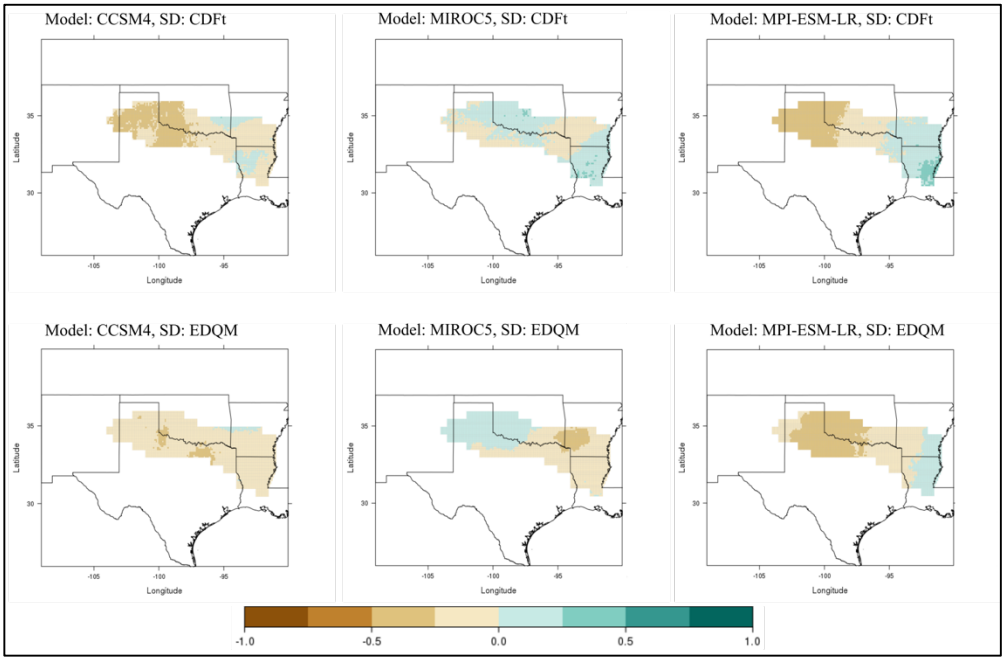


**Figure A3. Difference fields for mean daily precipitation (in mm/day) between historical (1981-2005) and mid-century (2046-2070) timeframes for RCP 8.5. Columns represent the GCMs (CCSM4, MIROC5, and MPI-ESM-LR, from left to right respectively); rows represent downscaling methods, with CDFt on top and EDQM on bottom. Brown and tan colors represent future decreases in precipitation compared to the historical period; blue-green colors represent future increases in precipitation.**

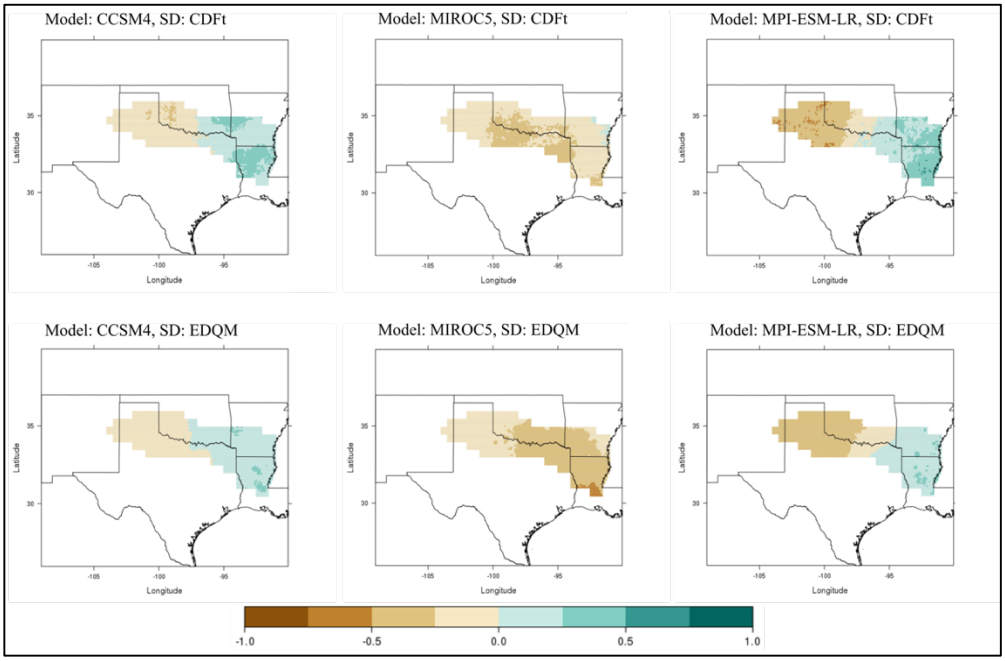


**Figure A4. Difference fields for mean daily precipitation (in mm/day) between historical (1981-2005) and end-of-century (2075-2099) timeframes for RCP 8.5. Columns represent the GCMs (CCSM4, MIROC5, and MPI-ESM-LR, from left to right respectively); rows represent downscaling methods, with CDFt on top and EDQM on bottom. Brown and tan colors represent future decreases in precipitation compared to the historical period; blue-green colors represent future increases in precipitation.**

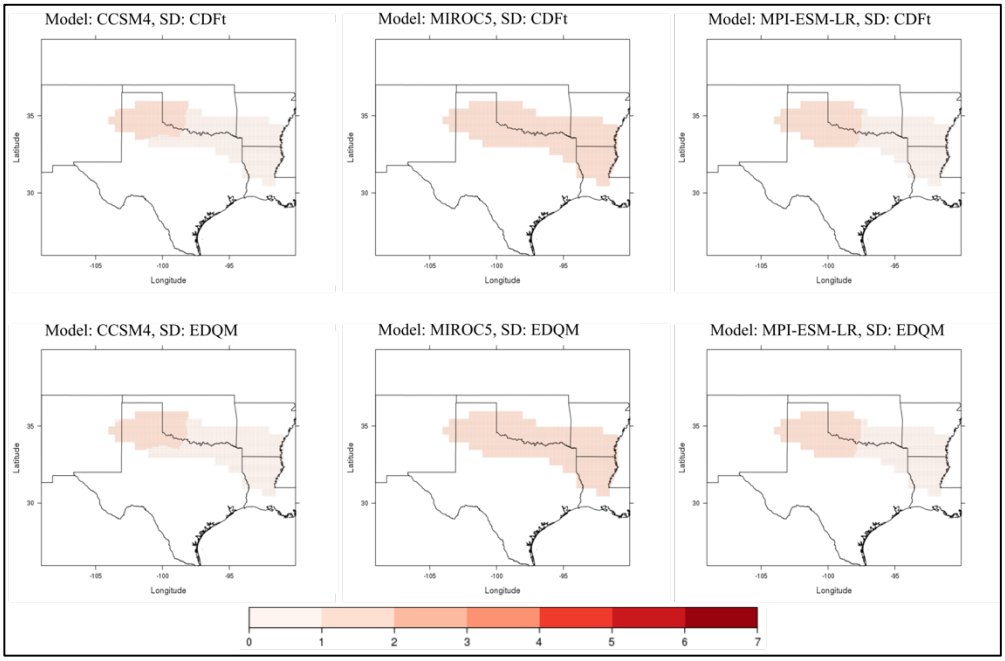


**Figure A5. Difference fields for mean daily minimum temperature (°C) between historical (1981-2005) and mid-century (2046-2070) timeframes for RCP 2.6. Columns represent the GCMs (CCSM4, MIROC5, and MPI-ESM-LR, from left to right respectively); rows represent downscaling methods, with CDFt on top and EDQM on bottom. Darker shades of red represent higher minimum temperature values.**

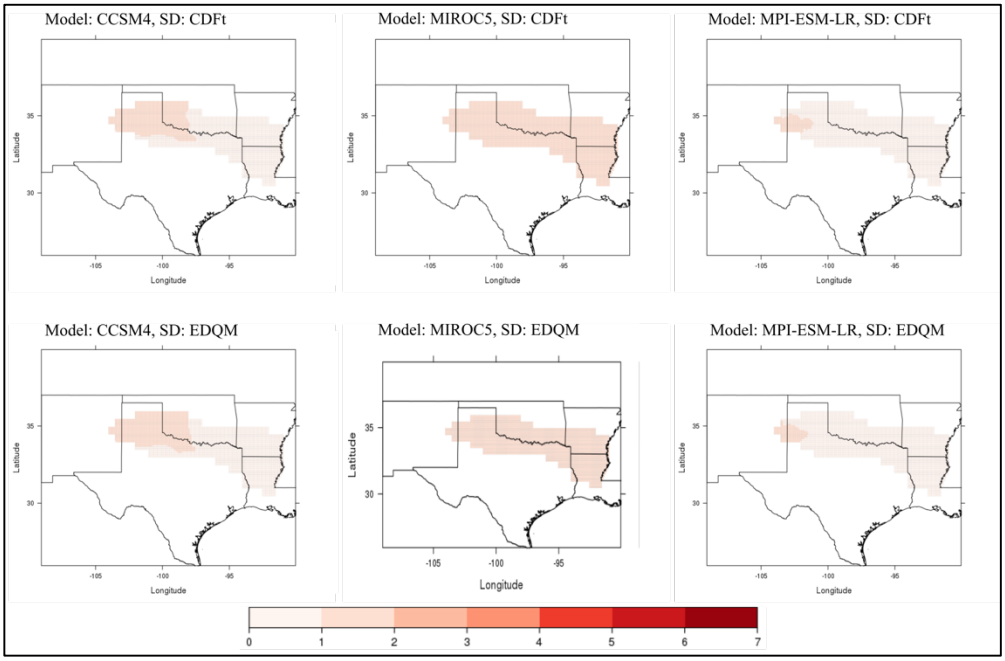


**Figure A6. Difference fields for mean daily minimum temperature (°C) between historical (1981-2005) and end-of-century (2075-2099) timeframes for RCP 2.6. Columns represent the GCMs (CCSM4, MIROC5, and MPI-ESM-LR, from left to right respectively); rows represent downscaling methods, with CDFt on top and EDQM on bottom. Darker shades of red represent higher minimum temperature values.**

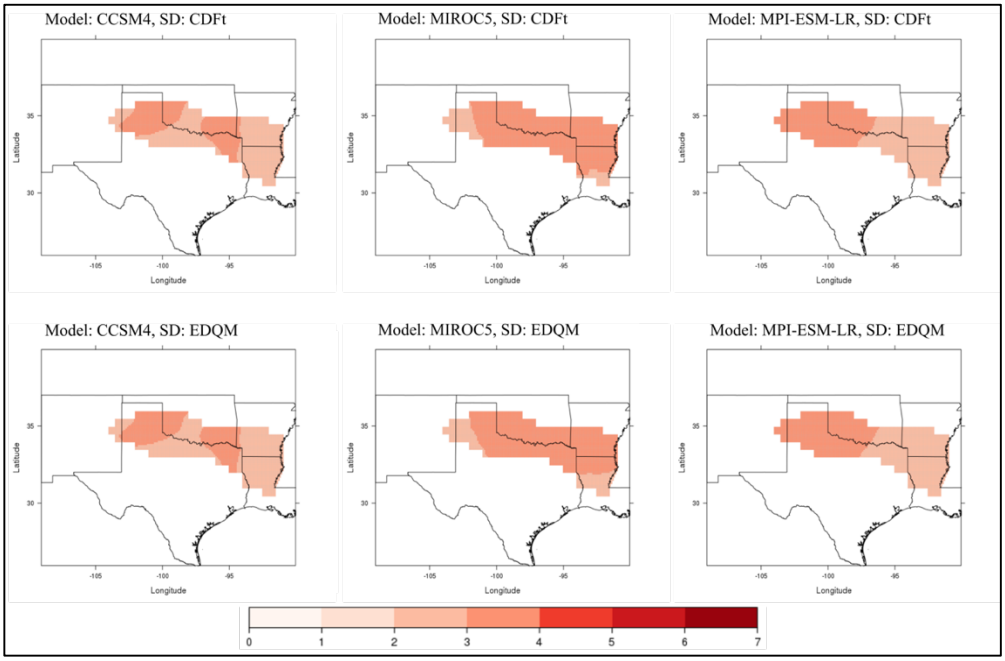


**Figure A7. Difference fields for mean daily minimum temperature (°C) between historical (1981-2005) and mid-century (2046-2070) timeframes for RCP 8.5. Columns represent the GCMs (CCSM4, MIROC5, and MPI-ESM-LR, from left to right respectively); rows represent downscaling methods, with CDFt on top and EDQM on bottom. Darker shades of red represent higher minimum temperature values.**

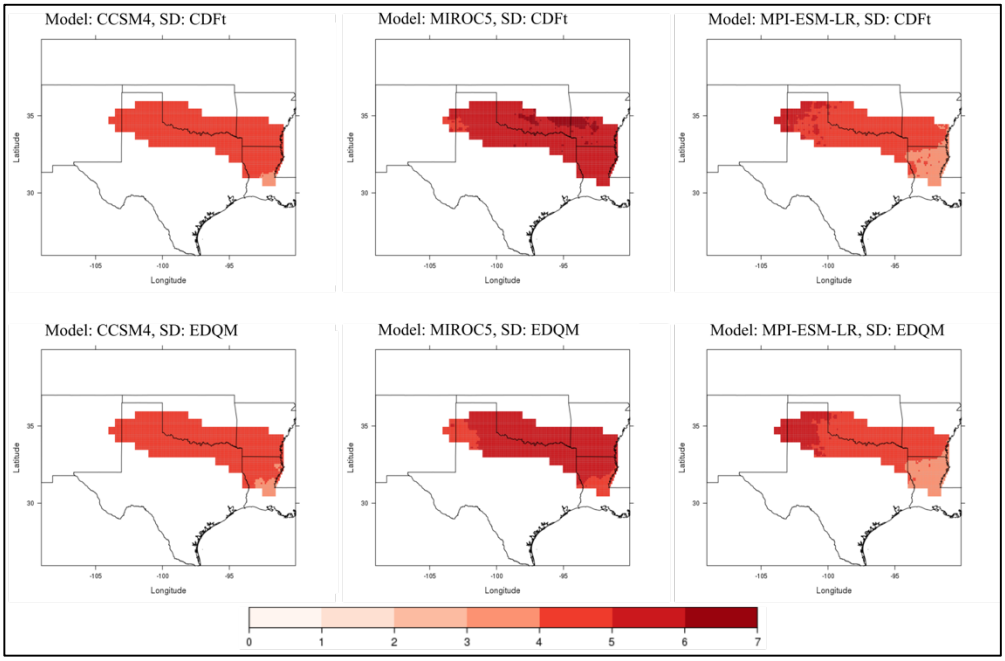


**Figure A8. Difference fields for mean daily minimum temperature (°C) between historical (1981-2005) and end-of-century (2075-2099) timeframes for RCP 8.5. Columns represent the GCMs (CCSM4, MIROC5, and MPI-ESM-LR, from left to right respectively); rows represent downscaling methods, with CDFt on top and EDQM on bottom. Darker shades of red represent higher minimum temperature values.**

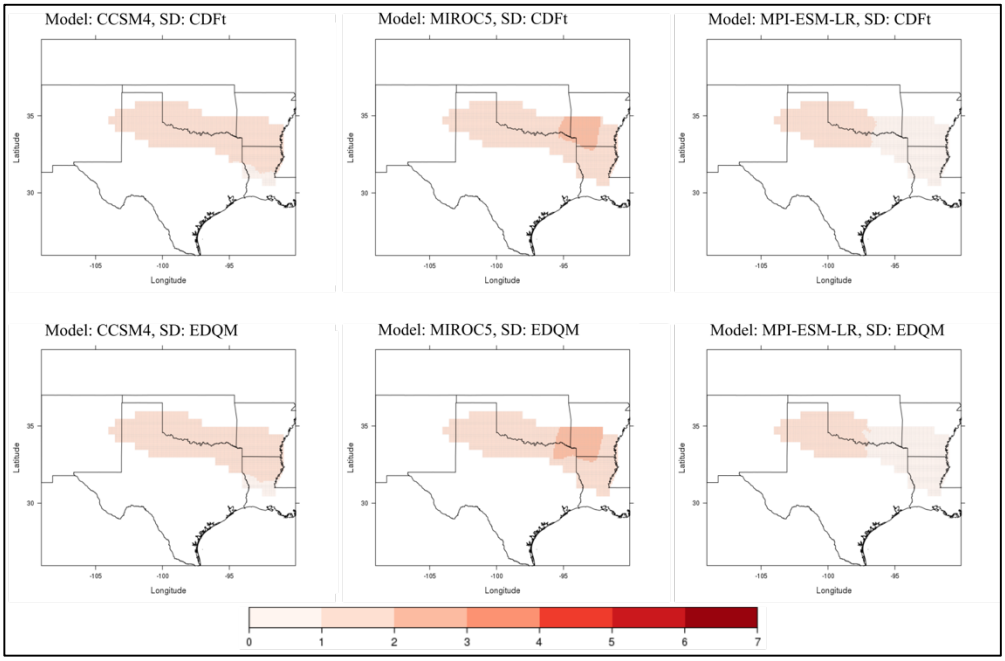


**Figure A9. Difference fields for mean daily maximum temperature (°C) between historical (1981-2005) and mid-century (2046-2070) timeframes for RCP 2.6. Columns represent the GCMs (CCSM4, MIROC5, and MPI-ESM-LR, from left to right respectively); rows represent downscaling methods, with CDFt on top and EDQM on bottom. Darker shades of red represent higher minimum temperature values.**

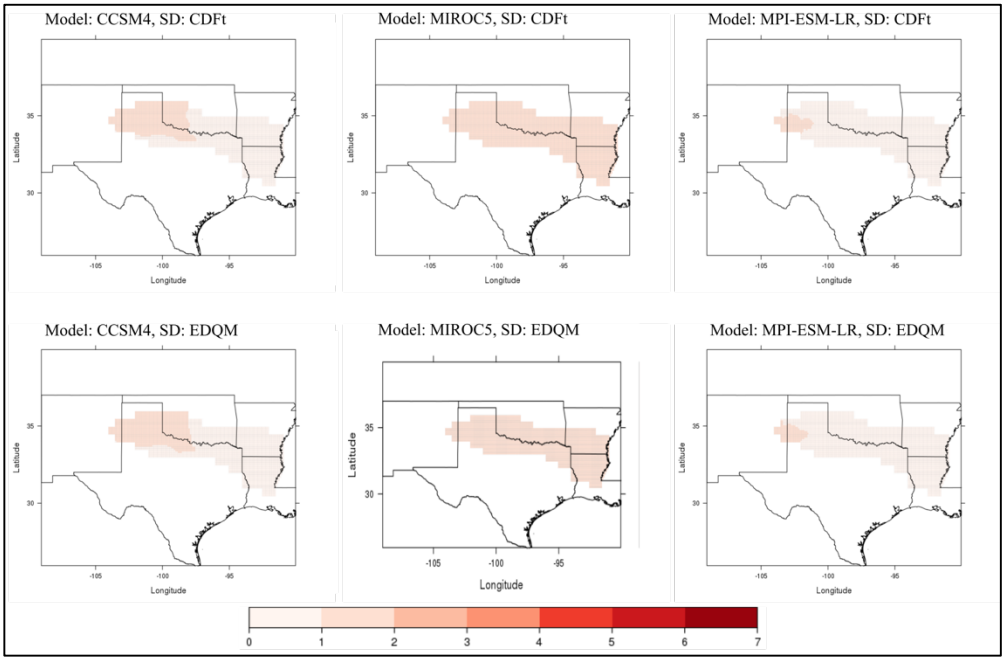


**Figure A10. Difference fields for mean daily maximum temperature (°C) between historical (1981-2005) and end-of-century (2075-2099) timeframes for RCP 2.6. Columns represent the GCMs (CCSM4, MIROC5, and MPI-ESM-LR, from left to right respectively); rows represent downscaling methods, with CDFt on top and EDQM on bottom. Darker shades of red represent higher minimum temperature values.**

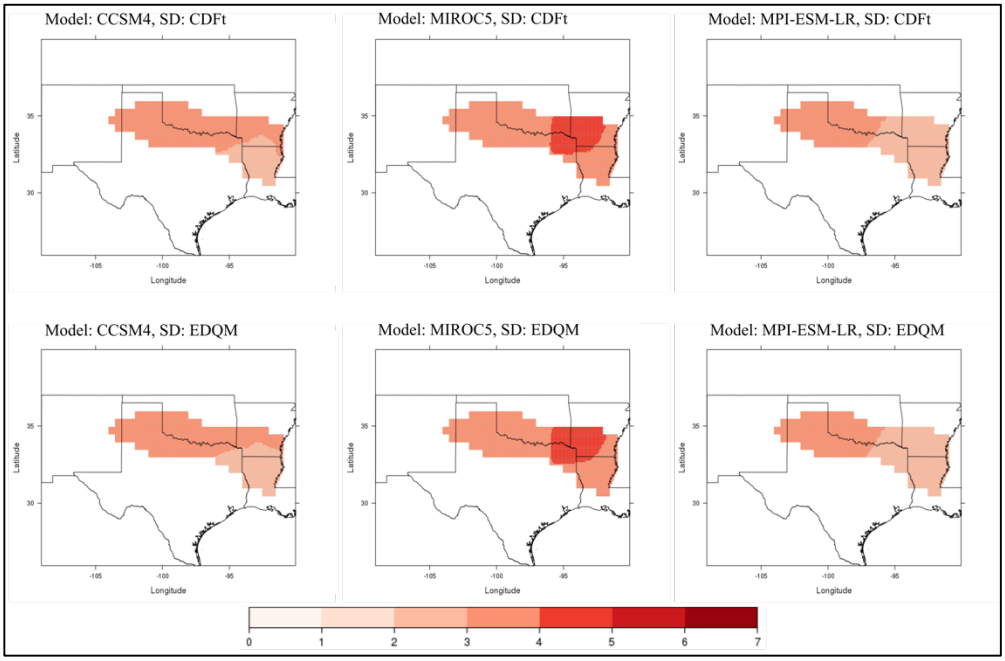


**Figure A11. Difference fields for mean daily maximum temperature (°C) between historical (1981-2005) and mid-century (2046-2070) timeframes for RCP 8.5. Columns represent the GCMs (CCSM4, MIROC5, and MPI-ESM-LR, from left to right respectively); rows represent downscaling methods, with CDFt on top and EDQM on bottom. Darker shades of red represent higher minimum temperature values.**

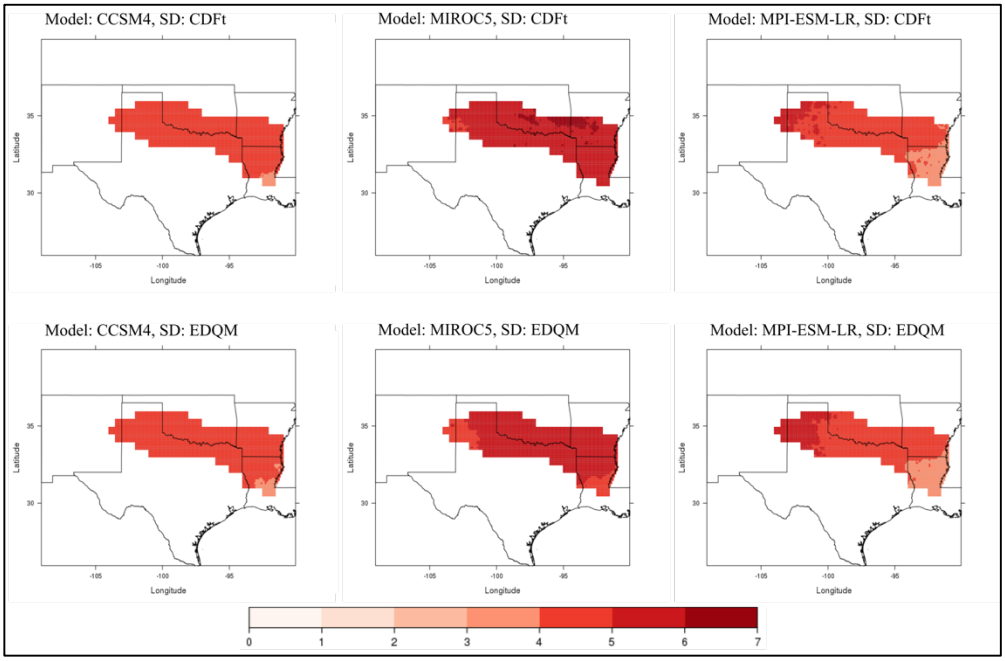


**Figure A12. Difference fields for mean daily maximum temperature (°C) between historical (1981-2005) and end-of-century (2075-2099) timeframes for RCP 8.5. Columns represent the GCMs (CCSM4, MIROC5, and MPI-ESM-LR, from left to right respectively); rows represent downscaling methods, with CDFt on top and EDQM on bottom. Darker shades of red represent higher minimum temperature values.**

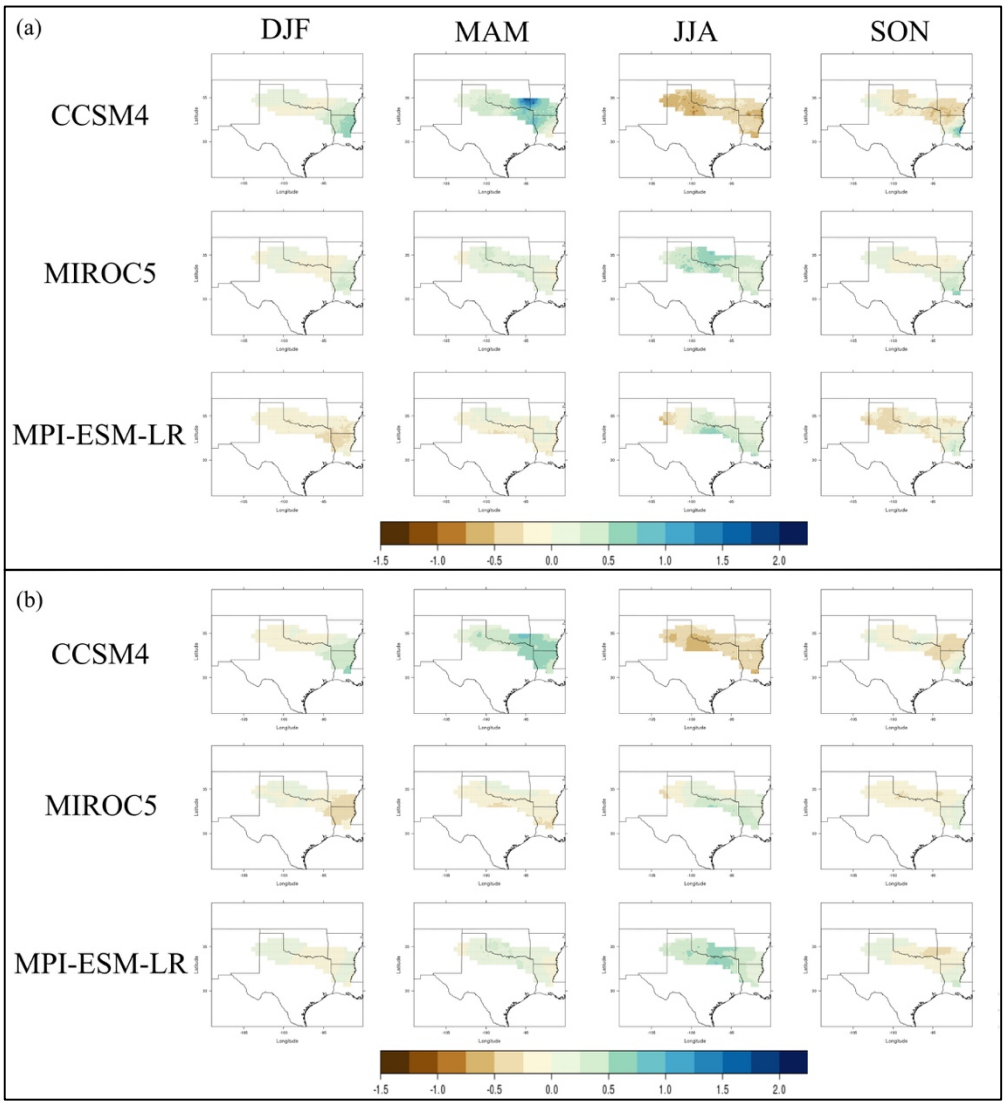


**Figure A13. Difference field in seasonal changes in mean daily precipitation (mm/day) between the historical (1981-2005) and mid-century (2046-2070) timeframes for RCP 2.6 using the (a) CDFt downscaling technique and (b) EDQM technique. Columns represent seasons (DJF, MAM, JJA, SON). Brown colors represent a decrease in daily precipitation and blues represent an increase.**

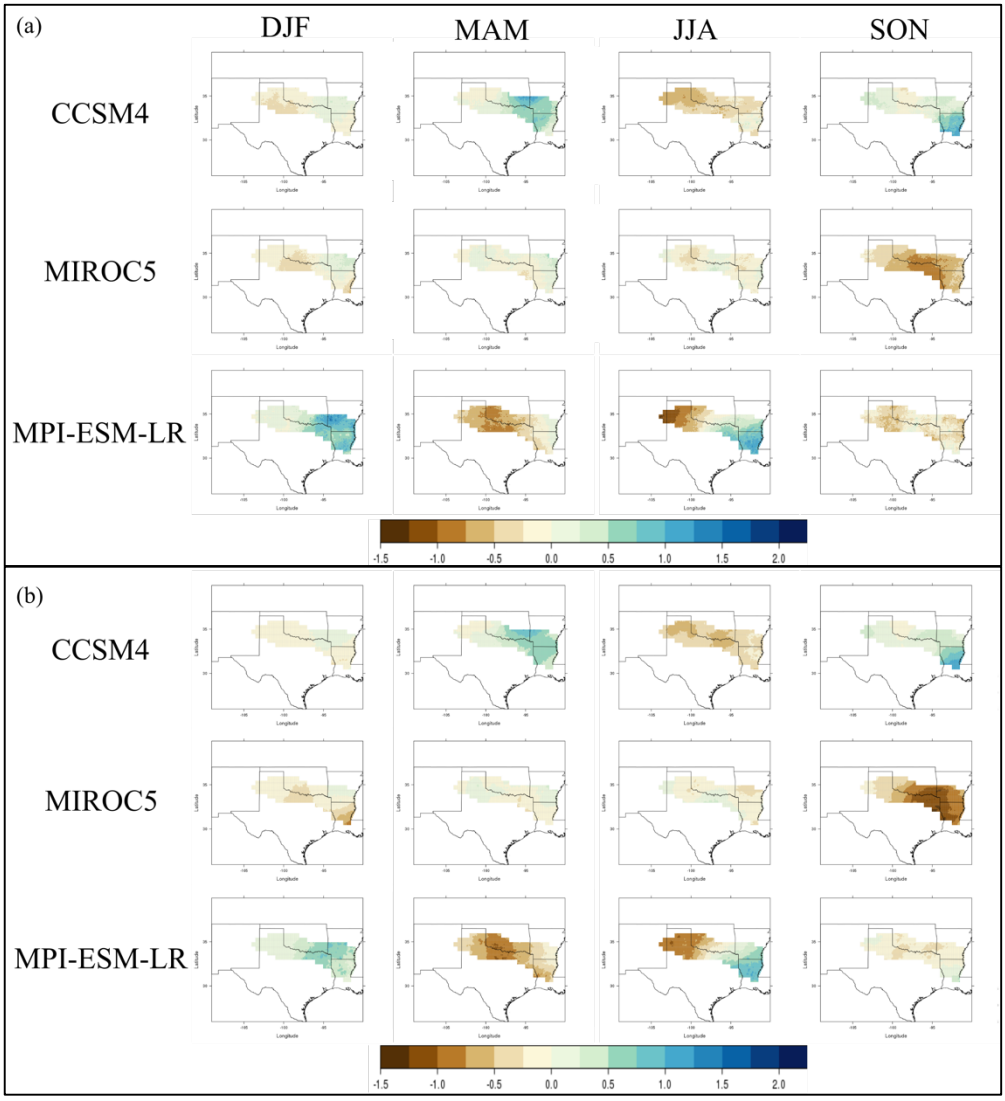


**Figure A14. Difference field in seasonal changes in mean daily precipitation (mm/day) between the historical (1981-2005) and end-of-century (2075-2099) timeframes for RCP 8.5 using the (a) CDFt downscaling technique and (b) EDQM technique. Columns represent seasons (DJF, MAM, JJA, SON). Brown colors represent a decrease in daily precipitation and blues represent an increase.**

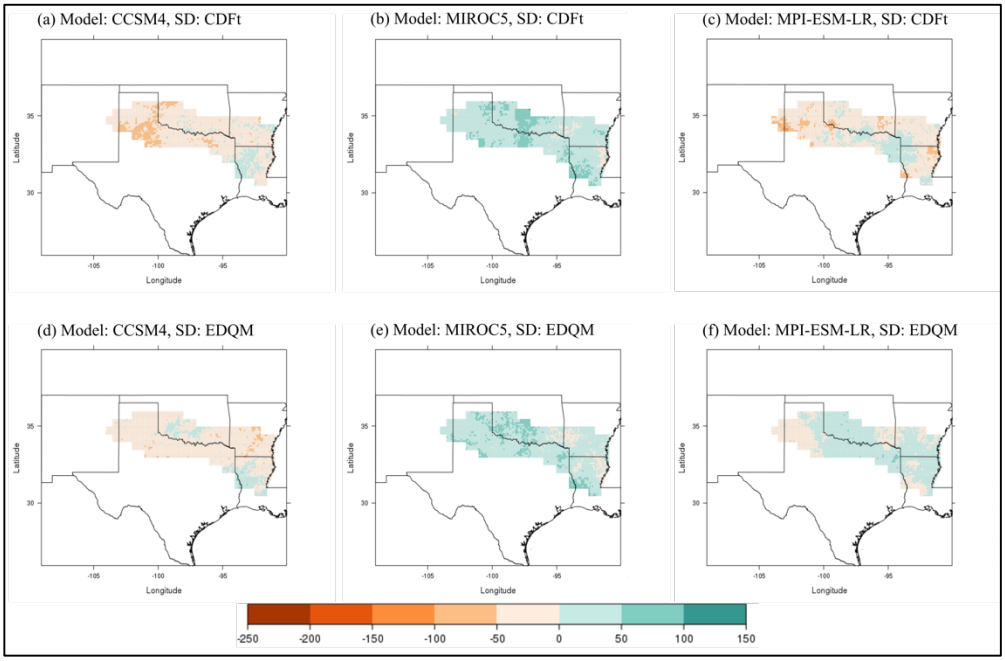


**Figure A15. Change in 25-year total frequency of all heavy rainfall days over 25 years at the 90th percentile between the historical period (1981-2005) and mid-century period (2046-2070) under a RCP 2.6 scenario. Orange colors represent a decrease in events and blue/greens represent an increase.**

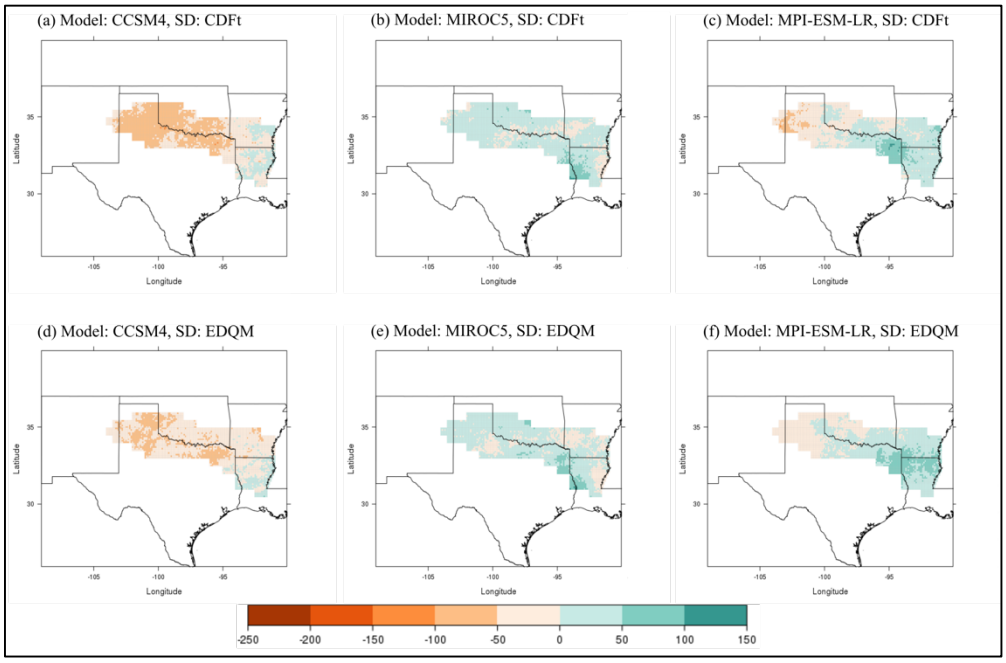


**Figure A16. Change in 25-year total frequency of all heavy rainfall days over 25 years at the 90th percentile between the historical period (1981-2005) and end-of-century period (2075-2099) under a RCP 2.6 scenario. Orange colors represent a decrease in events and blue/greens represent an increase.**

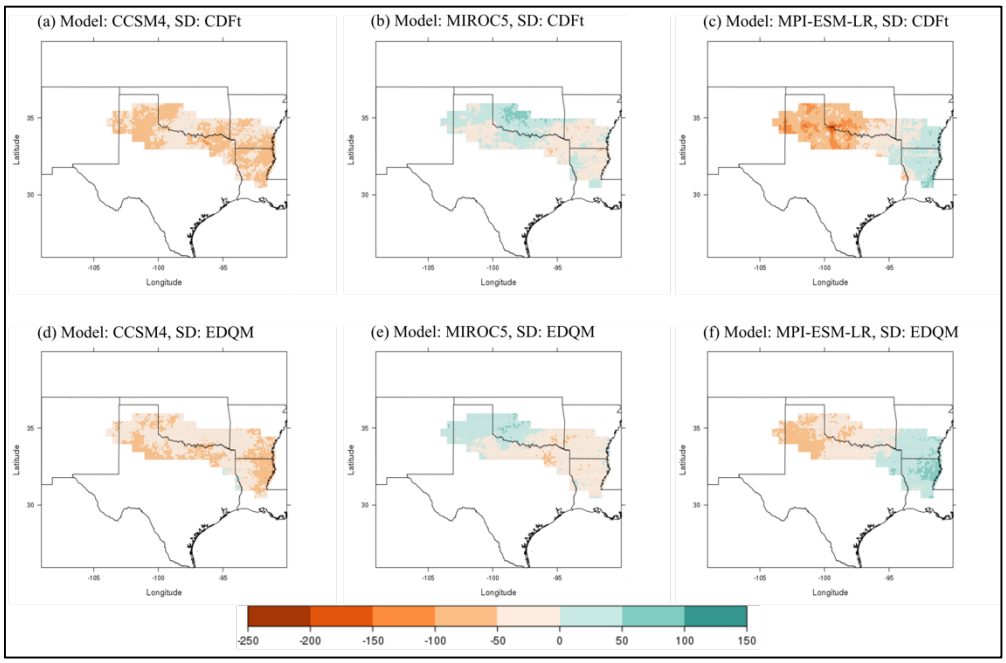


**Figure A17. Change in 25-year total frequency of all heavy rainfall days over 25 years at the 90th percentile between the historical period (1981-2005) and mid-century period (2046-2070) under a RCP 8.5 scenario. Orange colors represent a decrease in events and blue/greens represent an increase.**

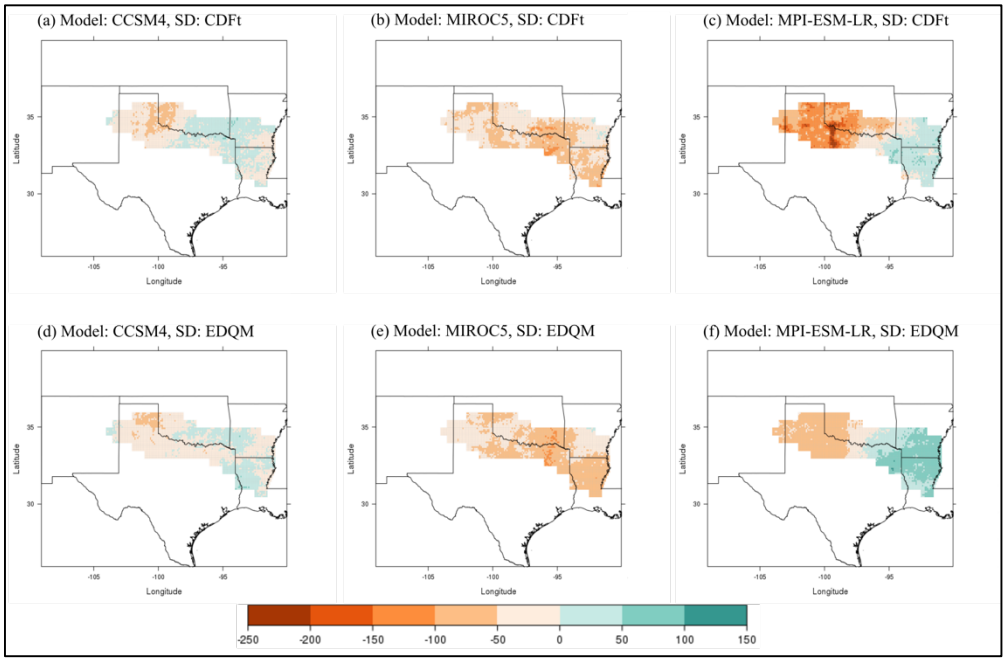


**Figure A18. Change in 25-year total frequency of all heavy rainfall days over 25 years at the 90th percentile between the historical period (1981-2005) and end-of-century period (2075-2099) under a RCP 8.5 scenario. Orange colors represent a decrease in events and blue/greens represent an increase.**

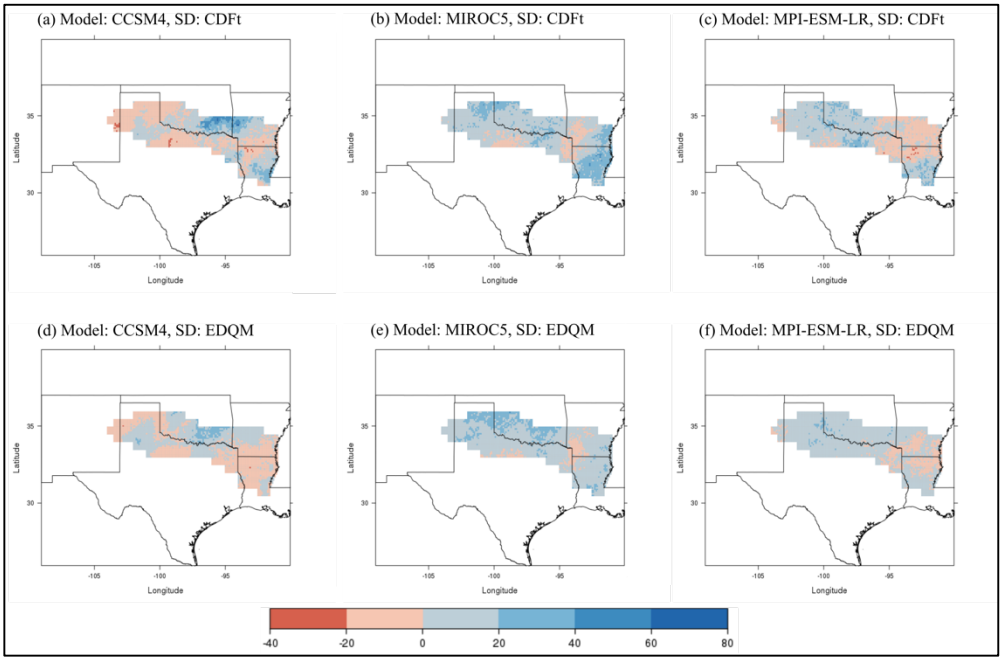


**Figure A19. Change in 25-year total frequency of all heavy rainfall days over 25 years at the 99$^{th}$ percentile between the historical period (1981-2005) and mid-century period (2046-2070) under a RCP 2.6 scenario. Red colors represent a decrease in events and blues represent an increase.**

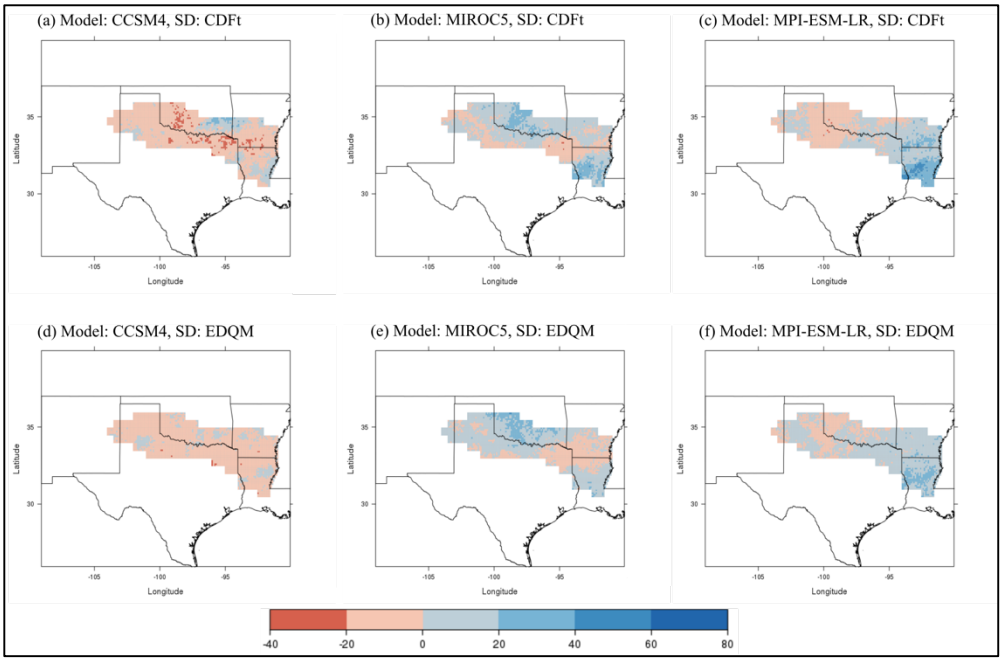


**Figure A20. Change in 25-year total frequency of all heavy rainfall days over 25 years at the 99$^{th}$ percentile between the historical period (1981-2005) and end-of-century period (2075-2099) under a RCP 2.6 scenario. Red colors represent a decrease in events and blues represent an increase.**

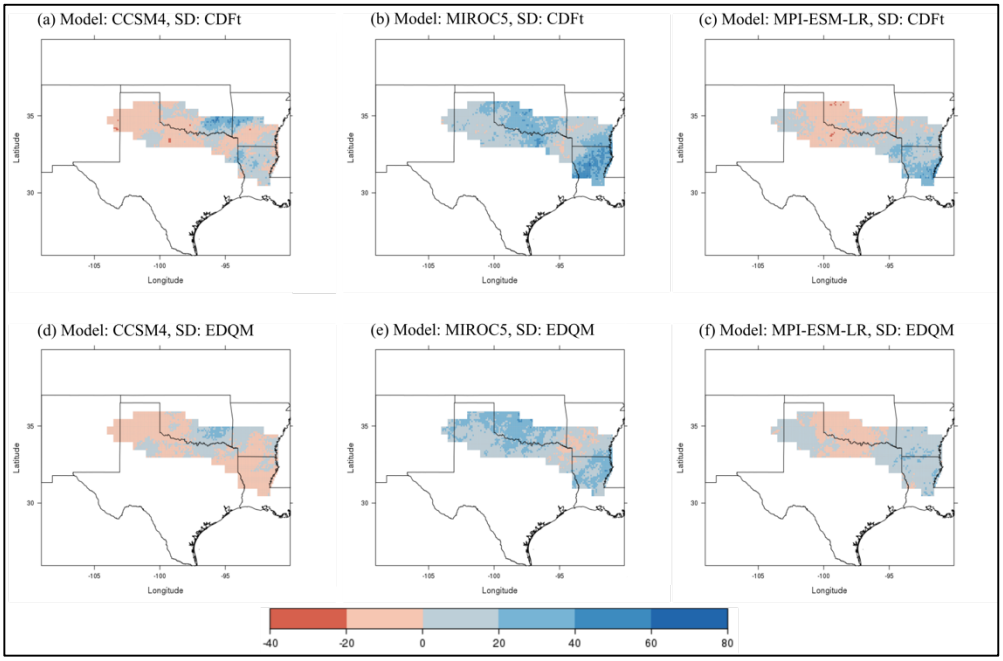


**Figure A21. Change in 25-year total frequency of all heavy rainfall days over 25 years at the 99$^{th}$ percentile between the historical period (1981-2005) and mid-century period (2046-2070) under a RCP 8.5 scenario. Red colors represent a decrease in events and blues represent an increase.**

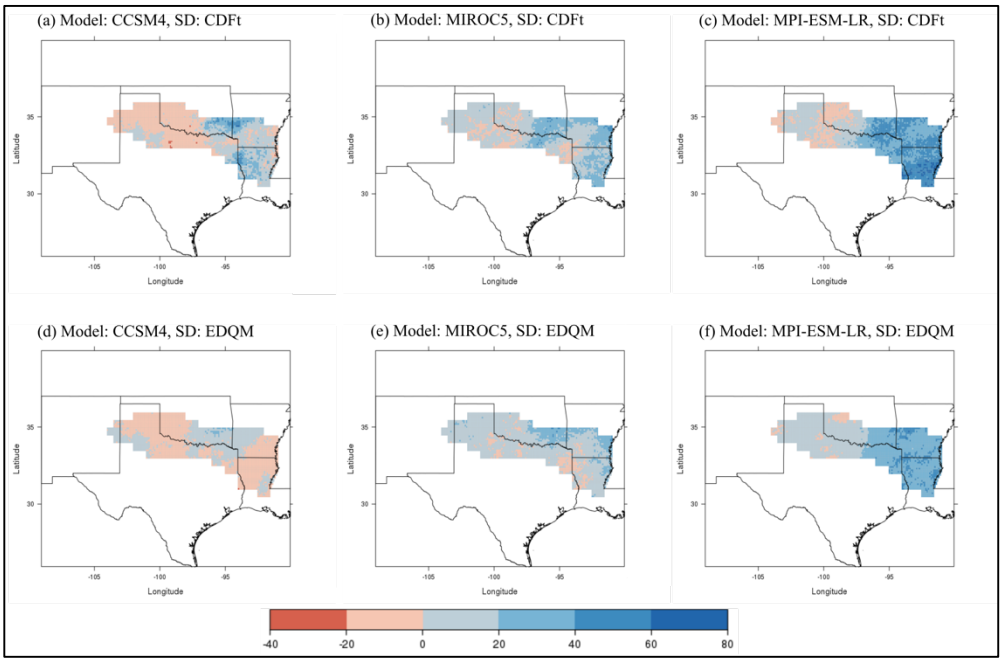


**Figure A22. Change in 25-year total frequency of all heavy rainfall days over 25 years at the 99$^{th}$ percentile between the historical period (1981-2005) and end-of-century period (2075-2099) under a RCP 8.5 scenario. Red colors represent a decrease in events and blues represent an increase.**

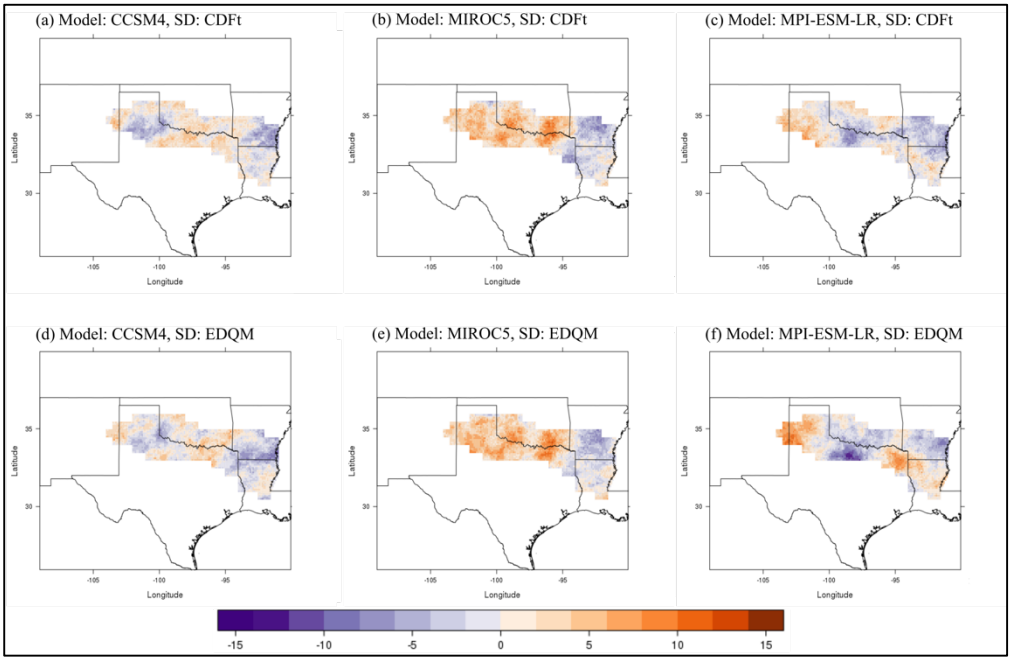


**Figure A23. Change in 25-year total frequency of severe drought at a 1-month timescale between the historical period (1981-2005) and mid-century period (2046-2070) under a RCP 2.6 scenario. Purple colors represent a decrease in events and oranges represent an increase.**

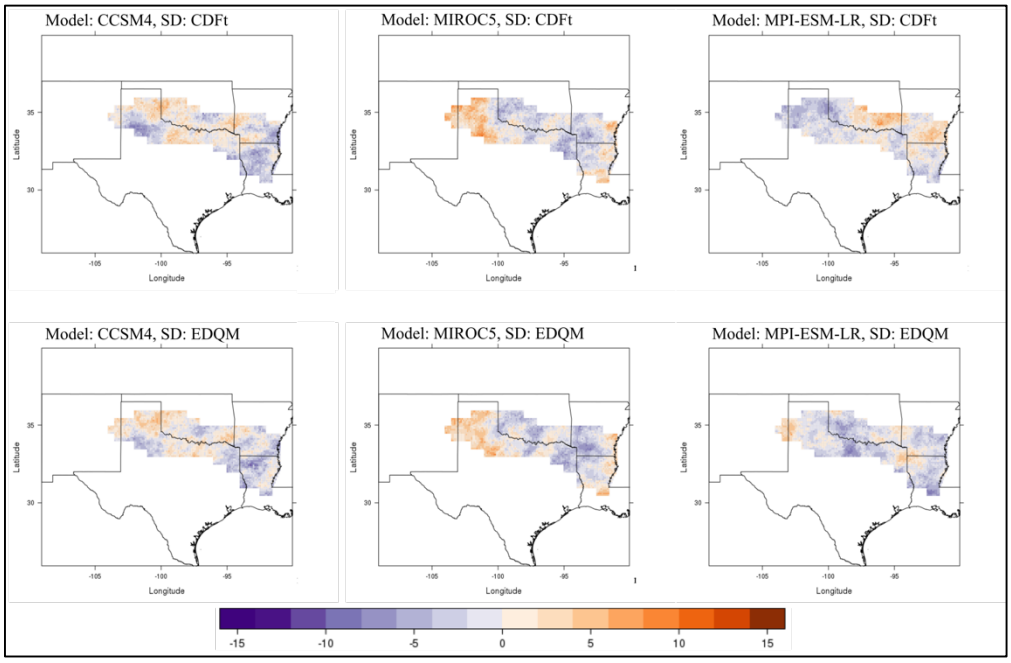


**Figure A24. Change in 25-year total frequency of severe drought at a 1-month timescale between the historical period (1981-2005) and end-of-century period (2075-2099) under a RCP 2.6 scenario. Purple colors represent a decrease in events and oranges represent an increase.**

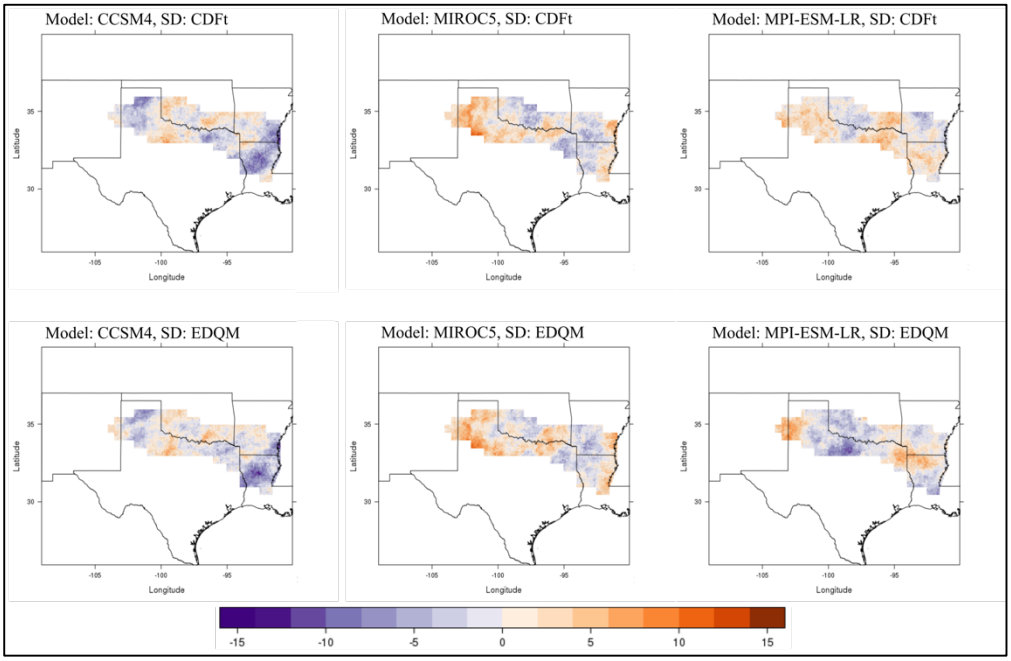


**Figure A25. Change in 25-year total frequency of severe drought at a 1-month timescale between the historical period (1981-2005) and mid-century period (2046-2070) under a RCP 8.5 scenario. Purple colors represent a decrease in events and oranges represent an increase.**

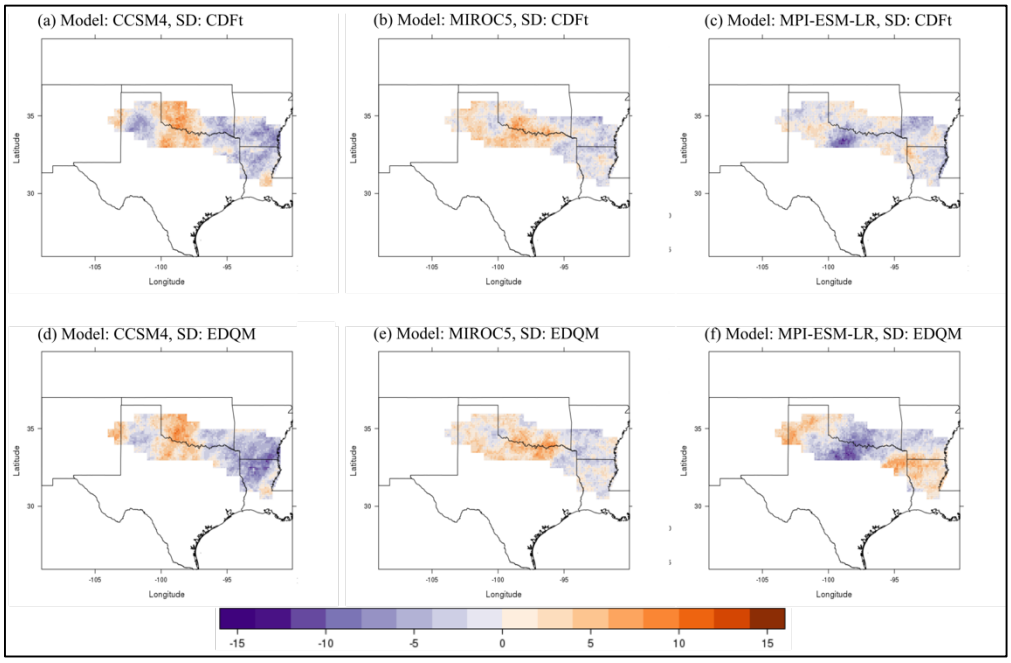


**Figure A26. Change in 25-year total frequency of severe drought at a 1-month timescale between the historical period (1981-2005) and end-of-century period (2075-2099) under a RCP 8.5 scenario. Purple colors represent a decrease in events and oranges represent an increase.**

## Appendix B: Survey Questions

Title of survey: Red River Basin Survey: Hydrologic Extremes

[Online consent form]

I agree to participate:

❍ Yes (1)

❍ No (2)

*If Yes, participant is directed to Question 1.

*If No, participant is directed to the End of Survey message.

1. What type of jurisdiction best describes your area of decision responsibility? (Please select all that apply.)

❑ International (1)

❑ National / Federal (2)

❑ State (3)

❑ Sovereign Tribal Nation / Indian Lands (4)

❑ Watershed / Drainage Basin / Catchment (5)

❑ County (6)

❑ Village / Town / City (7)

❑ Neighborhood (8)

❑ University / College (9)

❑ Other (Please describe.) (10) _____

2. In what area of the basin are you working in?

- ❍ New Mexico (1)
- ❍ Texas (2)
- ❍ Oklahoma (3)
- ❍ Arkansas (4)
- ❍ Louisiana (5)

3. For decisions pertaining to heavy rainfall and/or drought events, which option best represents your role(s)? (Please select all that apply.)

- ❑ Agricultural producer (1)
- ❑ Other agricultural decision maker (not a producer) (2)
- ❑ Fossil fuel energy producer (generation) (3)
- ❑ Renewable energy producer (generation) (4)
- ❑ Energy utility manager (transmission or distribution) (5)
- ❑ Water resources manager (6)
- ❑ Natural resources manager (excluding energy and water resources) (7)
- ❑ Conservation manager (8)
- ❑ Engineer (e.g., civil engineer, water resources engineer, hydrologic engineer, dam operations manager) (9)
- ❑ Hydrologist (10)
- ❑ Transportation planner (11)
- ❑ Risk manager (e.g., insurance) (12)
- ❑ City or regional planner (13)
- ❑ Emergency manager (14)

- ❑ Public safety official / First responder (e.g., police officer, fire chief) (15)
- ❑ Researcher (e.g., academia) (16)
- ❑ Educator (e.g., K-12, college, university) (17)
- ❑ Legislator or elected official (18)
- ❑ Weather or climate services expert (19)
- ❑ Public health official or provider (20)

Questions 4-9 pertain to extreme drought.

4. What products or indices do you use to gather drought information? (Please select all that apply.)

- ❑ U.S. Drought Monitor (1)
- ❑ U.S. National Weather Service (includes Climate Prediction Center) (2)
- ❑ Palmer Drought Severity Index (PDSI) (3)
- ❑ Standardized Precipitation Evapotranspiration Index (SPI or SPEI) (4)
- ❑ Crop Moisture Index (CMI) (5)
- ❑ Soil moisture data (e.g., Oklahoma Mesonet) (6)
- ❑ Other (Please describe.) (7) _____

5. For each season, what U.S. Drought Monitor category would cause adverse impacts to your jurisdiction, resulting in you or your organization to begin taking action (e.g., water conservation measures, water use restrictions)?

| | D0 (abnormally dry) (1) | D1 (moderate drought) (2) | D2 (severe drought) (3) | D3 (extreme drought) (4) | D4 (exceptional drought) (5) |
|---|---|---|---|---|---|
| Winter (1) | ❍ | ❍ | ❍ | ❍ | ❍ |
| Spring (2) | ❍ | ❍ | ❍ | ❍ | ❍ |
| Summer (3) | ❍ | ❍ | ❍ | ❍ | ❍ |
| Fall (4) | ❍ | ❍ | ❍ | ❍ | ❍ |

6. How many consecutive months of drought would cause adverse impacts to your jurisdiction?

7. What impacts would you expect to see in your jurisdiction if this occurred (e.g., infrastructure damage, ecological damage, impacts on water quality or quantity, etc.)?

8. What specific actions do you or your organization take in the event of your previously selected drought category being reached (e.g., water conservation measures, water use restrictions)?

9. Do you use any other specific triggers to determine if action is needed, such as reservoir level or water use exceeding a threshold? (If yes, please explain.)

❍ Yes; Explain: (1) _____

❍ No (2)

Questions 10-13 pertain to extreme rainfall.

10. What amount of rainfall in a two-week period would cause adverse impacts to your jurisdiction, resulting in you or your organization to begin taking action (e.g., activating emergency response procedures, releasing water resources, disseminating public warnings or advisories, or relocating resources or people)? (Please give a response in inches.)

11. If the rainfall amount from your previous response occurred, what impacts would you expect to see in your jurisdiction (e.g., flooded streets, fish kills, disease outbreaks, water contamination)?

12. What specific actions do you or your organization take in the event of your selected rainfall amount being reached (e.g., activating emergency response procedures, releasing water resources, disseminating public warning or advisories)?

13. Do you use any other specific triggers to determine if action is needed, such as reaching the 99th percentile of rainfall or the 100-year flood threshold? (If yes, please explain.)

❍ Yes; Explain: (1) _____

❍ No (2)

14. Does your workplace have a current plan or a plan in progress for future climate conditions? (If yes, please explain.)

❍ Yes; Explain: (1) _____

❍ No (2)

15. Would you like to be contacted with the research results for your jurisdiction in the Red River Basin? This would include information about the future frequency of extreme drought and rainfall events in your area. If so, please click the following link to provide us with your contact information.
https://ousurvey.qualtrics.com/jfe/form/SV_a2Asnx8NMlaRDcV

End of survey message:
Thank you for your time! If you are interested in the results of this research, then you can check the South Central Climate Science Center's webpage (www.southcentralclimate.org) in summer of 2017. If you chose to complete this survey, your responses will be of great help to this research regarding the impacts of extreme drought and rainfall in the Red River Basin. If you opted in to participate in this research further, then you will be contacted soon.

The following is a secondary survey that was created to keep contact information separate from previous survey responses.
Title of survey: Red River Basin Survey 2: Contact Information

Thank you for completing the previous survey! This is the contact page for the Red River Basin: Extreme Drought and Rainfall survey. If you chose to be contacted with research results for your jurisdiction, then please answer the following questions. If you would not like to provide contact information, you may exit this survey.

1. Would you like me to contact you with my research results for your jurisdiction in the Red River Basin? If yes, please provide contact information (email and/or phone number).

- ❍ Yes; Contact info: _____
- ❍ No

2. What is your name? (Optional)

End of survey message:

Thank you for your time! If you are interested in the results of this research, then you can check the South Central Climate Science Center's webpage (www.southcentralclimate.org) in summer of 2017. If you opted in for the opportunity to receive research results for your jurisdiction, then you will be contacted soon.